ATOMIC ENERGY REVIEW 17 1 (1979)

# THE MAIN CAUSES OF FUEL ELEMENT FAILURE IN WATER-COOLED POWER REACTORS

F. GARZAROLLI, R. von JAN, H. STEHLE
Kraftwerk Union Aktiengesellschaft,
Erlangen,
Federal Republic of Germany

ABSTRACT. The fuel failures observed in water-cooled power reactors (PWR, BWR, HWR) are classified according to the underlying mechanisms, i.e. hydriding, pellet-clad interaction (PCI), corrosion, clad collapsing, Zircaloy growth, rod and assembly bowing and fretting wear. The historical development of fuel designs and failure rates is briefly reviewed. Over the last decade the average fuel rod failure rate has dropped to near 0.02% and the majority of failures are at present caused by particular incidences. The present technological understanding of these failure types and their interpretation are presented in more detail. Hydriding, clad collapsing, unanticipated growth and fretting have mainly been caused by inadequate design or manufacturing in the early days and should not be a problem in future. PCI, external corrosion at high burnup and rod and assembly bowing are more generic mechanisms and need further consideration. Experience from the continued operation of defective fuel rods has confirmed that the selection of materials is also adequate for safe behaviour in the defective state.



## 1. INTRODUCTION

The fuel for water-cooled reactors has become a highly standardized and reliable industrial product over the past years. Present operational experience in the western world is based upon more than 9 million fuel rods, including 3.5 million short CANDU-type rods (no exact figures are available for the CMEA countries). Many countries and organizations have contributed to this outstanding success.

Uranium dioxide was used for bearing the fissionable material in all fuel designs from the early beginnings, whereas the present standard Zircaloy cladding material was not used in some early light water reactors. Being vital for heavy water reactors,

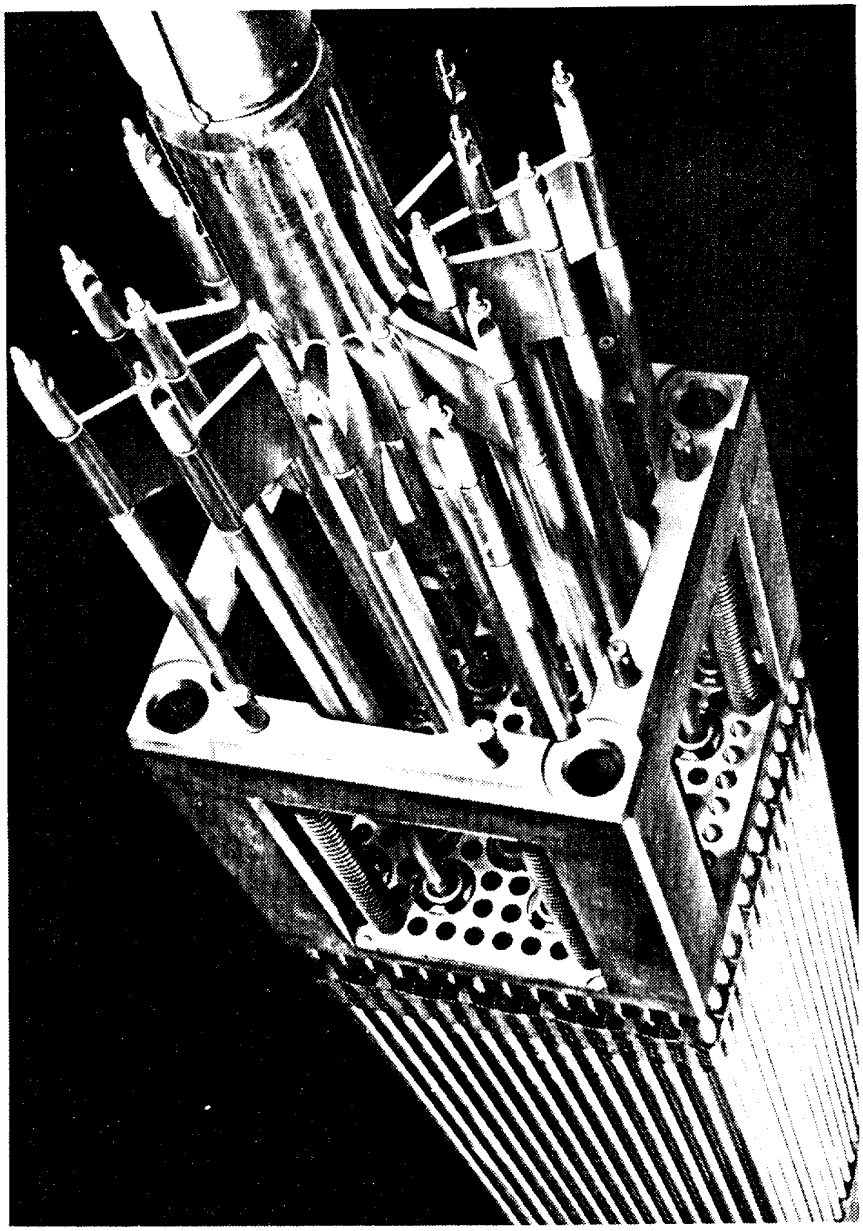

*FIG. 1. PWR fuel assembly.*

Zircaloy has always been used in these systems. Improvements in neutron econo provided an incentive to change from stainless steel to Zircaloy cladding for ligh water reactors as well. Although several problems related to the properties of Zircaloy are still of some concern, this step has been successful and is fully justi fied under the aspect of high fuel utilization.

The different reactor systems have a very similar fuel rod design. The main differences are outer dimensions (length, and to a lesser degree diameter), cladd

wall thickness and initial internal pressure. Prepressurization with helium is quite common for PWR fuel rods and is also applied to the BWR fuel rods in the present KWU design. It was originally introduced as a measure for reducing the cladding creep-down, but later proved to be an important step in stabilizing the thermal-mechanical fuel rod performance.

Unlike the fuel rod design, the bundle or assembly design varies from system to system since there are many correlations with the system design, especially with the layout of control rods and refuelling machines.

PWR fuel assembly design follows the rod cluster control (RCC) concept (Fig.1), with the exception of a few older reactors. The assembly structure consists of the control rod guide tubes, the grid-like spacers, and the lower and upper end pieces. These parts are fixed together, whereas the fuel rods are mainly clamped by the spring-force of the spacer grids. This design allows for independent

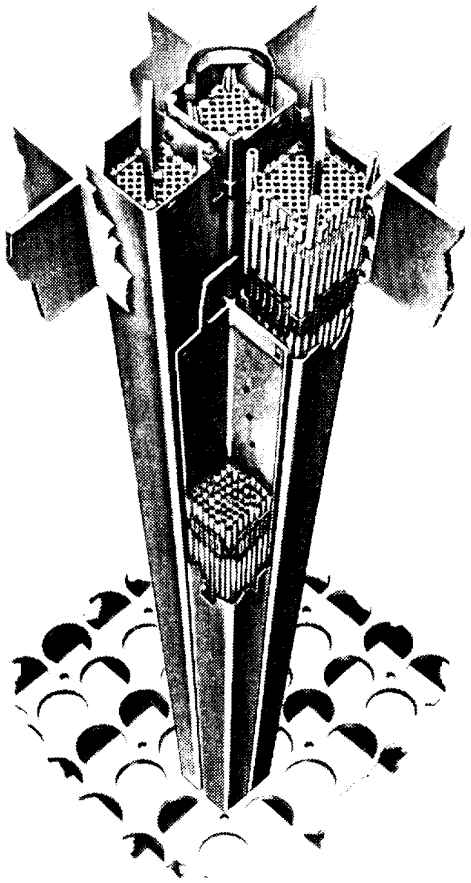

*FIG.2. BWR fuel assembly.*

TABLE I. OPERATIONAL REQUIREMENTS FOR LWR FUEL (TYPICAL VALUES)

| | PWR | BWR |
|---|---|---|
| Average linear heat generation rate (W/cm) | 155 – 225 | 155 – 230 |
| Residence time (a) | 3 | 4 |
| Hot channel factor | | |
| steady state | 1.5 – 2.1 | 1.8 – 2.2 |
| transient | 2.3 – 2.5 | 2.3 – 2.5 |
| Neutron flux, thermal ($cm^{-2} \cdot s^{-1}$) | $4 - 6 \times 10^{13}$ | $3 - 5 \times 10^{13}$ |
| fast ($cm^{-2} \cdot s^{-1}$) | $6 - 9 \times 10^{13}$ | $4 - 6 \times 10^{13}$ |
| Burnup target (assembly average) (GW · d/t(U)) | 28 – 34 | 22 – 28 |
| Coolant pressure (bar) | 145 – 158 | 72 |
| Coolant temperature (°C) | 303 – 316 | 287 |

expansion of structure and fuel rods and for easy visual inspection of the assemblies. In some of the current designs the assemblies are reconstitutable, and therefore fuel rods can be withdrawn or replaced. The number of rods and guide tubes per assembly varies slightly in the different designs of the leading companies. Most of them used stainless steel (or Inconel) for the structural parts in their first design approach but are currently using or going to 'low parasitic' Zircaloy structures. This will further improve the fuel utilization in PWRs.

In BWR fuel assemblies (Fig.2) the supporting connection between lower and upper end pieces is normally provided by eight fuel rods (tie rods). The spacer grids are fixed to either a segmented fuel rod or an inert rod (empty tube or solid). The grids are fabricated from a Zircaloy basic structure and Inconel spring members. Another characteristic difference compared with PWR assemblies is the Zircaloy channel, which confines the individual assembly coolant flow. The cruciform control rods and the in-core instrumentation are in the space left between the channels. In general, bundles and channels are considered as interchangeable parts. In addition, BWR assemblies are easily reconstitutable.

The main operational requirements for LWR fuel are reviewed in Table I. The coolant pressure in PWRs is higher than in BWRs by about a factor of 2; however, the coolant temperature is only slightly different in both systems. The

residence time of the fuel in the core for full burnup typically amounts to three or four years respectively. Average burnup and accumulated fast fluence (order of magnitude $10^{21}$ cm$^{-2}$) are slightly higher in PWRs.

The main design data and operational requirements of HWR fuel vary in different systems. A common feature is the circular bundle geometry. Most HWRs ($U_{nat}$ fuel) have flux and burnup targets smaller by a factor of 4 to 5 than have LWRs.

Fortunately, only one type of zirconium alloy has been developed and applied in the western countries, i.e. the well-known Zircaloy. There are only minor differences between Zircaloy-2 (~ 1.5% Sn, ~ 0.15% Fe, ~ 0.10% Cr, ~ 0.05% Ni, balance Zr) and Zircaloy-4 (~ 1.5% Sn, ~ 0.2% Fe, ~ 0.10% Cr, balance Zr) and their preference in one or the other system may be explained mainly on a historical basis.

With regard to their in-pile performance as cladding tubes the experts agree that the properties of interest are very similar. Only the hydrogen pickup in coolants with hydrogen additions is markedly different. Since Zircaloy-4 hydrides less than Zircaloy-2 under typical PWR conditions, only Zircaloy-4 is used in PWRs. In Russian reactors Zr-Nb alloys are used, obviously with adequate success. Several other alloys have been investigated on an experimental scale by several organizations.

Plutonium is considered as a future additional energy source in many countries. During the past ten years many Pu-bearing fuel assemblies have been fabricated and inserted in PWRs and BWRs, mainly in western Europe. The design and specifications of these assemblies closely follow those of uranium fuel. The operational performance of thermal Pu recycle fuel has been very satisfactory and only in a few cases will special reference be made to mixed-oxide fuel.

Good review articles are available on the subject of worldwide fuel performance [1–4] as well as on the fuel performance of individual reactor types or companies [5–13]. It is not the aim of this paper to repeat or exhaustively summarize these previous publications. The authors' intention is to give:

(1) A concise review of the classification, history and significance of fuel failures with today's understanding and judgement, and with emphasis on recent developments (sections 2 and 3);

(2) A more extended review of the present technological understanding of failure mechanisms (sections 4 and 5).

To satisfy different needs, both parts have been written so that they can be read independently. This aim should justify the occasional repetition of arguments.

TABLE II. CLASSIFICATION OF OBSERVED FUEL FAILURES (ZIRCALOY CLAD)

| Phenomenon | Main causes | Origin | Time of occurrence | Consequences | Reactor type |
|---|---|---|---|---|---|
| 1. Hydriding | Moisture in pellets/rods | Manufacture + specification | Early | Perforation local attack | All types |
| | Contamination, end plug stringers, weld deficiencies | Manufacture | Early | Perforation | All types |
| 2. Pellet clad interaction (PCI) | Power ramp | Operation | Mid to late | Perforation incipient cracks | All types |
| | Local hydriding + power ramp | Manufacture + operation | Mid to late | Perforation | BWR |
| 3. Corrosion (burnout) | Weld contamination | Manufacture | Early | Perforation | All types |
| | Crud deposits | External | Early to late | Perforation | BWR, SGHWR |
| | Coolant blockage | External or design | Early | Perforation | One BWR |
| | High heat flux/clad temperature | Operation or design | Late | Perforation | Experimental rods only |
| 4. Clad collapsing | Axial gaps by fuel densification | Specification | Early | Deformation (some perforations) | PWR |
| 5. Zircaloy growth | Irradiation-induced growth and pellet-clad interaction | Design | Early to late | Structural misfit rod bowing | BWR, SGHWR PWR |
| 6. Rod bowing | Relaxation of cladding tube | Specification | Early | Deformation + burnout | One BWR |
| | Rod growth + interaction with endplate | Design | Continuous | Deformation | PWR |
| | Interaction with assembly structure | Design | Continuous | Deformation | PWR |

| | | | | | |
|---|---|---|---|---|---|
| | Rod growth + interaction with endplate | Design | Continuous | Deformation | PWR |
| | Interaction with assembly structure | Design | Continuous | Deformation | PWR |

TABLE II. (cont.)

| Phenomenon | Main causes | Origin | Time of occurrence | Consequences | Reactor type |
|---|---|---|---|---|---|
| 7. Fretting wear | Foreign particles | External | Early | Perforation, wear marks | All types |
| | Vibration rod/spacer grid | Manufacture or repair | Early | Perforation | PWR |
| | Vibration of assembly | External or design | Early | Perforation, wear marks | PWR |
| | Vibration of incore components | External | Early | Channel wear | BWR |

## 2. CLASSIFICATION AND CHARACTERIZATION OF FUEL FAILURES

In general, the failure rate characteristics for an engineering device follow the well-known 'bath-tub' shaped curve with an early failure maximum, an extended period of useful life with low constant failure rate, and a wearout phase late in life. Besides the fact that manufacturing deficiencies often have led to an early failure rate maximum, this bath-tub curve approach has little relevance for the following reasons. First, the burnup target of present fuel design is not near to a threshold for irradiation-induced loss of integrity; secondly, the failure rate of proper fuel under well-controlled operation is practically zero; thirdly, the majority of fuel failures during useful life so far had to be attributed to 'deterministic events', i.e. to abnormalities in fabrication or operation or to early design deficiencies.

Another difficulty arises from the definition of a fuel failure, or more precisely from the question of to what extent a fuel defect or a leaking fuel rod really has to be considered as a 'failure', since usually the operation of a reactor is not influenced by the presence of minor defects or a limited number of leaks. Nevertheless, following Bobe [1], we define a fuel failure as a "perforation or defect of the fuel cladding, or any structural change which causes abnormal maintenance or early replacement of a fuel assembly or its component parts".

Any classification of fuel failures is always to some extent arbitrary because of the various criteria that can be applied, and because of the possibility of multiple causes. Several classifications have been offered in the literature [1–4], depending on the goal of the various authors. For the purposes of this report fuel failures are classified according to the **phenomena** that establish a failure as defined above. Using this, seven different failure mechanisms can be defined (see Table II):

(1) Primary **hydriding** due to hydrogenous impurities and sometimes promoted by halogenous impurities in the fuel rod or end-plug defects.

(2) Stress corrosion cracking of the clad due to mechanical and fission product-induced chemical **pellet-clad interaction (PCI)**.

(3) Accelerated **corrosion** (in cases of overheating called **burnout**) due to oxidation of the clad outer surface.

(4) Rod **collapsing** or flattening due to insufficient support of cladding because of $UO_2$ stack shortening by fuel **densification**.

(5) Structural changes that exceeded design margins from **growth of Zircaloy** (or differential growth effects).

(6) **Rod bowing** to the extent that the assembly design criteria (e.g. rod to rod spacing) are violated. (Rod bowing must be distinguished from assembly bowing, where all the rods and structure components are equally bowed.)

(7) Wear and **fretting** corrosion on fuel rods and structural parts due to foreign particles or due to vibration of single fuel rods, entire assemblies, or in-core components.

Many of these mechanisms (i.e. PCI, corrosion, densification, growth, bowing) are generic effects which occur to a minor extent in all operating fuel and are considered in standard design procedures. It is only the excessive or more than anticipated degree that makes them a failure mechanism in several cases. On the other hand, several mechanisms that were often feared as a potential risk in the past have never led to fuel failures in power reactor application; for instance, late in life fuel swelling, hydrogen uptake of the cladding, cladding fatigue, and severe Zircaloy embrittlement (cladding or spacers). Faulty end-plug welds because of weld contamination occurred only in the early days of Zircaloy-clad fuel fabrication. Indeed, the welding of Zircaloy is a process with an outstanding high degree of reliability if proper welding techniques are applied. More than other metals, Zircaloy is rather insensitive to welding failures like microfissures, second-phase precipitates etc.

In the past there have also been infrequent failures of other types, e.g. (i) misloading of pellet enrichments, rods or assemblies; (ii) defective as-delivered material; (iii) breach of some structural parts during operation; (iv) mechanical damage by handling; and (v) specific design or manufacturing deficiencies resulting in replacement/repair of as-delivered fuel batches or irradiated fuel. A more recent example of the latter failure type is the unexpected axial displacement of the spacer grids in Swedish fuel assemblies. In the former ASEA Atom design the spacers were not fixed to the assembly structure and tended to shift axially after relaxation of the springs. ASEA Atom decided to repair all operating assemblies by introducing an inert rod and fixing the spacer grids to this rod, similar to the present design of ASEA Atom and all other BWR fuel suppliers. However, these occasional failures and the corresponding preventive action have to be treated on a case by case basis and cannot be the subject of a review of the main causes of fuel failures.

The second column of Table II summarizes the main causes of the seven categories of fuel failures. They will be discussed in more detail in section 4. In the early days it was sometimes difficult to distinguish between cause and effect, since in-pile degradation of defective fuel rods by 'secondary defects' may mask the primary cause of the failures (see section 5). Defective fuel rods operated in water reactors suffer from substantial secondary hydriding which dominates the visual appearance, and it happened that failures were erroneously attributed to

primary hydriding where later post-irradiation examination revealed the true primary cause to be fretting or PCI. Longitudinal splits in the cladding may also be a source of misinterpretation. Intuitively this failure is attributed to PCI, and frequently this is accurate since PCI failures (i.e. tiny pinholes or cracks in the cladding) may develop into longitudinal splits. However, secondary splits have frequently been observed in LWRs, even in the fission gas plenum area where severe hydriding has been the cause of the split and a contribution from PCI is impossible. Observations in SGHWR and hot cell examinations also support the interpretation that longitudinal splitting, if observed under normal operating conditions, is a typical secondary defect which may occur in any defective fuel rod and particularly in a BWR due to the more frequent local power changes by control rod movement. From this evidence the authors propose to classify longitudinal splits in most cases as secondary defects and not as a primary PCI failure.

After having established the technological cause of the failure, it is important to find its origin in order to design preventive actions and remedies. As can be seen from column 3 of Table II, the origin is approximately equally distributed in the areas of

Design and specification
Manufacturing
Operation
External influences.

This shows that no single area can be blamed for the fuel failures and that quality assurance programmes have to cover not only fuel design and manufacturing but the whole reactor system and reactor services.

For practical reasons there are two more characteristic features of interest:

(1) The time of occurrence, in order to assess the consequences of continuing fuel operation or the advantage of repair action

(2) The consequences of the failure and, in particular, the extent of rod perforation and fission product release to the primary coolant.

The majority of fuel failures occurred early in life. In particular, hydriding is generally classified as an early-in-life failure referring to the more severe cases of residual moisture in the fuel. However, the result may also be a non-penetrating hydride attack of the inner clad surface, which may perforate later in life. The evidence from operational experience is the continuing high failure rate of those fuel batches that suffered from initial hydriding.

Several failure phenomena can be detected early in life before any damage may occur. For instance, rod bowing, length growth and the corrosion rate can be checked by visual examination or by simple pool measurements during refuelling outages. One exception is the PCI mechanism, which typically occurs mid to late in life when mechanical pellet-clad contact is established and sufficient fission products are available to initiate stress corrosion cracking. No measuring technique is yet known to determine the PCI propensity of a fuel rod. However, a device has been described [14] for measuring the residual gap between clad and $UO_2$ by determining the 'interaction force' during ovalization by a line force. Applicable results are not yet available.

In principle, the failure phenomena discussed above may occur in all water reactors. The failure propensity, however, has differed depending on the system design and on the state of the art at the time when the reactor system was designed or fuel mass production started. Hydriding has occurred in all reactor types, although to a variable extent. Corrosion of production fuel by crud deposits has mainly been reported from old BWR plants and from the SGHWR. Heat flux accelerated water-side corrosion of the cladding was only observed in some experimental high power fuel rods. Under present design conditions and burnup targets there is no problem with this type of accelerated corrosion, neither with uniform corrosion nor with the so-called nodular corrosion frequently observed in a BWR environment. Rod collapsing occurred only in some early PWRs with unpressurized rods and has never been observed in highly pressurized PWR fuel or in a BWR ('free standing' clad design). Only 2–20% of the collapsed rods showed rod perforation. Problems with the assembly structure (growth, bowing, fretting) were more pronounced in LWRs than in HWRs because of the greater length of the assemblies and partly because of higher coolant velocity or the possibility of cross-flow. Rod perforations were confined to severe cases of fretting.

The remedies for the above-mentioned failures have been design and manufacturing improvements. The only generic failure phenomenon that cannot be easily eliminated by design modifications, selection of materials or fabrication improvements is the PCI failure risk at severe power ramps. However, substantial progress has been made recently in understanding the underlying mechanisms and in designing remedies. In particular, it has been clearly established that PCI failures in sound fuel rods are not caused by power cycles within the previous steady-state power level (preconditioned envelope). They are always correlated to power ramps, i.e. the **first** severe (fast and large) power increase beyond the preconditioned envelope. Many experimental efforts in the area of power ramping are known from companies and nuclear research centres.

It can be stated today that – owing to the major efforts of the nuclear industry in fuel testing and in post-irradiation examination (PIE) of defective and non-defective fuel – the main causes of all known failure mechanisms are well understood and no longer present the confusing picture of several years ago.

TABLE III. MAIN FUEL TYPES FOR WATER REACTORS (WESTERN COUNTRIES)

| Type | Reactor Manufacturer | Former fuel design | | | | Present fuel design | | | |
|---|---|---|---|---|---|---|---|---|---|
| | | Number of rods | Rod o.d. (mm) | Ave. LHGR (W/cm) | Number of plants[a] | Number of rods | Rod o.d. (mm) | Ave. LHGR (W/cm) | Number of plants[a] |
| PWR | Babcock & Wilcox and BBR | 15 X 15–17 | 10.92 | 177–200 | 8 | 17 X 17–25 | 9.63 | 170–180 | 0 |
| | Combustion Engineering | 14 X 14–4 X 5 | 11.18 | 184–194 | 6 | 16 X 16–4 X 5 | 9.70 | 170–180 | 0 |
| | Kraftwerk Union | 14 X 14–16<br>15 X 15–20 | 10.75 | 177–226 | 1<br>3 | 16 X 16–20 | 10.75 | 207 | 2 |
| | Westinghouse[b] and Framatome | 14 X 14–17<br>15 X 15–21 | 10.72 | 150–220 | 17<br>16 | 17 X 17–25 | 9.50 | 170–180 | 6 |
| BWR | ASEA Atom | 8 X 8 | 12.25 | 126–155 | 3 | 8 X 8–1 | 12.25 | 158–175 | 2 |
| | Gen. Electric[c] and Kraftwerk Union | 6 X 6<br>7 X 7[d] | 14.3 | 150–234 | 7<br>30 | 8 X 8–2 | 12.5 | 170–200 | 4 |
| HWR | AECL[e] ($D_2O$-CANDU) | 19/28 | 15.2 | 80–260 | 8 | 37 | 13.08 | 210 | 2 |
| | Kraftwerk Union (PHWR) | 37/36 | 11.9 | 116/232 | 2 | – | – | – | – |
| | UKAEA/BNFL (SGHWR) | 36 | 16.0 | 210 | 1 | 60 | 12.2 | – | 0 |

[a] Number of plants (>20 MW(e)) in operation since January 1978.
[b] Including Mitsubishi.
[c] Including Hitachi and Toshiba.
[d] 8 X 8 reload since 1973/74.
[e] 50 cm length of bundle.

3. P
F

3.1. L
S
histor
the m
increa
rod di

If failu
irradia
costs a
to one

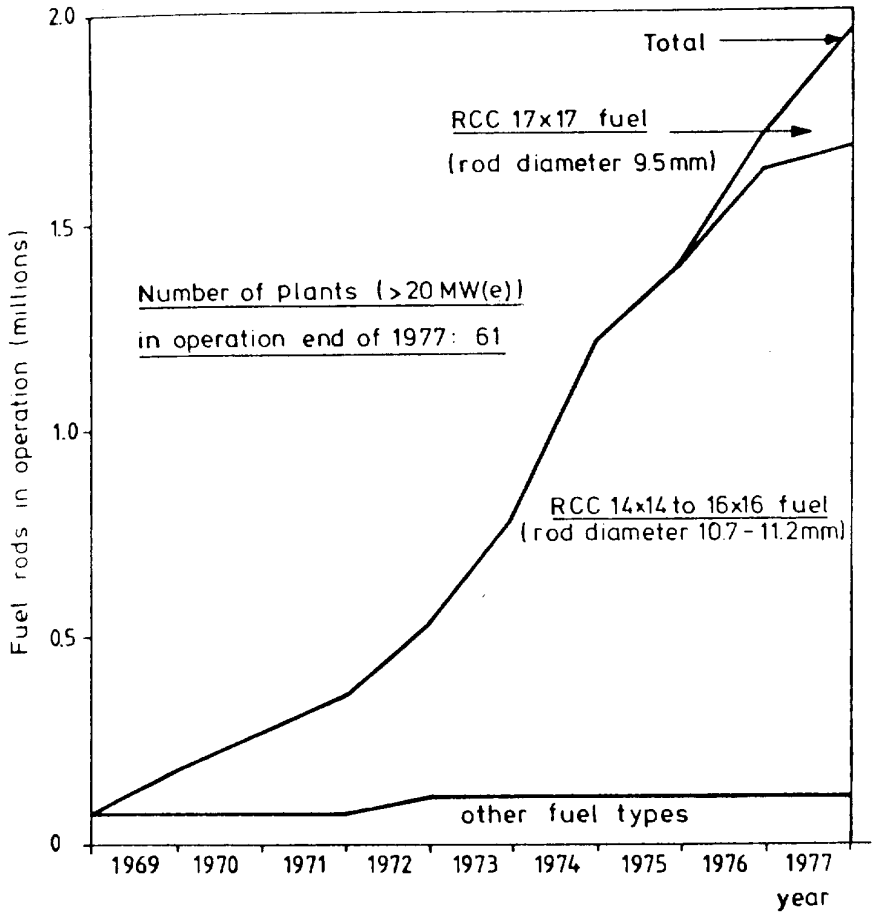


*FIG.3. Number of PWR fuel rods in operation.*

If failures are declared as "unexplained", this is simply due to the fact that post-irradiation examination cannot be performed in each case because of the high costs and other limitations. It does not mean that the failure could not be traced to one of the known mechanisms.

## 3. HISTORICAL BACKGROUND AND SIGNIFICANCE OF FUEL FAILURES

### 3.1. Development of fuel design and fuel duty

Some remarks on fuel design and duty should be helpful to understand the history and significance of fuel failures in different reactor systems. A survey of the main fuel types for water reactors is given in Table III. The variety has increased during recent years since several manufacturers have changed to smaller rod diameters (lower heat rating) in order to increase the margins to design limits.

[a] Number of plants (>20 MW(e)) in operation since January 1978.
[b] Including Mitsubishi.
[c] Including Hitachi and Toshiba.
[d] 8 × 8 reload since 1973/74.
[e] 50 cm length of bundle.

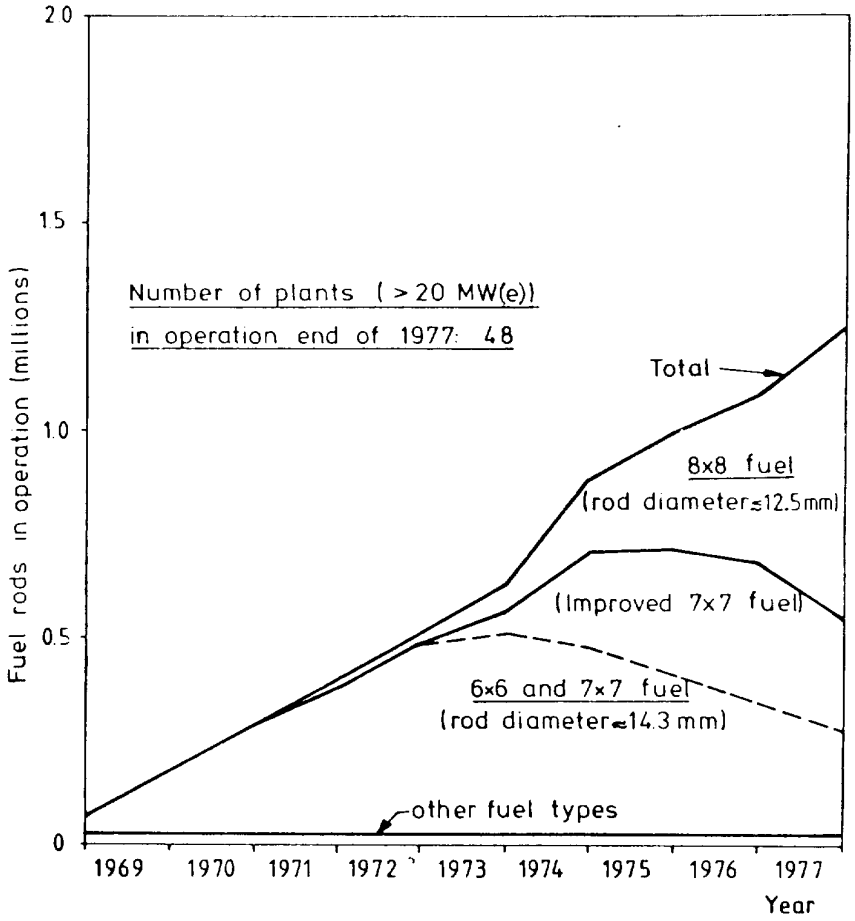


*FIG.4. Number of BWR fuel rods in operation.*

PWR fuel assemblies (RCC type) of the former designs are characterized by a fuel rod diameter near 11 mm and a 14 X 14 or 15 X 15 rod array (160 to 208 fuel rods per assembly). The present designs are of 16 X 16 and 17 X 17 geometry (224 to 264 fuel rods per assembly) with varying rod diameters. The US companies (and licencees) use rod diameters near 9.5 mm, since with the original design the average linear heat rating in a 1300 MW(e) plant would have been near and above 230 W/cm. Only Kraftwerk Union (KWU) designed their 1300 MW(e) standard plants with lower heat rating (207 W/cm) and therefore decided to keep the larger rod diameter for the present generation of plants. The vast majority of operating PWR fuel is (and in the near future will be) of those types with ≈ 11 mm rod diameter, as only 6 out of 61 operating plants are designed for using 17 X 17 fuel (see Fig.3).

An 'all rod' 6 X 6 to 8 X 8 array (36 to 64 fuel rods per assembly) has been typical for former commercial BWR fuel with rod diameters of either 14.3 mm (GE/KWU) or 12.25 mm (ASEA Atom). Since GE and KWU have changed to a

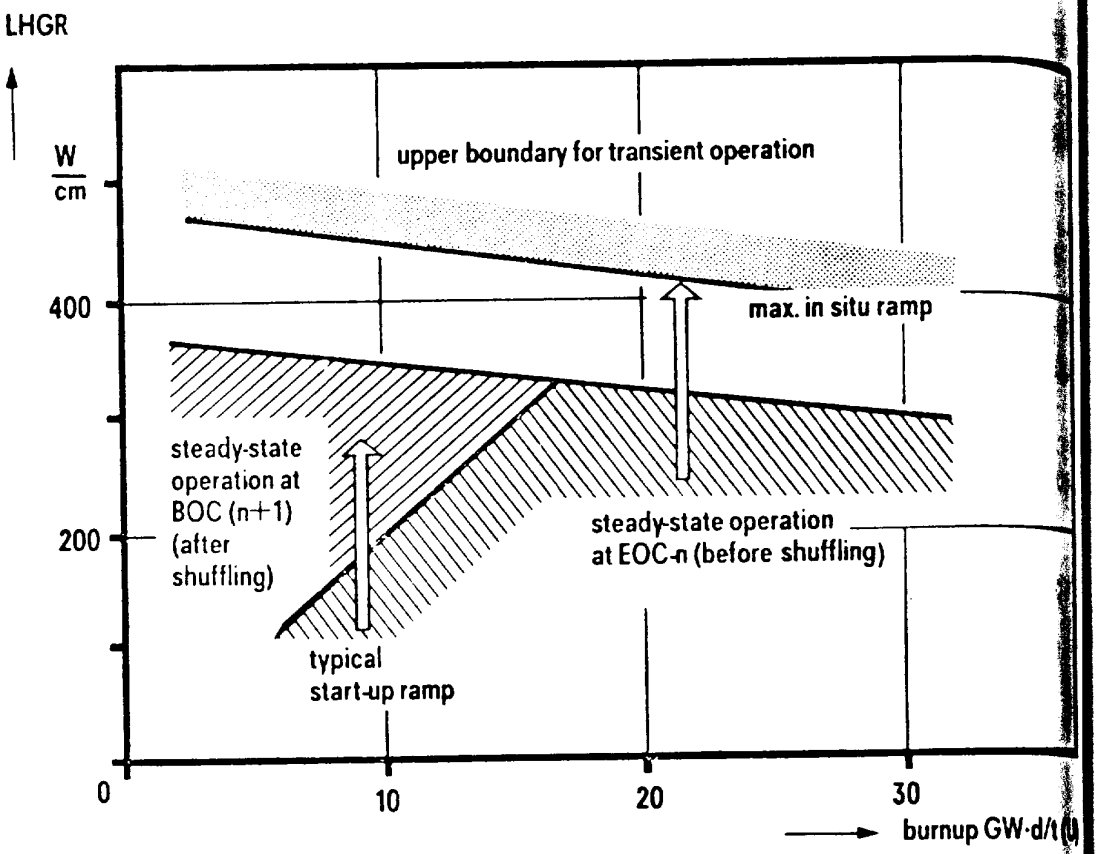


*FIG.6. Maximum LHGRs and anticipated ramps in a KWU PWR.*

countries. Including already discharged fuel, the total number of irradiated rods is estimated as follows:

PWR: over 3 million fuel rods
BWR: over 1.7 million fuel rods
HWR: 130 000 (short) fuel bundles (≈ 3.5 million rods)
100 000 (long) fuel rods.

Another interesting feature is the historical development of fuel rating (Fig.5). With the exception of the ASEA Atom BWR design, the plant average power density and linear rod power continuously increased during the late sixties and the early seventies, changing from 80–150 W/cm in the early plants to the range of 160–230 W/cm in later LWR plants, and even up to the range above 250 W/cm in several HWR plants. This was accompanied by a corresponding increase in average design burnup to typically 34 (PWR), 28 (BWR) and 7–20 (HWR) GW·d/t(U). Although the feasibility of operating high-rated fuel had been well

established by various high-performance test programmes, the value of these tests had been limited with respect to the later requirements in fuel reliability. The combined change to fuel mass production and high-rated plants necessarily had the consequence of initially enhanced failure risks.

With respect to the PCI effect, an important remark has to be made to the power history of fuel rods in operating LWR plants. In most of the physical design strategies used today the maximum heat rating occurs at a burnup below 15 GW·d/t(U). This can be seen, e.g., from the design curve of a modern German PWR (Fig.6). In this case under steady-state conditions the maximum heat rating decreases with increasing burnup. Significant ramps have to be considered due to reshuffling after one cycle exposure or to transient operations at any time. According to Fig.6 the maximum ramp height as well as the maximum power that might be reached decreases with increasing burnup. Such a design excludes that highly burned fuel is ramped to the maximum design heat rating during normal operating conditions. Since modern power plants are also equipped with sophisticated power distribution control and power-limiting systems, the effective fuel duty of highly burned fuel is not at all characterized by the maximum design heat rating, but depends on many details of the individual reactor system, design and operating mode.

### 3.2. The main incidences of fuel failure (Table IV)

To evaluate the significance of fuel failures during the last decade, the available published data ([1–13] and references given there) together with unpublished data on fuel failures and their causes have been accumulated and analysed. In addition, a distinction has been made between reported abnormal occurrences (incidents) and unsystematically occurring failures with known or unknown cause. For several plants the failure levels had to be estimated from coolant activity, and only trends can be indicated for the 1977 data since the available information covers less than 50% of the operating plants.

As a first approach the individual plant failure levels have been plotted against time. One remarkable result is that the bulk of the data points for each failure category can be enveloped and separated, as schematically shown in Figs 7–9, giving typical ranges of failure levels for each category. The decreasing slope of the block of hydriding/PCI data for BWRs is a consequence of the elimination of old fuel in GE/KWU plants.

It is evident from Figs 7–9 that mainly three phenomena, i.e. hydriding, PCI and clad collapsing, have had a significant effect on fuel performance. In the early seventies failure rates of 0.1–1% due to these mechanisms were experienced at many plants and massive failures beyond 1% of the rods occurred in some fuel batches where particular circumstances or manufacturing deficiencies added to the general failure risk. Fuel batches or even whole core loads had to be replaced in some of these cases, with a corresponding impact on fuel management.

TABLE IV. MAIN REPORTED INCIDENCES OF FUEL FAILURES
Zircaloy-clad water reactor fuel

| Failure mechanism | PWR plant (cycle No.) | BWR plant (cycle No.) | HWR plant (year) |
|---|---|---|---|
| Hydriding (≳0.1% failures) | Beznau 1 (1,2)<br>Ginna (1,2)<br>Mihama 1 (1)<br>Obrigheim (1)<br>Pt. Beach 1 (1) | All BWR 1, 2, 3 (several cycles)<br>Fukushima 2<br>Lingen<br>Vermont Yankee | None |
| Pellet clad interaction [a] | Maine Yankee (1)<br>Obrigheim (6)<br>Pt. Beach 1 (3) | Dresden 3 (3)<br>Gundremmingen (5)<br>Oskarshamn 1 (2)<br>Peach Bottom 2 (1)<br>Quad Cities 2 (2) | Douglas Point (≲1972)<br>Pickering 1 (≲1972) |
| Clad collapsing | Beznau 1 (1,2)<br>Ginna 1 (1,2)<br>Mihama 1 (1)<br>Pt. Beach 1 (1,2)<br>Robinson 2 (1) | None | None |
| Corrosion (crud) | None | Big Rock Point (several cycles)<br>Tsuruga | SGHWR (1968) |

| | Robinson 2 (1) | | |
|---|---|---|---|
| Corrosion (crud) | None | Big Rock Point (several cycles)<br>Tsuruga (several cycles) | SGHWR (1968) |

TABLE IV. (cont.)

| Failure mechanism | PWR plant (cycle No.) | BWR plant (cycle No.) | HWR plant (year) |
|---|---|---|---|
| Rod bowing (growth/ interaction) | Beznau 1 (1)<br>Ginna 1 (1)<br>Mihama 1 (1)<br>Mihama 2 (2)<br>Obrigheim (1)<br>Zorita (1) | Dresden (1) | None |
| Fretting<br>(a) foreign particles (≳0.1% failures) | None | Gundremmingen (1)<br>Nine Mile Point (1) | Gentilly 1 |
| (b) assembly vibration [b] | Borssele (1)<br>Mihama 1 (2)<br>Pt. Beach 1 (3)<br>Zorita (2) | None | – |
| (c) channel wear [c] | – | Mühleberg (1)<br>Pilgrim (1)<br>Vermont Yankee (1) | – |
| (d) rod to spacer [d] (≳0.1% failures) | Stade (5) | None | None |

[a] Confirmed ramp incidents.
[b] Borssele weak hold-down spring. Other plants cross-flow.
[c] Vibration of incore components.
[d] Spacer spring distortion by assembly repair.

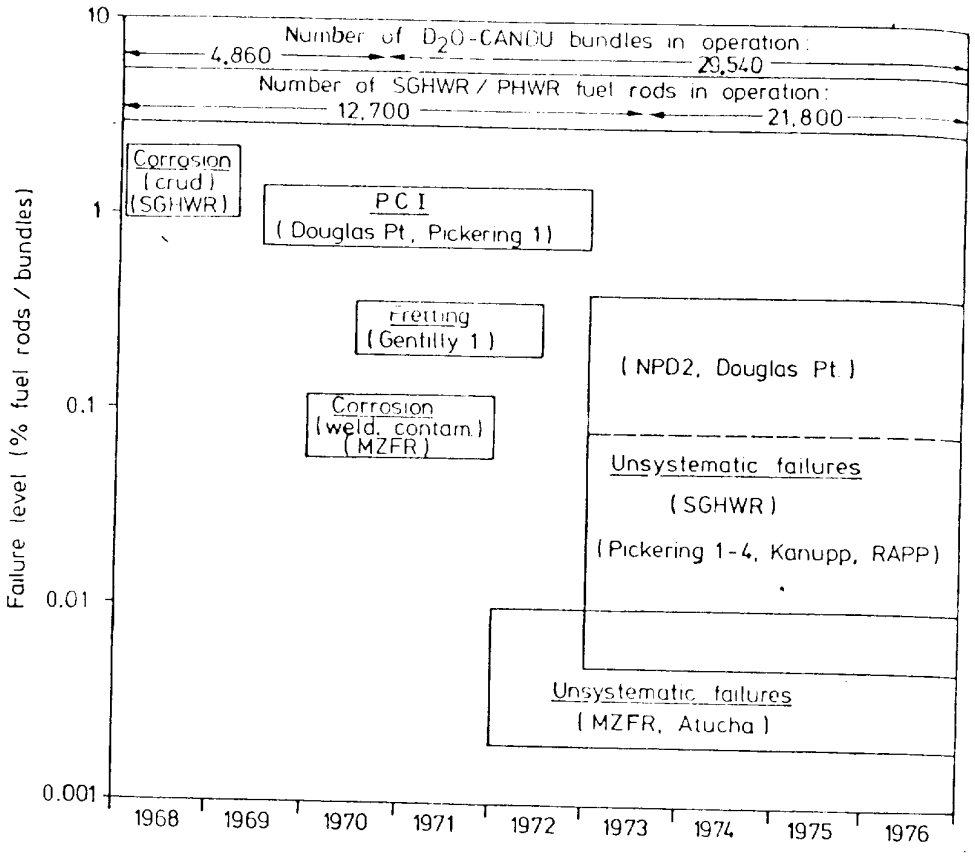


*FIG. 7. Fuel performance summary of HWR plants.*

The remaining phenomena were of less significance for the overall fuel performance. Still, high failure rates and substantial surveillance and repair campaigns resulted in individual plants.

### *3.2.1. Hydriding*

The effects of hydriding can be separated into low-frequency failures (e.g. through occasional end-plug defects) and the well-known hydriding epidemics of the early seventies. Hydriding has dominated BWR fuel performance to the present time, despite the fact that only those fuel batches were affected that had been manufactured before 1970–1972. The reason is that these old batches showed consistently high failure rates of $\gtrapprox 0.2\%$ rods per cycle even after repair and throughout their lifetime of four to five operating cycles. This effect is attributed to a combined hydriding/PCI effect. In 1976/1977 the vast majority of fuel failures in BWRs still occurred in these old batches, whereas improved 7 X 7 fuel types remained in the range 0.01–0.03% of unsystematic failures, and 8 X 8 reload fuel had essentially zero failure rates [7].

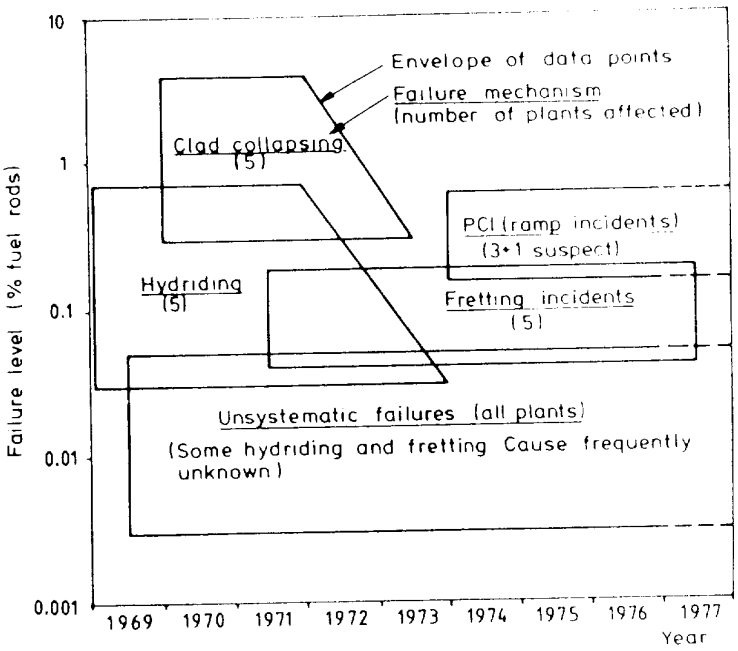


*FIG.8. Fuel failure levels in individual PWR plants.*

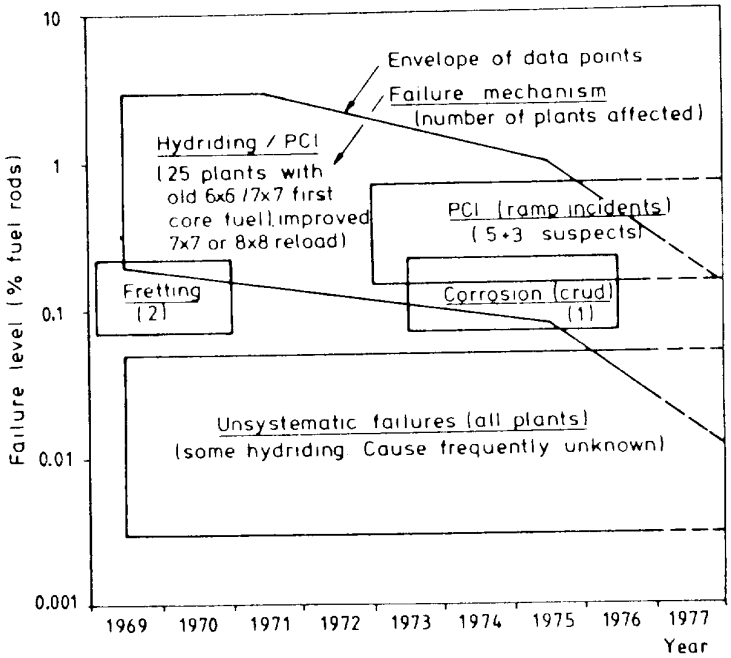


*FIG.9. Fuel failure levels in individual BWR plants.*

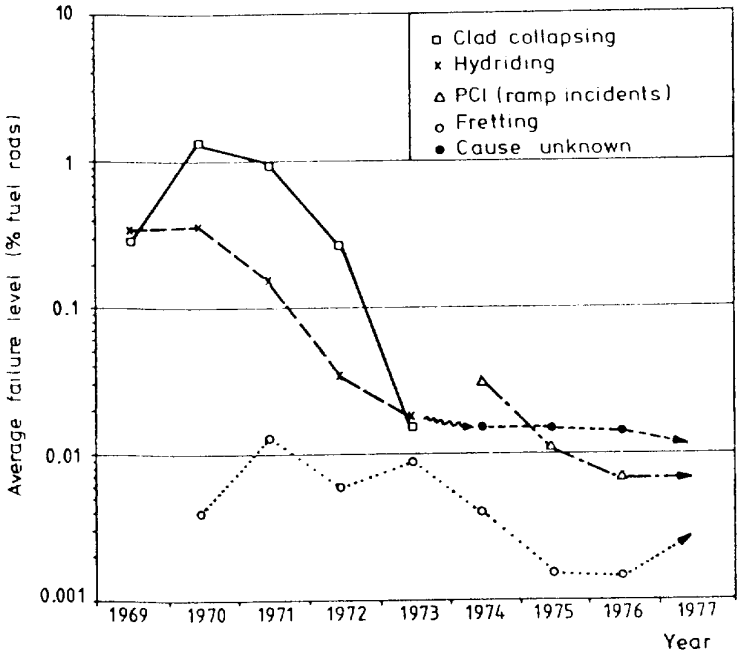


*FIG.10. Overall significance of fuel failures in PWR plants.*

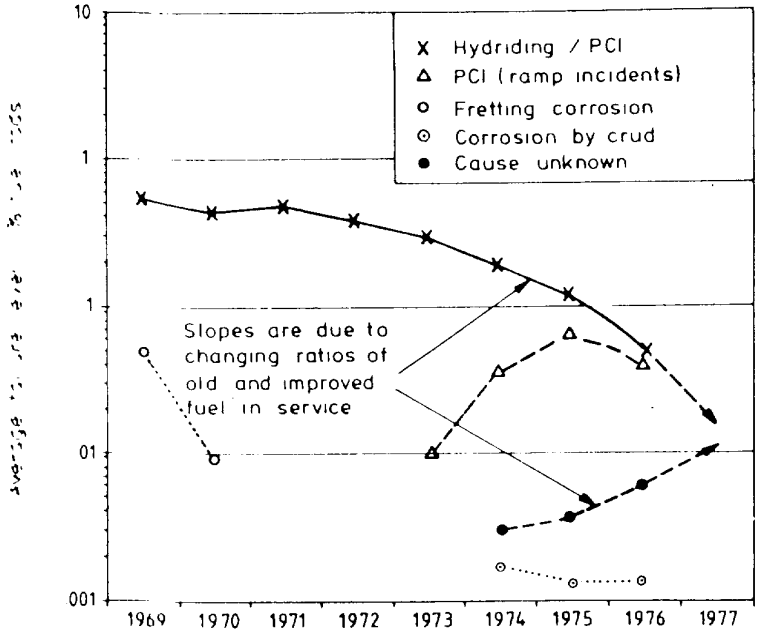


*FIG.11. Overall significance of fuel failures in BWR plants.*

Fewer cases of massive hydriding were reported from PWR fuel. Since most of these failures occurred in early discharged first-core fuel and because of the policy of some PWR fuel vendors in USA of discharging and not repairing defective fuel, the problem was essentially eliminated within a few years or was at least emerging into the background of unknown failure causes. HWRs have not been affected by massive hydriding.

### 3.2.2. *Pellet-clad interaction*

If one disregards the old BWR fuel, the PCI problem seems to be surprisingly similar in PWRs and BWRs – PCI failures are mainly related to severe power ramp incidents [15–17] or corresponding ramp experiments [12] in operating plants.

The typical failure rate resulting from such an incident is of the order of 0.3% of the rods in the core with substantial scattering depending on the fuel type, the severity of the ramp and fuel burnup, with the failures being concentrated mostly in a limited number of fuel assemblies. In addition, experience shows that fuel batches that suffer from a ramp incident may also have high activity release and high failure rates in the subsequent reactor cycle, indicating that predamaged fuel rods with incipient cracks have been left in the core. In these cases the failures in the subsequent cycle were also attributed to PCI.

The cause of these ramp incidents has been plant operation, either fast BOC startup rates after refuelling, or xenon transients resulting from errors in control rod manoeuvring. Therefore, specific recommendations and operating guidelines were given to the operators, to be discussed in section 3.3. Despite the high failure rate in individual plants, ramp incidents did not make the largest contribution to the overall fuel failures (Figs 10 and 11).

In HWRs only the CANDU-type reactors have been affected by PCI, with up to 0.9% of fuel bundles failing before 1972 [6]. The main cause was power ramps resulting from the specific fuelling procedure used at that time which involved bundle movements from low to high flux positions. A change in the fuelling method was successful in preventing further failures.

### 3.2.3. *Clad collapsing*

The effect of clad flattening or clad collapsing after fuel densification has been limited to five Westinghouse plants, but in terms of rod failure rates had the largest effect on PWR fuel in the early seventies. The effect on activity release, however, has been less significant because of the small percentage of perforated rods. Since this phenomenon is extensively covered in the literature and has been completely eliminated, the reader is referred to section 4 for further discussion.

several assemblies in three PWRs, induced by cross-flow through the baffle plate [1,17]. Most of these incidents occurred in the first or second operating cycle. Repair of the system components and removal of the particles during the maintenance outage solved the problems.

More severe – though without rod perforation – has been the 'channel wear' problem mainly in three BWRs by flow-induced vibration of temporary poison curtains and (to a minor extent) in-core monitors [17]. The channel wall was worn through in many of the fuel assemblies of these three plants and channels had to be replaced. Temporary power restrictions and extended channel surveillance were other consequences of this incident.

Compared with externally induced fretting, the number of fretting failures from deficiencies in the fuel itself has been very low. In Europe two incidences have been reported during the last few years. One PWR plant had failures in the first operating cycle from flow-induced vibration of fuel assemblies because the hold-down springs were too weak and had to be reinforced. Another plant experienced fretting by vibration of fuel rods against spacer grids in a few repaired fuel assemblies, where the spacer springs had been distorted by improper repair tooling. In as-manufactured fuel the fretting of rods against spacers seems to be very infrequent, and generally the failure rate is below 0.01% of rods.

As can be seen from Figs 7–9, a fretting incident typically produces a failure rate of the order 0.1% of the fuel rods in the plants affected. For the overall fuel performance, however, these effects are generally not very significant.

### 3.3. The present significance of fuel failure

Figures 10 and 11 show the average failure levels of PWRs and BWRs versus time, with the average being taken over all plants in operation at that time and on which failure information is available. They indicate the relative significance of different failure mechanisms and the continuously decreasing overall failure rates. The slower decrease for BWR fuel is exclusively due to the old fuel batches still in service. An important factor is that an increasing number of plants and fuel batches complete operating cycles with near zero failures (< 0.01%).

Despite this, we find the astonishing result that the data blocks of "unsystematic failures with unknown cause" show a continuously large scattering band in PWRs and in BWRs (Figs 8,9). Certainly, most of these failures would be attributed to known causes if post-irradiation examination were performed.

By extrapolating the failure levels in Figs 7–11 to 1977, the present significance of fuel failures in the western countries can be summarized as follows. On an overall view, the operation of water reactors is not much affected by fuel failure. Disregarding the delayed effects of old BWR fuel, the worldwide average rod failure rate in LWRs should now be near or below 0.02% per operating cycle.

Outstandingly good results are also reported from high-rated HWR plants with $< 0.03\%$ bundle failures in CANDU reactors and with $\lesssim 0.01\%$ rod failures in PHWRs delivered by KWU.

These figures mark a great success for the nuclear industry, as they are one to two orders of magnitude lower than several years ago. However, the success has not been a hundred per cent. About one half of the recent LWR fuel failures has been concentrated in very few plants, where abnormal incidents produced typically 0.1 to 0.3% failures. In such a case the effects on plant operation and maintenance are no longer negligible, in particular, when the leakage of the primary coolant system is high. Although it might be difficult to eliminate these incidents completely, major efforts should be made – and actually are being made – to avoid them in future.

Again disregarding the old BWR fuel, there is now surprisingly little difference between PWR and BWR fuel performance. In general, there is also no significant difference between the band width of failure rates of different plant or fuel manufacturers as long as similar fuel types are compared. It is a promising outlook that a few more recent fuel types perform substantially better than the average, although in all these cases the high burnup experience is not yet sufficient to prove that near zero failure rates will be maintained over the whole lifetime.

One lesson learned from the PCI histories has been that the plant operation modes have to be submitted to certain rules with regard to the PCI phenomenon. Today all fuel vendors provide fuel management schemes, operating guidelines and/or control rod manoeuvring strategies which at least implicitly aim at minimizing local power ramps in the fuel. The experience in the past has been that losses in availability of 0–2% (1% average) in PWRs and of 2–8% (3.5% average) in BWRs were the consequence [11].

With present knowledge and present fuel types there is no doubt that thorough optimization of operating modes to minimize PCI effects is necessary for all plants. However, it seems that in most cases this could be done without significant losses in availability for two reasons:

(i) Very often the criteria for minimizing ramps are similar to the criteria already applied to optimize plant flexibility (e.g. axial off-set control in PWRs).

(ii) Some existing recommendations seem to be overconservative and can be relaxed with increasing experience, as can be seen by comparing the BOC startup rates recommended by different manufacturers. GE and ASEA [19] recommend 0.06 kW/ft · h ($< 0.5\%$/h), KWU 1–5%/h for BWRs. For PWRs typical recommendations are 3–5%/h [9,15,20]. This broad range of recommended values shows that there should be margins for further optimization, in particular for lower-rated fuel.

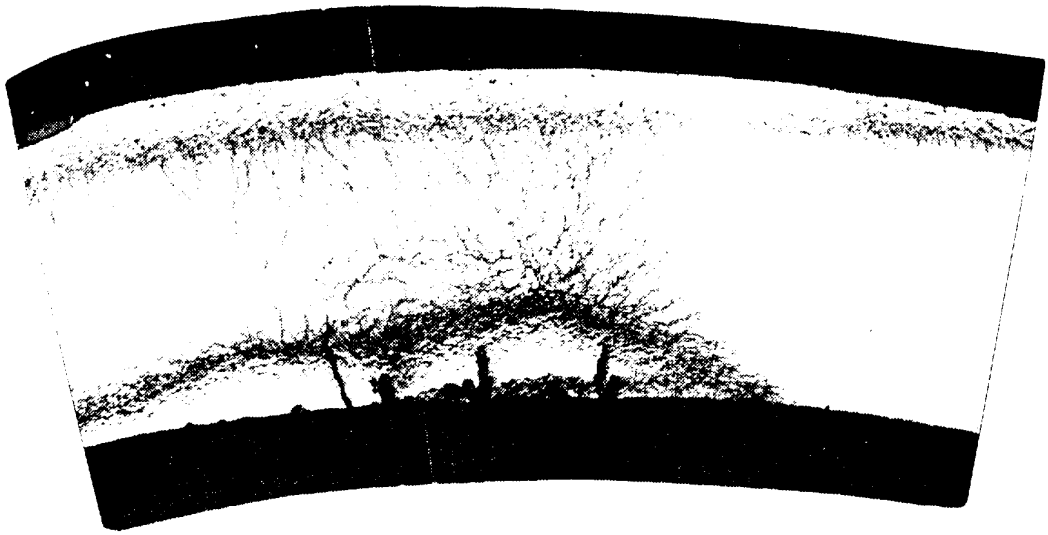

*FIG.12. Metallographic cross-section at a sunburst.*

Therefore, the authors believe in the general trend that future fuel operating guidelines must not be more restrictive than existing restrictions from other system components or other design limits.

## 4. CAUSES AND MECHANISMS OF FUEL FAILURE

### 4.1. Primary hydriding

Hydrogenous impurities in a fuel rod will ultimately hydride the Zircaloy cladding regardless of their initial chemical state. As long as the hydrogen pickup is uniform, no significant consequences arise. However, if the hydrogen pickup is locally enhanced, high concentrations of hydride, 'sunbursts', tend to form at these points (e.g. Ref.[21]). Figure 12 shows an example of localized hydriding, characterized by heavy zirconium hydride precipitation. The cracks in Fig.12 result from the associated increase in volume. Massive localized hydriding leads (1) to hydride blisters (Fig.13(a)), where the volume change is visually evident on the outside of the fuel rod, (2) to deterioration of the mechanical properties of the clad so that splits (Fig.13(b)) can easily develop, and (3) eventually to perforation of the clad after local breakthrough (Fig.13(c)). This breakthrough of the hydride blisters is accelerated by thermodiffusion of the hydrogen, which results in gross migration of the hydrides from the hotter inner side to the cooler outer side of the wall [22]. The statistical distribution of the probability for local

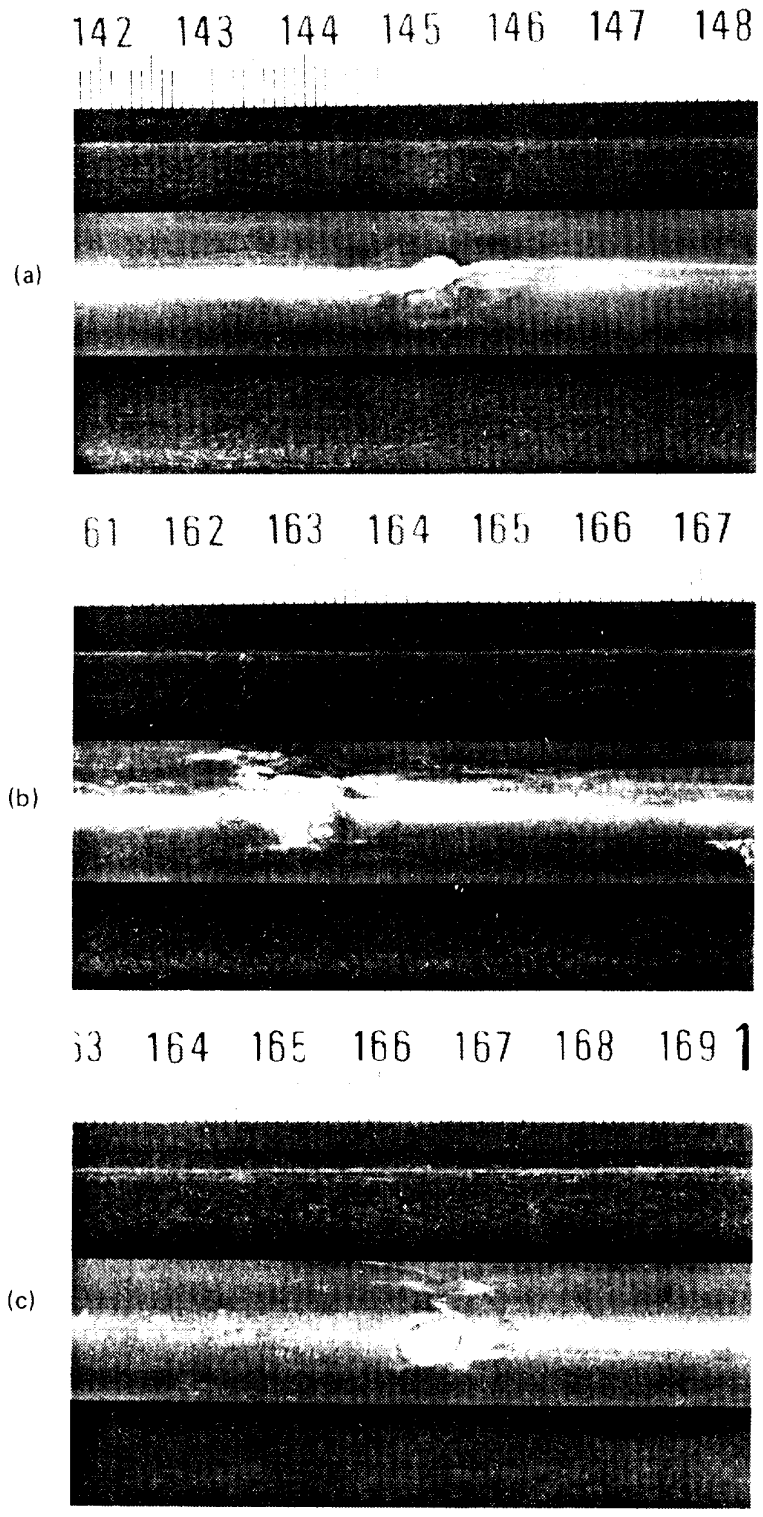


*FIG. 13. Typical hydride defects: (a) blister; (b) split; (c) perforation.*

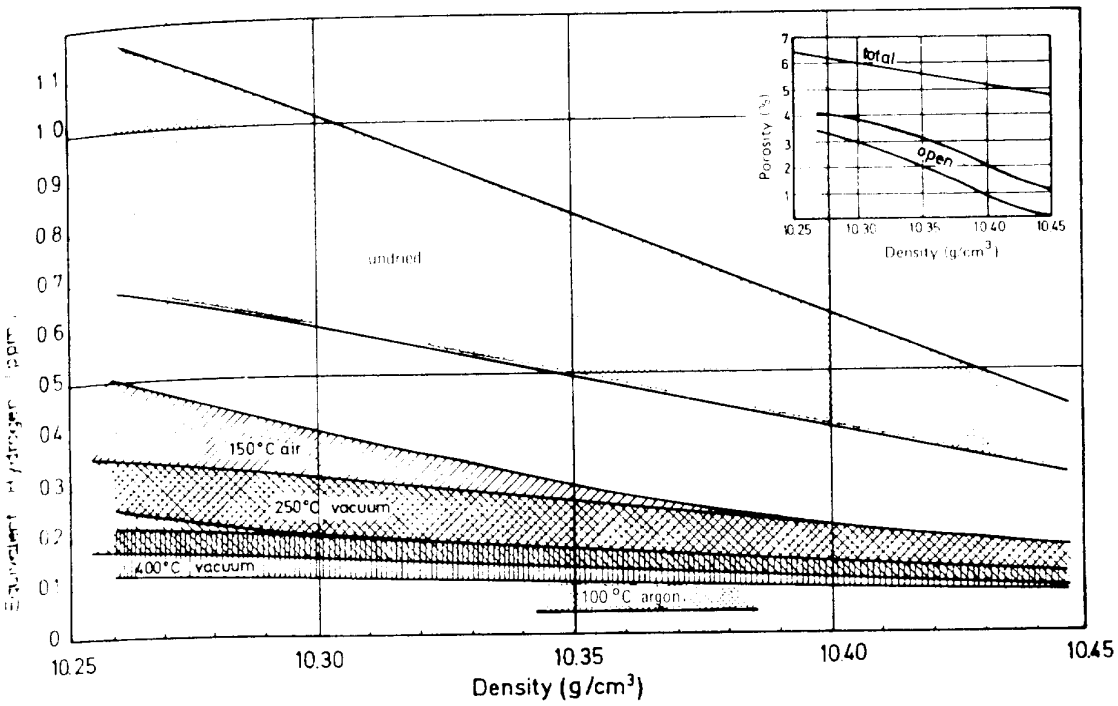


*FIG. 14. Influence of density and drying procedure on the hydrogen content of fuel pellets* [26].

hydriding along the length of the fuel rods is rather random [21]; only the welds and their heat-affected zones seem to have a higher susceptibility for local hydriding [23]. The same type of failure can develop due to secondary hydriding (see section 5).

### *4.1.1. Sources of hydrogen*

The main source of hydrogen in fuel rods is the residual moisture in the $UO_2$ fuel pellets. This moisture results from the manufacturing procedures, i.e. from the adsorption of water layers on the 'inner' surface of the $UO_2$ pellets and from water entering open pores during wet grinding. The final residual moisture in the loaded pellets depends on the drying and handling procedures, the open porosity, and the shape of the pores [24–27]. The open porosity is related to the bulk density after sintering, to the $UO_2$ powder properties, and to the type of additives (e.g. pore formers etc.).

Water can be adsorbed in pellets after sintering even by storing in air. The adsorption rate increases with increasing open porosity and relative humidity of the environment. The amount of water adsorbed in equilibrium with wet air decreases with increasing temperature. As shown by Assmann et al. [24], the

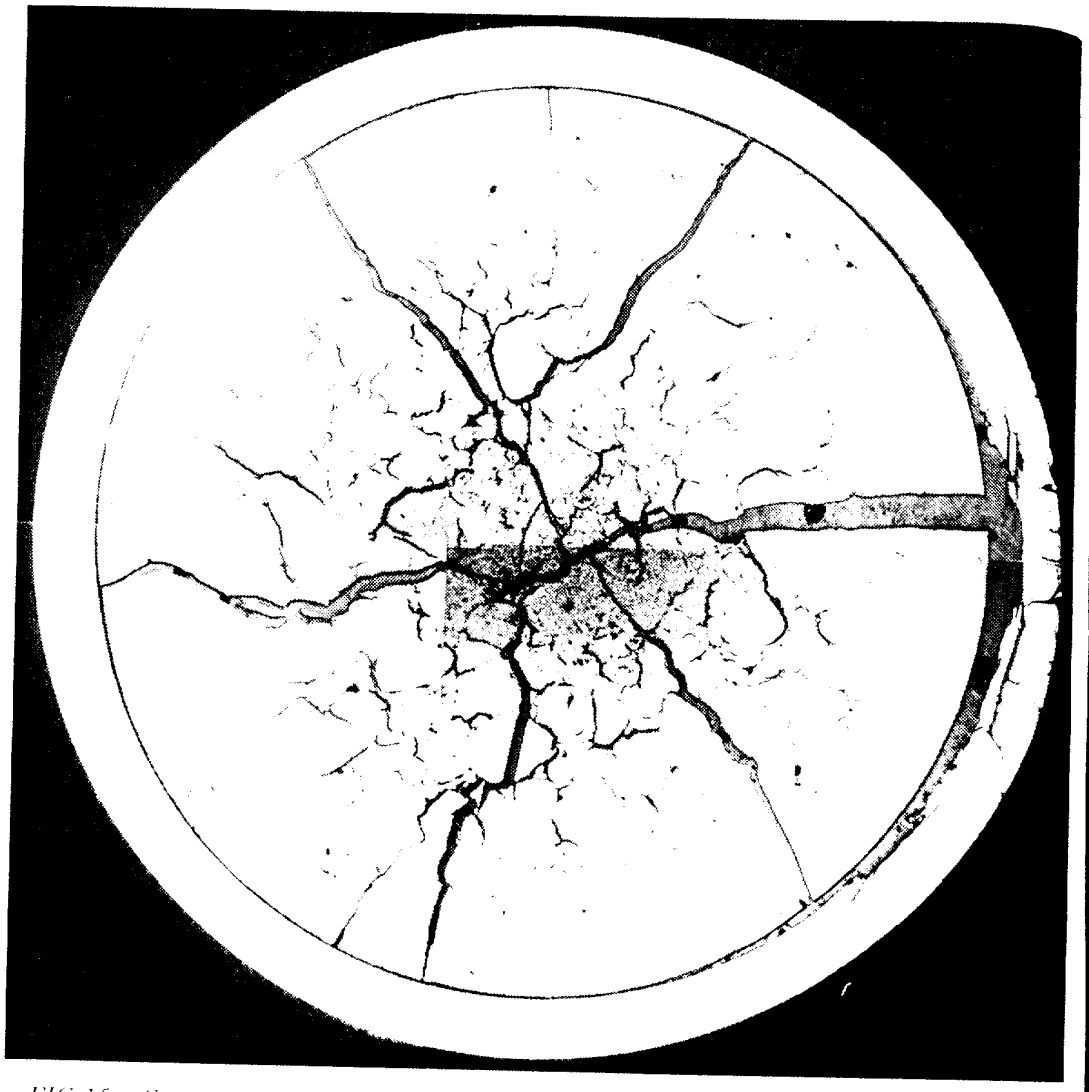

*FIG.15. Cross-section through a hydride defect located opposite a poorly sintered pellet.*

reversible adsorption of water as a function of relative humidity of the surrounding air can well be described by a Langmuir adsorption isotherm. As a rule of thumb, the moisture of pellets stored long time in 'normal' air is between 3 and 10 ppm (= 0.3 – 1.1 ppm total equivalent hydrogen content), if the density is $\geq 10.25$ g/cm$^3$ (Fig.14), and may reach values of $> 20$ ppm at densities $< 10.2$ g/cm$^3$ [24 27].

Desorption of water by drying is very effective. As can be seen from Fig.14, 60% of the moisture is already desorbed by drying at 150°C. However, the effectiveness of the drying step also depends on the production steps between drying and loading of the pellets into the cladding tubes. Water penetration during grinding can lead to moisture contents of 100 ppm in poorly sintered pellets with long pores (e.g. around the original granules). Such pellets are 'hard to dry' and can cause hydride failures, as shown in Fig.15.

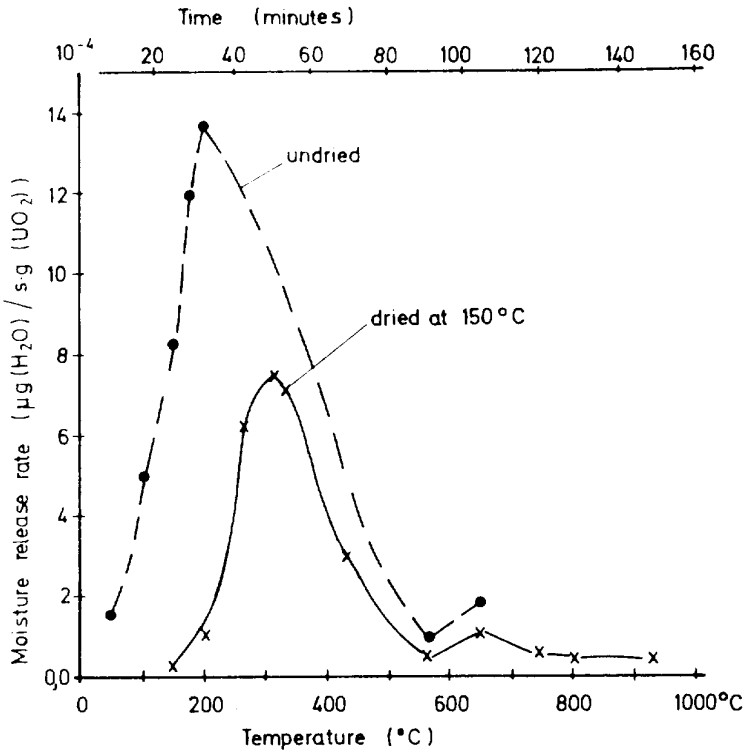


*FIG. 16. Moisture release rate of fuel pellets (10.35 g/cm³) as a function of temperature measured in out-of-reactor extraction tests.*

Contamination with organic materials may also be a source of hydrogen because hydrocarbons release hydrogen by radiolysis [28]. Therefore, droplets of oil, grease, contamination from organic gaskets etc. must be carefully excluded from the fuel rod interior.

Another source of hydrogen is the small amount of hydrogen atoms in solid solution or in closed pores. It is common practice today to check the total 'equivalent' hydrogen content of pellets by a high-temperature extraction method. This is of special importance for $UO_2/PuO_2$-pellets, where part of the moisture may be converted into hydrogen by $\alpha$-radiation decomposition during storage.

### 4.1.2. *Hydrogen pickup*

During start of operation the moisture in the fuel pellets is released very rapidly. Figure 16 shows the release rate as a function of temperature according to out-of-reactor extraction tests. It can be concluded that about 50% is released at temperatures up to 400°C and nearly 100% at 1000°C. This moisture will partly dissociate to oxygen and hydrogen by radiolysis and oxidize the cladding

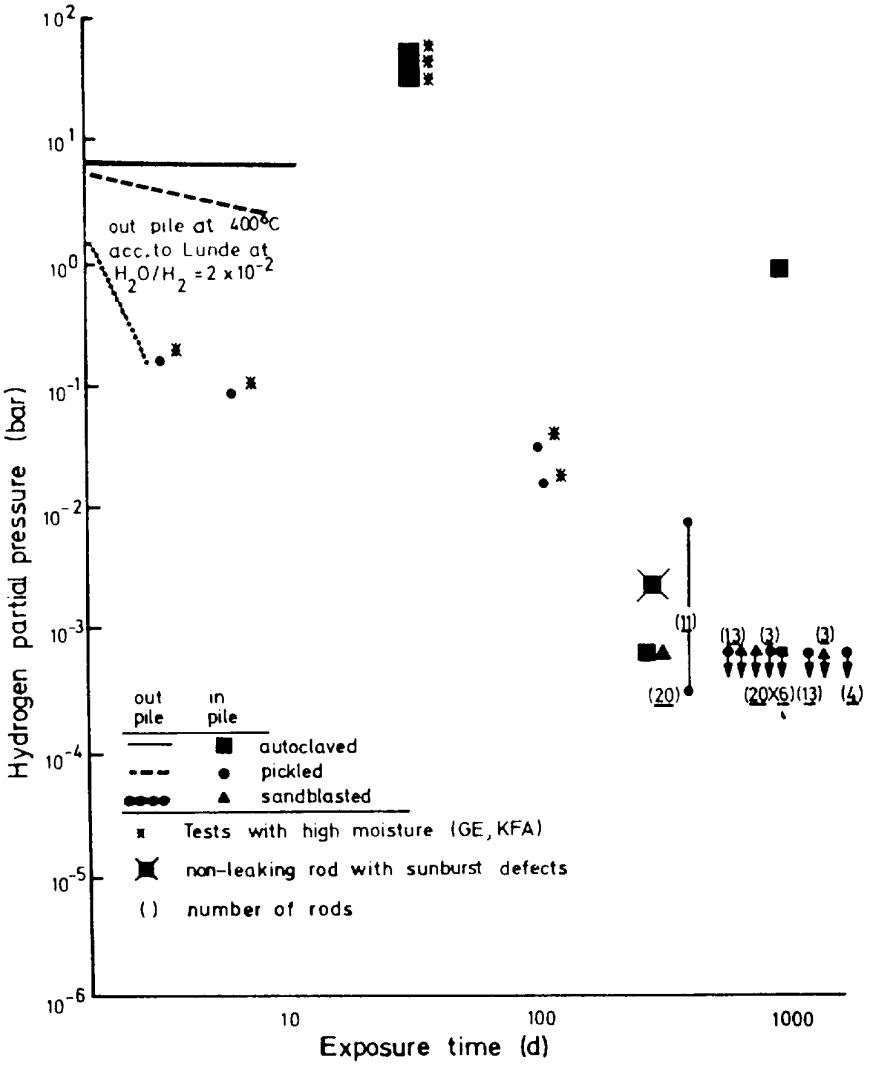


*FIG. 17. Hydrogen content measured in irradiated fuel rods compared with the out-of-reactor observed decreases in $H_2$ pressure in samples with various surface treatments as a function of the exposure time ([7, 29], KWU results and private communication).*

and the pellet surface. As a result, a substantial hydrogen partial pressure can be built up in the rod; at the same time the oxygen chemical potential decreases by oxygen starvation. The hydrogen is trapped by the cladding, but the rate of trapping depends on the temperature, the surface condition of the cladding and the oxygen partial pressure in the fuel rod [29–31].

Figure 17 shows the decrease of hydrogen pressure due to uniform pickup of samples with different surface treatments together with PIE measurements of the hydrogen content in the plena of the fuel rods. It can be seen from out-of-reactor tests that the uniform hydrogen pickup is slow in cladding with a pre-oxidized surface ('autoclaved') and fast in cladding with a sandblasted surface.

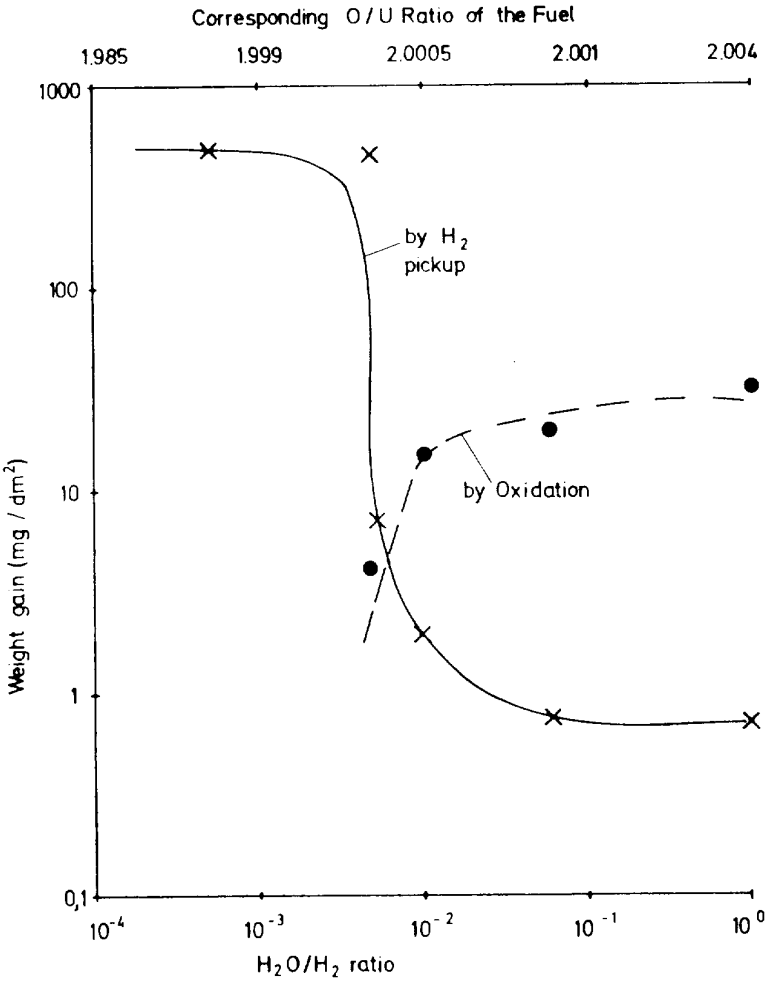


*FIG. 18. Influence of the $H_2O/H_2$ ratio on oxidation and hydriding of Zircaloy in 10 mbar $H_2O$-$H_2$ mixtures at 400°C after 8 hours* [31].

This tendency is also obtained from measurements on irradiated fuel rods, although the initial hydrogen pressure is unknown. As can be seen from Fig.17, high hydrogen partial pressure was measured after 50 and 900 days of reactor exposure in one experimental and in one production fuel rod with autoclaved cladding. Experimental rods with pickled cladding also showed measurable hydrogen contents after 2 to 100 days of exposure. For all other fuel rods, especially those with sandblasted surfaces, the hydrogen was below the detection limit. As indicated in Fig.17, there is one rod that revealed non-penetrating sunbursts during post-irradiation examination and had a relatively low hydrogen content in the plenum after irradiation, suggesting that most of the hydrogen must have entered the cladding locally at the sunbursts.

The large influence of the oxygen chemical potential on the hydrogen pickup rate is clearly seen in Fig.18. At $H_2O/H_2$ ratios between $10^{-3}$ and $10^{-2}$ the pickup rate changes by about 3 orders of magnitude. To understand the reason for this drastic change, the effect of the composition of the gas atmosphere on the electrical properties of $ZrO_2$ corrosion films was measured [31]. The results revealed a large decrease in the electric resistance when the atmosphere changed from oxidizing to non-oxidizing, indicating a drastic change of the morphology (passivity) of the oxide film. The critical $H_2O/H_2$ ratio where the pickup rate changes drastically is still uncertain. According to Ref.[32], this critical $H_2O/H_2$ ratio is $10^{-3}$, whereas in Ref.[33] it is reported that $H_2O/H_2$ ratios in excess of $10^{-5}$ are sufficient to maintain a protective film at 343°C. Zima [34] postulated that the protective ratio of water to hydrogen is a function of the hydrogen partial pressure. Reviewing the available data, he proposed the equation $\log(p_{H_2}/p_{H_2O}) = 6(p_{H_2})^{2/3}$ for the limiting conditions where protection may be lost. In any case, the obvious implication of all available results is that massive hydriding can start when the availability of oxygen to continuously repair the protective oxide film falls below a critical value. Since the depassivation of the surface becomes inhomogeneous under conditions close to this critical value, locally enhanced hydrogen pickup will occur frequently under adverse conditions.

The water to hydrogen ratio in a fuel rod under operation will be buffered for some time by fuel with an initial oxygen to uranium ratio of typically 2.00–2.01 (compare Fig.12). However, during continued operation the cladding is effective in capturing the excess oxygen by forming an oxide layer on the cladding inner surface. According to the measurements in Ref.[35], the $H_2O/H_2$ ratio in fuel rods with 10 GW · d/t(U) exposure is between $10^{-3}$ and $10^{-4}$. As can be derived from Fig.18, enhanced hydrogen pickup and sunburst formation could be possible under this condition if the oxide loses passivity locally or is removed locally, e.g. by mechanical interaction with the fuel.

Another often discussed reason for locally enhanced hydrogen pickup is that the protective qualities of the oxide film may be destroyed by some chemical catalysts, even in the presence of excess oxygen. This may lead to hydride defects early in life. Out-of-reactor tests showed that the halogenides (fluorine, chlorine and iodine) and caesium hydroxide can act as catalysts for massive local hydriding [21,23,29]. The reason for the loss of passivity due to the above species is probably a reaction with the oxygen layer and the formation of oxyhalogen complexes or caesium zirconate. Only two of these catalysts, fluorine and chlorine, may be present as impurities, whereas iodine and caesium are fission products which can be released to the inner surface of the cladding after some burnup at high power levels. Fluorine impurities have often been discussed as an important catalyst because of the possibility of local residues after pickling. Therefore, several vendors use sandblasted claddings and avoid internal pickling after the final annealing treatment.

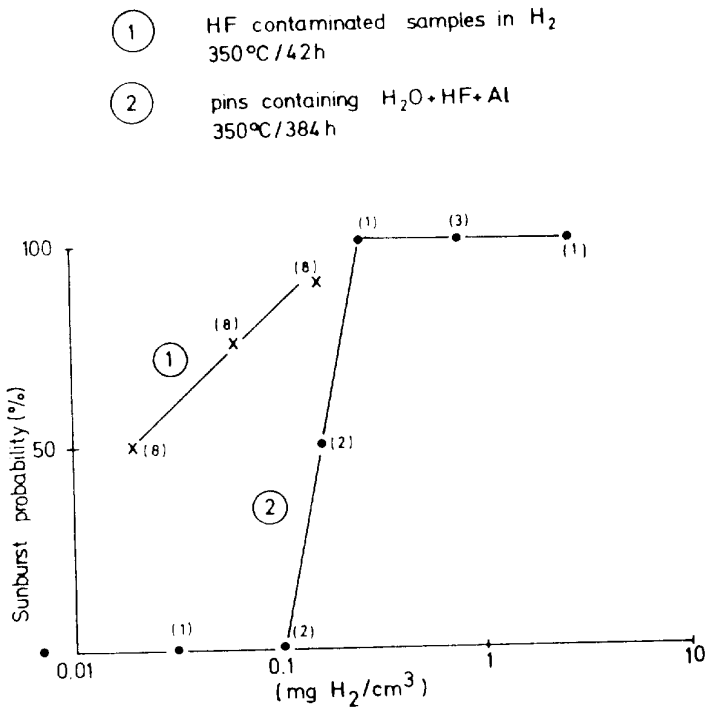


*FIG.19. Influence of the total hydrogen concentration on the out-of-reactor probabilities of sunburst formation in hydrofluoric acid-contaminated Zircaloy samples at 350°C under wet hydrogen in a water environment.*

### *4.1.3. Critical concentration of hydrogen*

The critical concentration of hydrogen in a fuel rod for local hydriding is not a simple number but depends on the source of hydrogen (e.g. moisture or hydrocarbons), the general absorption rate and the time to local depassivation.

Figure 19 compares measurements on the failure probability of HF-contaminated tube samples filled with wet hydrogen with the failure probability of tube samples filled with water, HF and aluminium chips. As can be seen from these data, the critical amount of hydrogen is about one order of magnitude lower in the experiments with wet hydrogen than in the experiments with water. This means that some of the hydrogen enters the clad uniformly when the surface is still passive, and that moisture prolongs or improves the passivity of the surface. It may also indicate that the critical amount of hydrogen is lower if organics are the main source instead of residual moisture.

Because of the large difference in the general absorption characteristics between surfaces with different surface treatments (see Fig.17), the amount of initial hydrogen that leads to a critical concentration in the moment of local

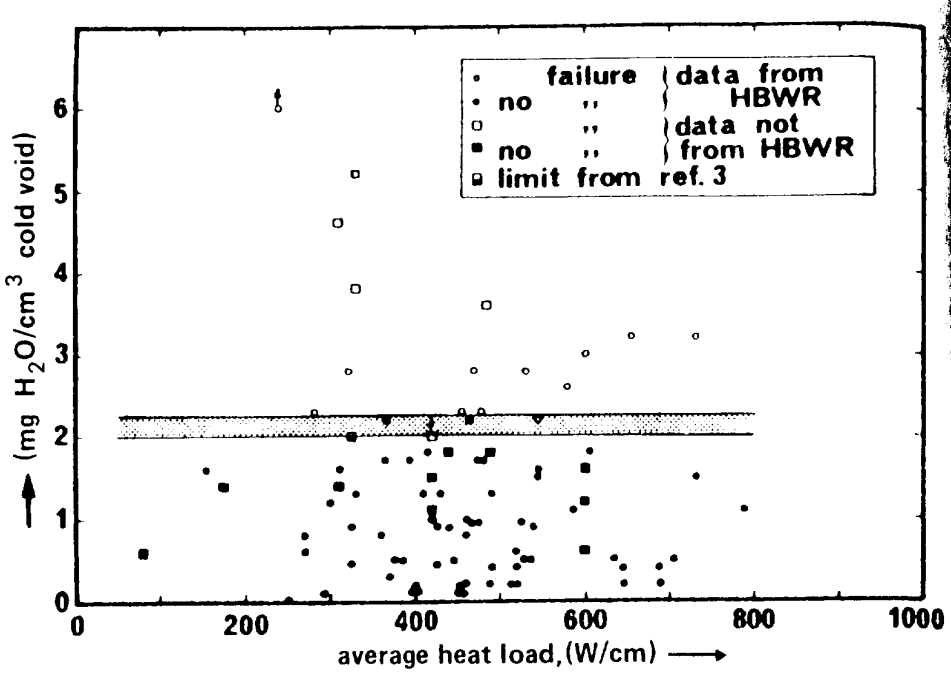


*FIG.20. Primary hydride defects in relation to initial gas phase moisture equivalent and linear heat generation rate* [36].

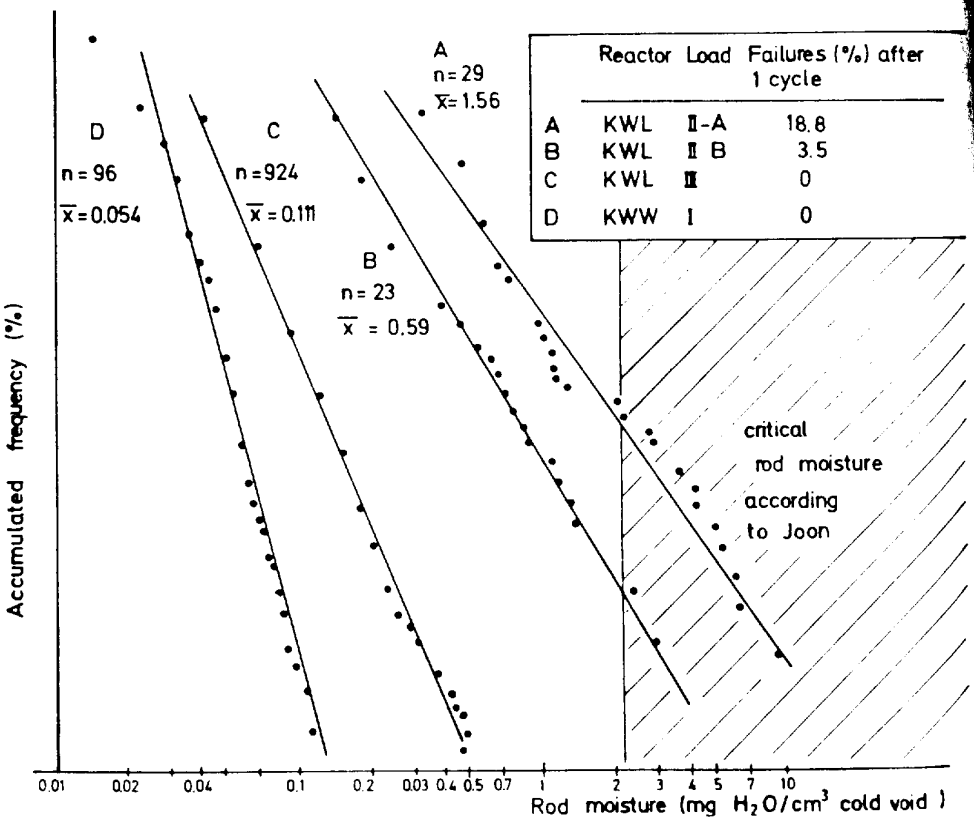


*FIG.21. Distribution of rod moisture and fraction of hydride defects in different BWR fuel batches.*

depassivation should be different in fuel rods with different inner surface treatment of the cladding. In general, the critical hydrogen concentration should be highest in sandblasted and lowest in autoclaved rods, because of their inability to trap hydrogen.

The time when local depassivation occurs may also be important. Contamination with pickling residues, for instance, may cause an early depassivation leading to low critical initial hydrogen concentrations, especially if organics are the main source of hydrogen. Therefore, contamination with organics is generally prohibited in fabrication routines.

As far as the moisture in the fuel is concerned, all specifications known to the authors limit either the pellet equivalent moisture content to 10 ppm or the total water inventory in the fuel rod to 2 mg $H_2O$ per $cm^3$ of free cold volume (e.g. Ref. [22]). These limits, especially the latter, are primarily based on Joon's analyses [36]. Joon reviewed reported moisture values and in-pile hydride failures from HBWR and other sources, and tried to correlate failure limits to various parameters such as mg $H_2O$, mg $H_2O/dm^2$ cladding internal surface, mg $H_2O/cm^3$ hot void, and mg $H_2O/cm^3$ cold void. His analyses showed that the parameter mg $H_2O/cm^3$ cold void provided the best approximation to a failure threshold, and that failures were only observed above 2 mg $H_2O/cm^3$ cold void (Fig.20). This result is in agreement with the correlation between the rod moisture and the number of hydride failures in different BWR fuel batches (Fig.21). It can be seen that for the KWL reload about 40% of the rods of batch A and 8% of the rods of batch B had a moisture content above the Joon criterion, whereas the moisture content of all rods of the KWW first core and especially of the KWL second reload were below the Joon criterion. The rod failure rates of these fuel batches after one cycle of operation were proportional to the percentage of rods exceeding the Joon criterion. It should be noted that the agreement can only be found for the ratio of the failure rates but not for the absolute values. Joon's analysis and the data in Fig.21 do not include all the potential sources of hydrogen and are based on moisture results obtained by old measuring methods at low temperatures. Therefore, as compared with modern measurement methods for moisture, these data underestimate the total amount of hydrogen.

## 4.2. External corrosion

The water chemistry in the primary coolant system and the main sources of corrosion products in the reactor coolant are different in pressurized and in boiling water reactor systems.

In PWRs, where the water chemistry of the primary circuit can easily be treated, boric acid additions (500–2500 ppm) are generally used to control

reactivity, lithium additions (0.2–2.2 ppm) to fix the pH value of the water, and hydrogen (2–4 ppm) to suppress radiolytic oxygen formation. The corrosion products released to the circuit are mainly from the steam generators (made either from Inconel or from Incoloy).

In BWRs the water is purified by demineralizers and degassed in the condensers. Since oxygen is formed by radiolysis, the water chemistry is different inside and outside the core. The feedwater line (carbon steel, stainless steel, or Cu-Ni alloys in early plants) is the main source of corrosion products.

### 4.2.1. *Stress corrosion of stainless steel cladding*

In a few first-generation LWRs austenitic stainless steel was used as cladding material. The experience with this cladding was excellent in PWRs. However, intergranular stress corrosion failures were observed under the oxygenated coolant conditions of BWRs [37]. The defects occurred at burnups beyond 3–6 GW·d/t, particularly in fuel rods with thin wall cladding. It was proposed [38] that the reason for this type of corrosion is an increased concentration of certain impurities at the grain boundaries, thereby reducing the corrosion resistance. Silicon phosphorus and sulphur were identified from simulation tests to be the active impurities [38]. Later [39] it was shown that vacuum-melted lots provide better resistance to this type of corrosion and that the susceptibility varies from ingot to ingot.

### 4.2.2. *Corrosion of Zircaloy cladding*

The corrosion problem observed with stainless steel cladding in BWRs and the intention to improve the neutron economy led to an early change from stainless steel to Zircaloy cladding material for all light water reactor systems.

Zircaloy has excellent corrosion resistance at normal LWR operating temperatures. However, at higher temperatures its corrosion rate increases markedly. Therefore, overheating of the Zircaloy cladding can cause corrosion failures. Such overheating may arise from a heat flow blockage through excessive crud deposits or abnormal corrosion layers as well as from a drastic reduction of the coolant flow. Attempts to develop a zirconium-base alloy for application in water or steam at higher temperatures have been unsuccessful.

Coolant flow reduction has never been a cause of fuel failures in power reactors. However, in some early BWRs marked increases of the pressure drop along the bundles have led to unscheduled shutdowns or to interim operation limitations. In all cases the increased pressure drop was caused by heavy deposits of copper-rich crud (60% Cu, 30% Fe, 20% Ni) at the fuel element inlet nozzles. The deposits could be removed mechanically (by brushing). The sources of these

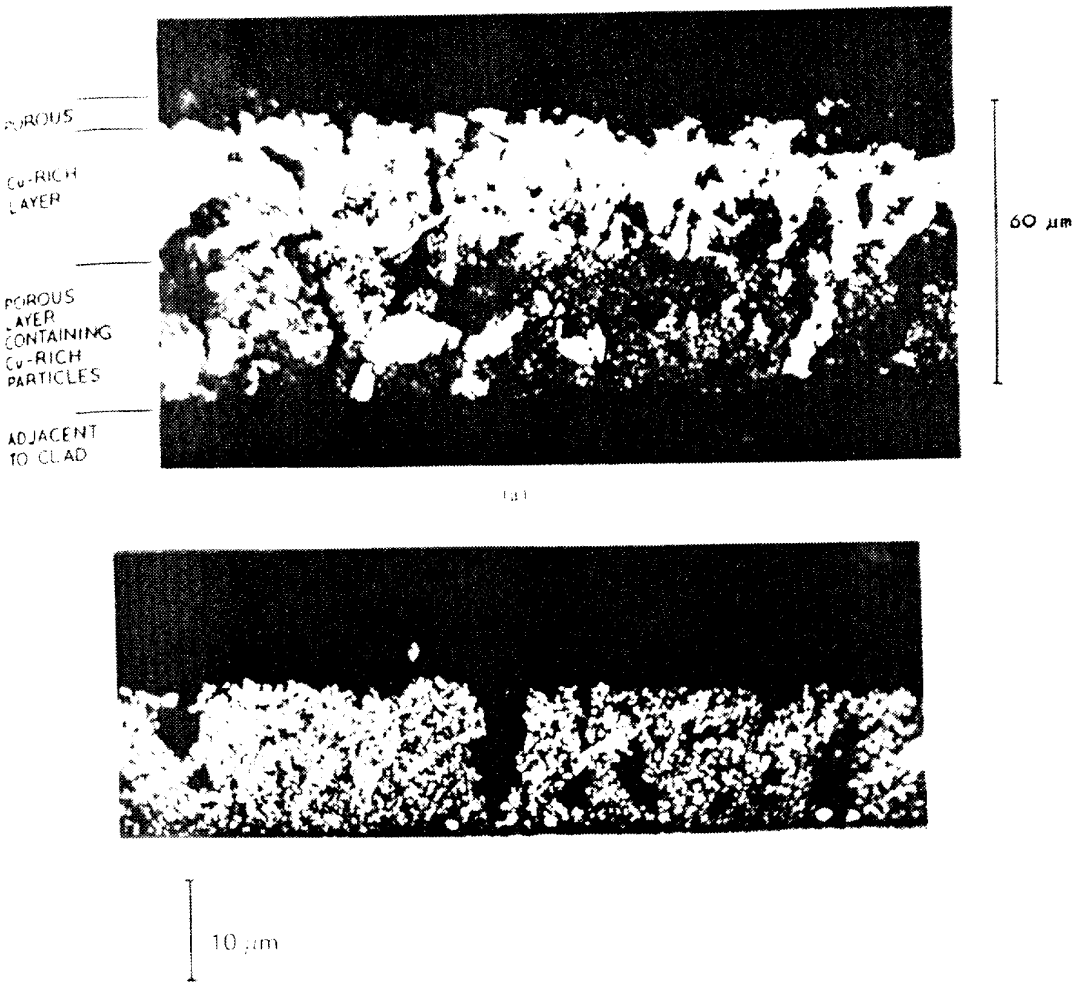


*FIG.22. Types of crud layer on fuel rods* [41]: *(a) dense crud; (b) porous crud.*

corrosion products were the Cu-Ni-alloy feedwater heaters. They were taken out of service and finally replaced with stainless steel units. As an intermediate measure, the oxygen concentration in the feedwater line was controlled in order to minimize the copper pickup [17].

Crud on fuel rod surfaces has been a source of failures in a few plants and in experimental high power test rods. The crud deposition rate depends on the water chemistry, the structural materials of the circuit, and the heat flux of the rods. The radiation field also has some influence. It has frequently been reported that crud deposition showed a sharp boundary at the lower end of the core (see, e.g., Ref.[40]). In principle, two different types of crud can be observed, i.e. porous crud and dense crud (Fig.22). According to Ref.[42], porous crud is rich in iron and forms

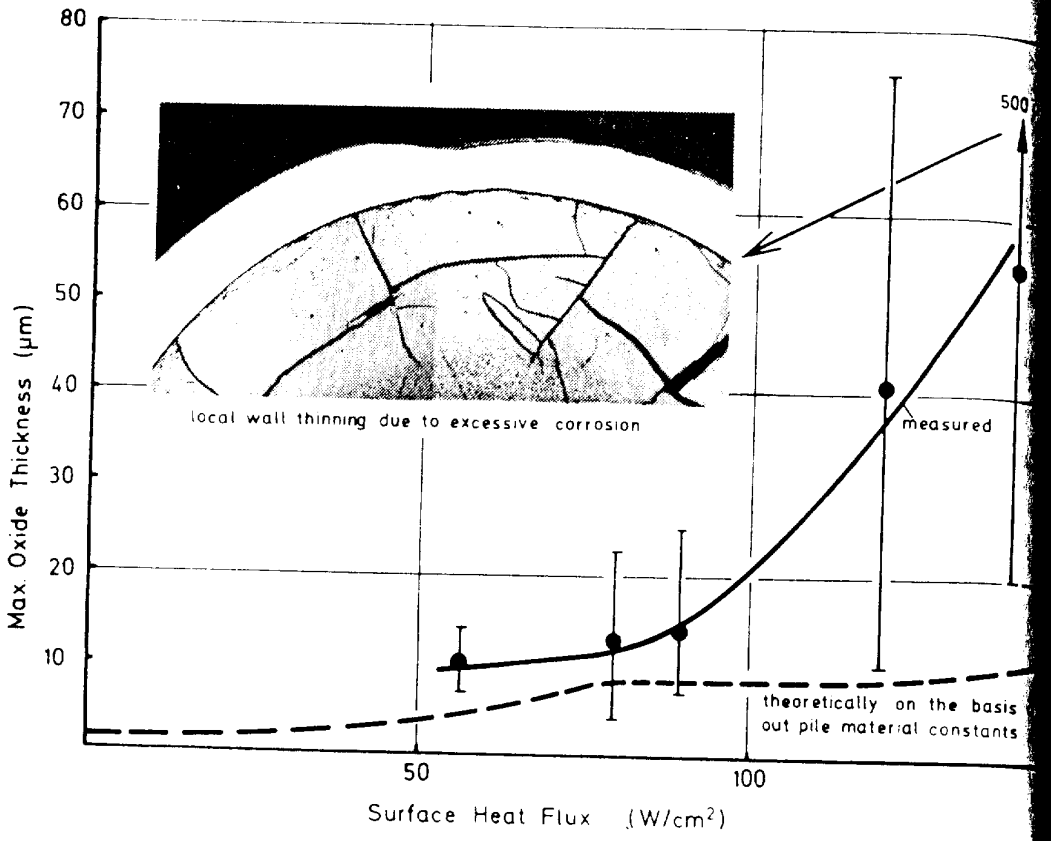


*FIG.23. Accelerated corrosion observed on experimental high power fuel rods in KWO aft two cycles of operation.*

first. Dense crud is attributed to the drying-out of the porous iron-rich crud leading to further deposition of copper, silicon etc. The thermal conductivity of the crud layer formed on the fuel rods of SGHWR during the first period of operation was found to be 0.02 W/cm · K [42].

According to Ref.[42], porous crud contains numerous boiling channels, 2–4 μm wide (Fig.22(b)), which permit an internal circulation of water and ste and impede the rise in temperature. This process has been referred to as "wick boiling". Dense crud is more dangerous because it can lift and form gaps filled with stagnant steam. This can cause a drastic increase in temperature, since stag steam has an extremely low thermal conductivity ($7 \times 10^{-4}$ W/cm · K).

Crud deposition can be minimized in PWRs by the addition of 1–2 ppm of lithium [43], in BWRs by using stainless steel tubes for the feedwater pre-heater, effective demineralization, and optimization of the oxygen content in the feedwater.

As the corrosion rate of Zircaloy is controlled by the temperature at the metal/oxide interface, the growing oxide layer itself leads to an acceleration of

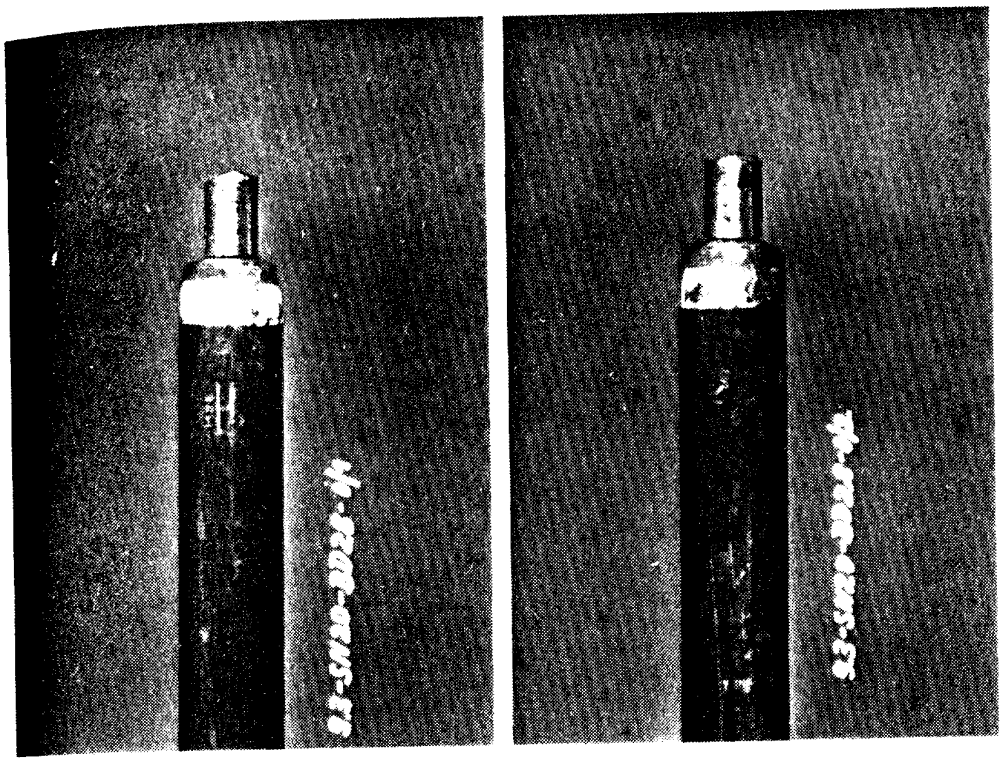

*FIG.24. Faulty end-plug weld from MZFR first core (1969) after 3900 MW·d/t (U) burnup [44]*

the corrosion rate of operating fuel rods as a consequence of the temperature increase with increasing oxide thickness. As shown by analytical treatment in Ref.[44], the acceleration depends on the heat flux, the thermal conductivity of the oxide layer, the basic corrosion rate and the activation energy. The thermal conductivity of the oxide layer is probably influenced by the macro and microstructure.

In the absence of crud this effect can lead to excessive corrosion at high rod powers after prolonged exposure. Indications of an unexpected accelerated corrosion were seen on experimental high power rods (Fig.23) irradiated in the PWR Obrigheim. The figure points out that the acceleration was much more pronounced than one would expect from a calculation taking into account out-of-pile estimated corrosion behaviour and a thermal conductivity of 0.016 W/cm · K. The deviations from the calculated values are most pronounced at higher heat fluxes. However, measurements on standard fuel rods operated in the same cycle at lower heat fluxes showed also some deviation from the values calculated. Therefore, the corrosion rate itself may be enhanced. The factor of enhancement depends on the thermal conductivity of the oxide layer used for the calculation. Fitting of the data is possible with enhancement factors between 1.7 to 2.5. Additional

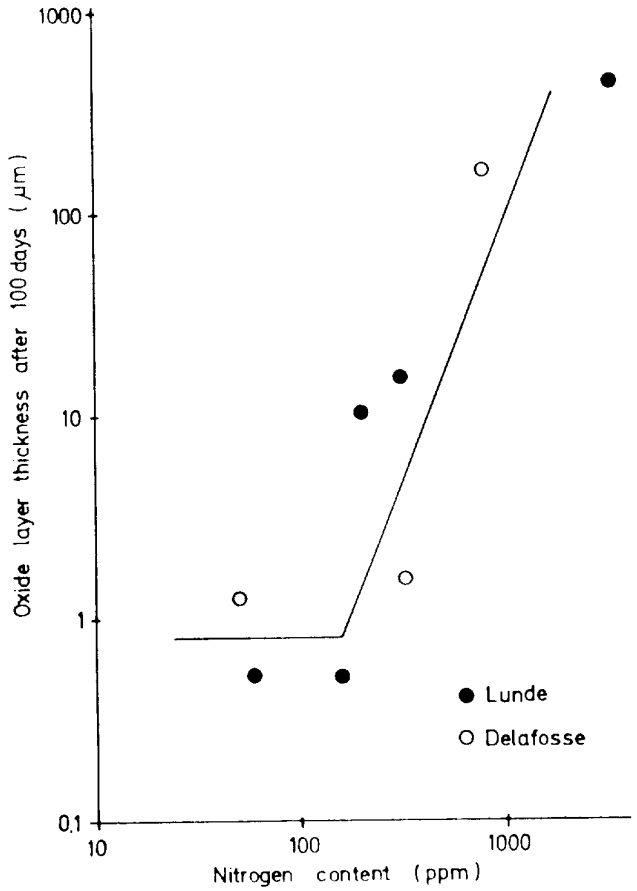


*FIG.25. Influence of nitrogen on the corrosion behaviour of Zircaloy at 300–310°C* [41, 47].

measurements on fuel rods irradiated in different reactor cycles in Obrigheim or in other PWRs revealed that a significant enhancement is not symptomatic for PWRs, but can be found occasionally [45]. Since these deviations are limited to few operational cycles in the same reactor, it is suggested that the main reason for the deviations must be attributed to the water chemistry. Such deviation may become significant with raising target burnups, therefore their causes need further clarification.

Internal and external contamination or poor heat treatment of the Zircaloy may be other reasons for excessive corrosion. Contamination of the welds with nitrogen from the surrounding atmosphere was the reason for some early failures at the end-plug welds [41,44] (Fig.24). Nitrogen reduces the corrosion resistance, as can be seen from Fig.25. Analyses have shown that the nitrogen content across a contaminated weld is not uniform. The highest concentration is normally found in the surface layer. According to the measurements reported in Refs [41,44],

...0 ppm of additional nitrogen is found in the weld surface for each ppm ...itrogen in the shielding gas. For quality control purposes the inert gas should ...ontrolled for a nitrogen content less than 20 ppm [44].

Contamination with pickling residues (fluorides) has often been discussed ...s another reason for increased corrosion [47] and, consequently, autoclaving ...the outer surface was or is still used for quality control of cladding tubes with ...final pickling treatment, although no failure has ever been reported due to local ...pickling residues.

It is well known that a slow cooling-down from the $\beta$-range through the ...$(\alpha + \beta)$-range or from the $(\alpha + \beta)$-range increases the corrosion rate of Zircaloy [...]. Spalling of heavy oxide layers in some early BWR fuel channels were found ...to be caused by poor temperature control during annealing of the strips whereby ...temperature was locally in the $(\alpha + \beta)$-range [45].

Both under boiling water conditions and in oxygen-rich PWR environments ...localized corrosion phenomenon known as 'nodular corrosion' is frequently ...observed. Although the average oxide thickness becomes larger than in normal ...behaviour, no operational problems have been reported so far. The hydrogen ...pickup in the course of nodular corrosion is obviously less than under normal ...corrosion. Furthermore, the thermal conductivity of the nodular oxide seems ...to be higher than that of the normal uniform oxide film.

### ...2.3. *Hydrogen uptake*

...00 310°C [41, 47].

Part of the hydrogen formed by the aqueous corrosion of Zircaloy is absorbed ...by the metal. Because of the increasing solubility of hydrogen with increasing ...temperature (Fig.26) and because of the transition from brittle to ductile behaviour ...of the zirconium hydrides [49], there is no risk of embrittlement under normal ...operation at hydrogen concentrations below 1000 ppm. However, at the low ...temperatures typical for refuelling periods and storage the ductility can be markedly ...reduced by the hydrides, as shown in Fig.27 where fracture energy is plotted versus ...temperature.

The accumulated hydrogen concentration depends on the exposure time and ...the wall thickness of the Zircaloy components. Cracking due to hydrogen embrittlement was found in an experimental fuel assembly with twisted Zircaloy-2 tapes (0.2 mm) after three years of exposure in the German BWR in Kahl. The tapes were broken at many positions at the periphery. Post-irradiation investigations revealed significant embrittlement at room temperature due to a hydrogen concentration of 1500 ppm.

Early BWR channels made from Zircaloy-2 also suffered from embrittlement at low temperature after very long exposure times ($\gtrsim$ 10 years). Zircaloy-2 structural components (isothermal conditions) pick up more hydrogen than Zircaloy-2 cladding tubes, as shown in Fig.28. Therefore, it is understandable that components

n Obrigheim
ymptomatic for
s are limited to
e main reason
ch deviation may
uses need further

of the Zircaloy
the welds with
ne early failures
rosion resistance,
en content across
is normally found
Refs [41,44],

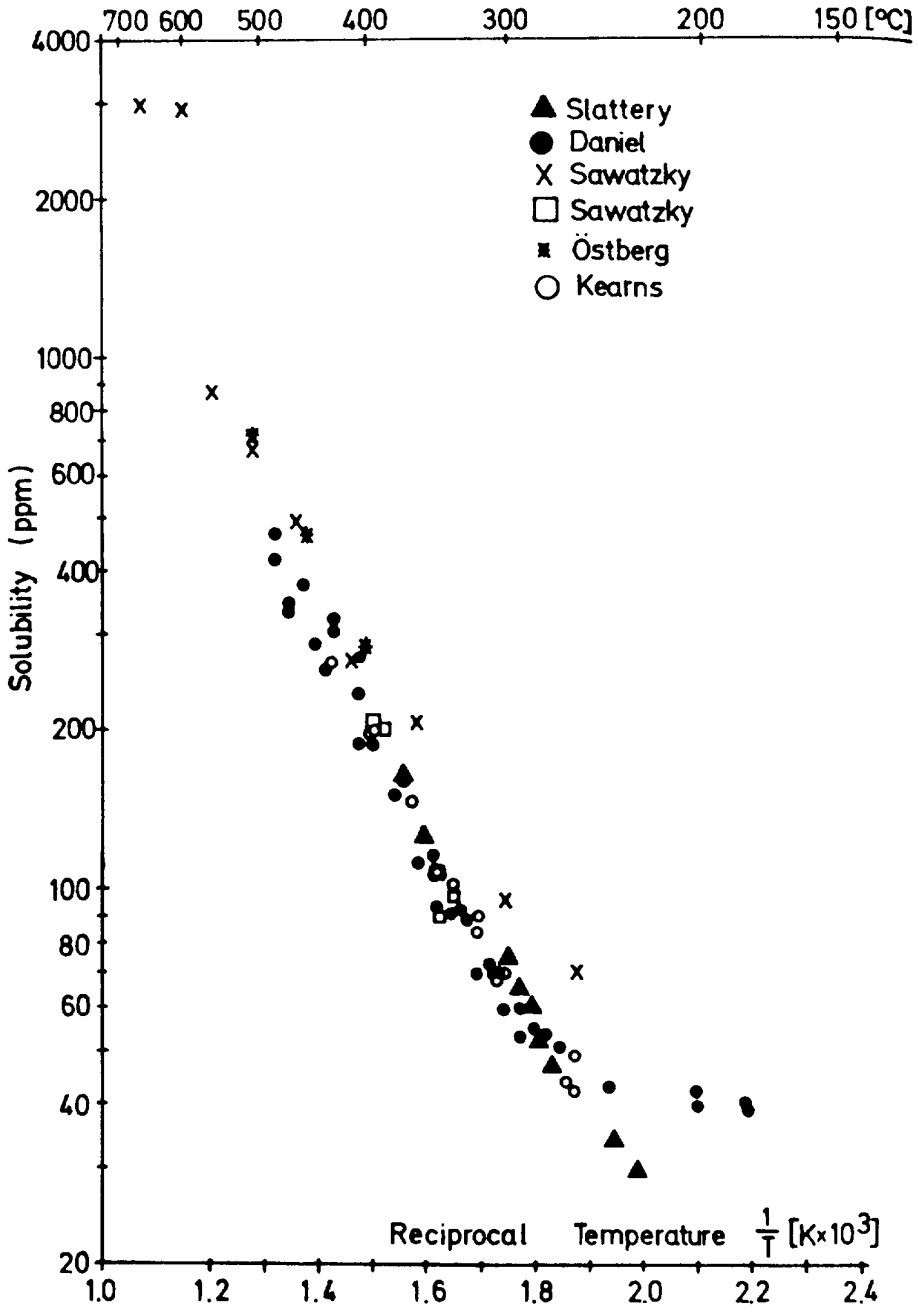


*FIG.26. Solubility of hydrogen in Zircaloy* [48].

150 [°C]

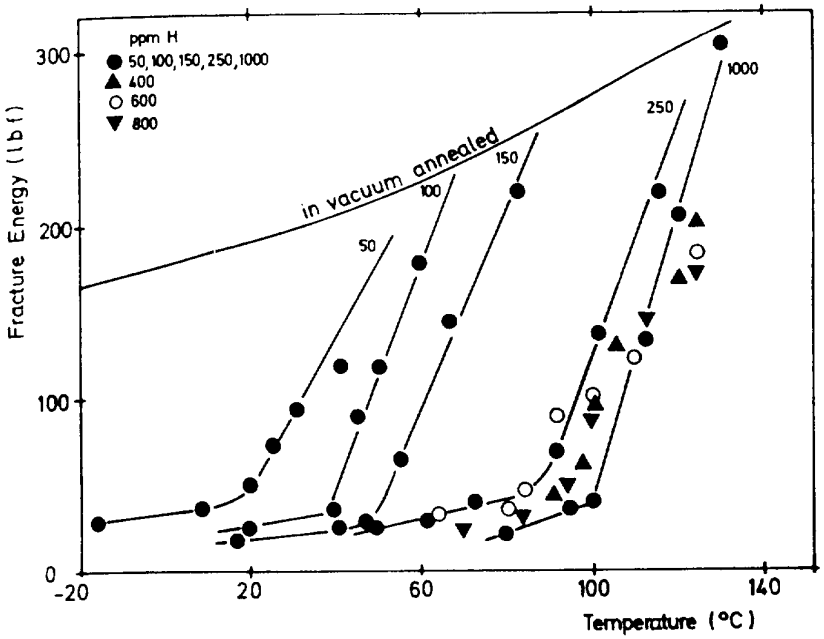


*FIG.27. Influence of hydrogen on the fracture energy transition temperature* [50].

[K×10³]

2.4

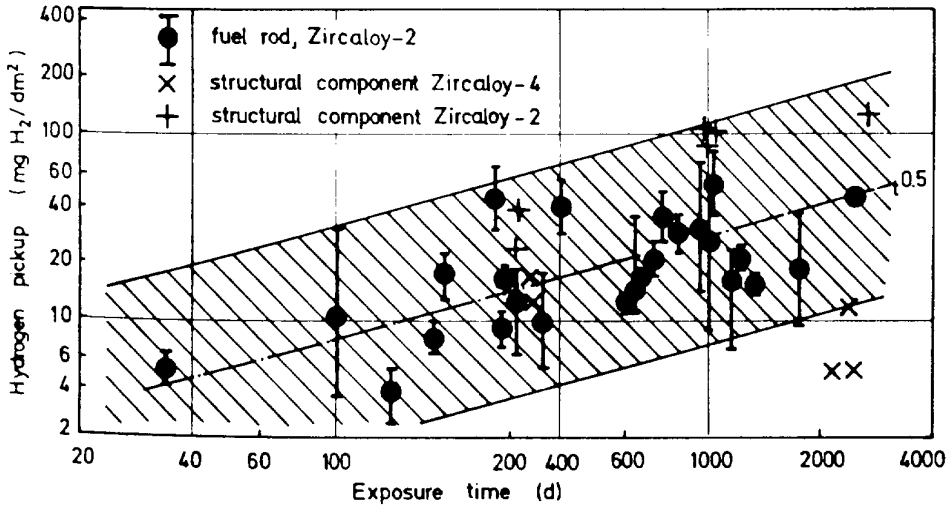


*FIG.28. Hydrogen pickup of Zircaloy fuel rod cladding and structural components in BWRs* [51].

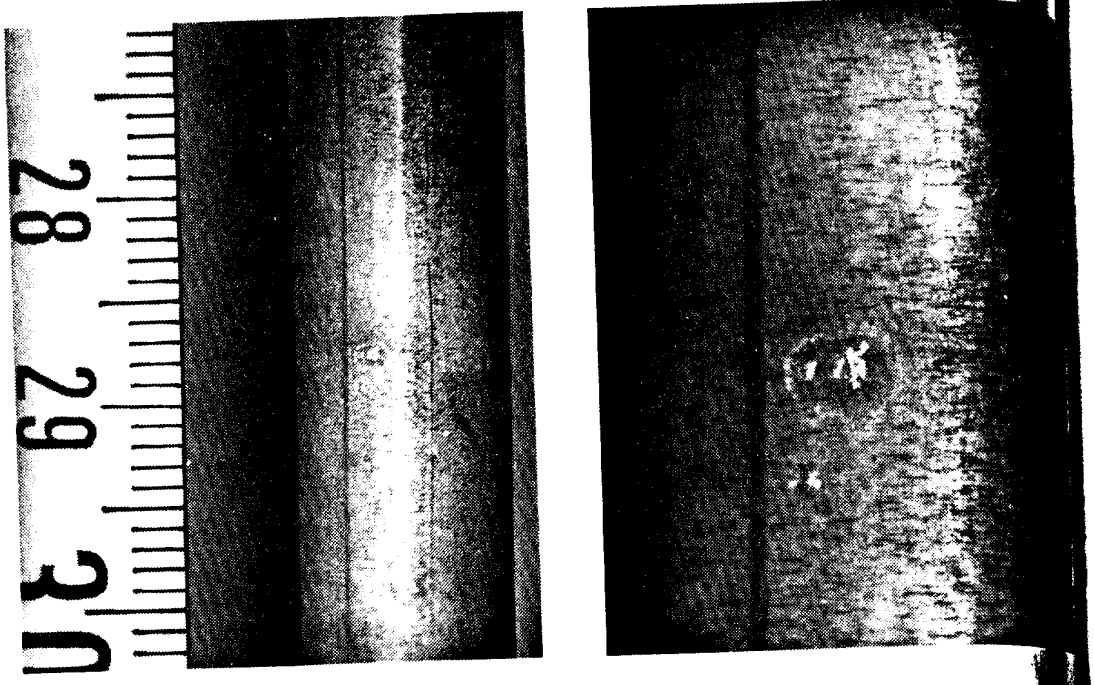


*FIG.29. Typical appearance of PCI defects.*

designed for long exposures in boiling water environments were later made fr
Zircaloy-4, which was developed for a lower hydrogen uptake. Under PWR c
tions only Zircaloy-4 is used.

## 4.3. Pellet-clad interaction (PCI)

### *4.3.1. Characteristics of PCI failures*

Mechanical/chemical pellet-clad interaction is at present the most extensively
studied effect of fuel performance. A final review cannot be written today and
would be a book rather than a few pages. The first observation of PCI failure
dates back to 1964 [52], but it was not before about 1970 that PCI was recogniz
as a performance-limiting effect. At that time failures were observed in HBWR
test rods [53], CANDU fuel [54] and BWR fuel [52] and were attributed to sev
local power ramps defined as a first and fast power increase after extended expos
accumulated at low power. In fact, power cycling on a daily or weekly basis nev
did lead to PCI failures. Early PWR fuel was not affected by PCI failures, which
was partly due to the lower effective power ramps as compared with HWRs and
BWRs, partly due to the early use of prepressurized fuel rods. However, several
power ramp incidences in PWRs since 1973 have confirmed that the propensity
to PCI failure is a generic feature of all Zircaloy-clad fuel.

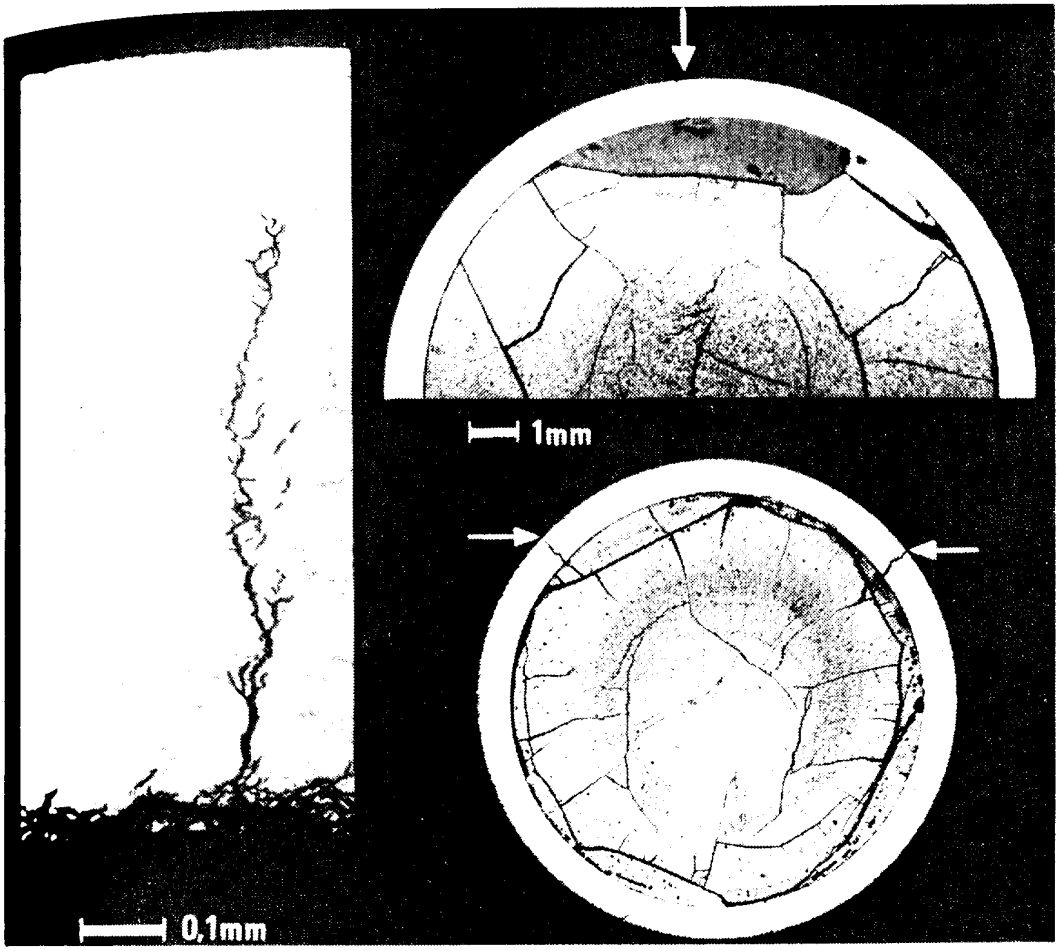


*FIG.30. Typical features of PCI defects in metallographic cross-sections* [63]

Soon the brittle nature of the PCI failures was recognized and the mechanism was attributed to stress corrosion cracking starting from the inner clad surface. Post-irradiation examination of PCI defects from power reactors and power ramp experiments [15,16,52–64] always showed the same failure characteristics, i.e. fine cracks (Fig.29) often associated with 'X'-marks on the clad outer surface. The axial position is predominantly at pellet/pellet interfaces or at transverse pellet cracks. The ridge height at the position of a defect is generally very small. Metallographic examination (Fig.30) revealed tiny brittle cracks starting from the inner clad surface, mostly opposite radial pellet cracks but sometimes opposite other pellet imperfections like missing chips or chips wedged into the pellet-clad gap. The nature of the fracture frequently changes over the length of the crack, being brittle and branched on the inner side and ductile on the outer side of the cladding. Detailed examination of these cracks by SEM showed transcrystalline facets (cleavage fracture) linked by flutings (ductile fracture), as well as intercrystalline fracture modes, depending on the crack propagation rate.

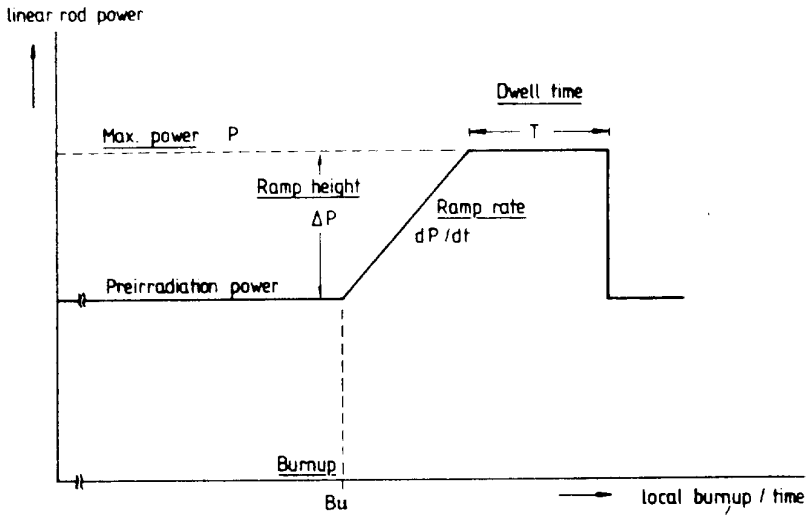


*FIG.31. Standard power ramp history and parameters.*

### *4.3.2. Operational conditions producing PCI failures*

The experimental efforts to clarify the critical operational parameters for PCI failure can be divided into four categories:

(1) Ramp tests in test reactors with individual test rods (mostly short rods or segments of standard design or with design variables) preferentially pre-irradiated in power reactors. In general, these are high-risk tests to establish failure thresholds for fast ramps and the conditions for safely exceeding the threshold power.

(2) Planned ramp tests in power reactors using either standard fuel or modified experimental fuel. Normally designed with low risk, these tests should mainly verify the zero or low-probability failure range on a statistically significant basis.

(3) Evaluation of inadvertent ramp occurrences or power transients in power reactors. These 'ramp incidences' have produced the most valuable data on PCI, because statistical significance was frequently combined with enhanced failure risk.

(4) Evaluation of power ramps associated with normal plant operation, e.g. startup after refuelling in LWRs, on-power fuelling in HWRs, or return to full power after control rod pattern changes in BWRs.

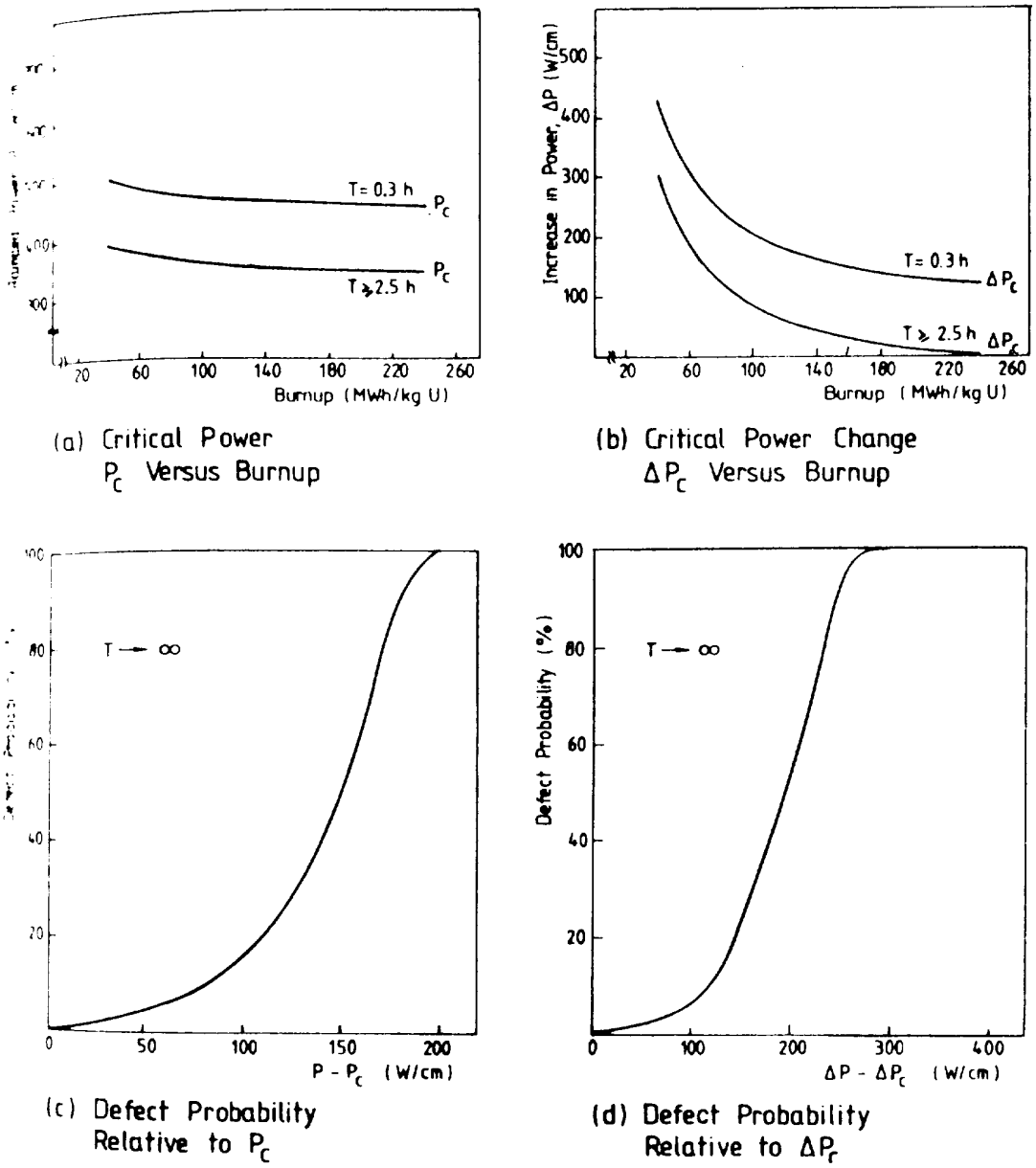


(a) Critical Power $P_c$ Versus Burnup

(b) Critical Power Change $\Delta P_c$ Versus Burnup

(c) Defect Probability Relative to $P_c$

(d) Defect Probability Relative to $\Delta P_r$

*FIG.32. CANDU experience with respect to PCI failures* [56].

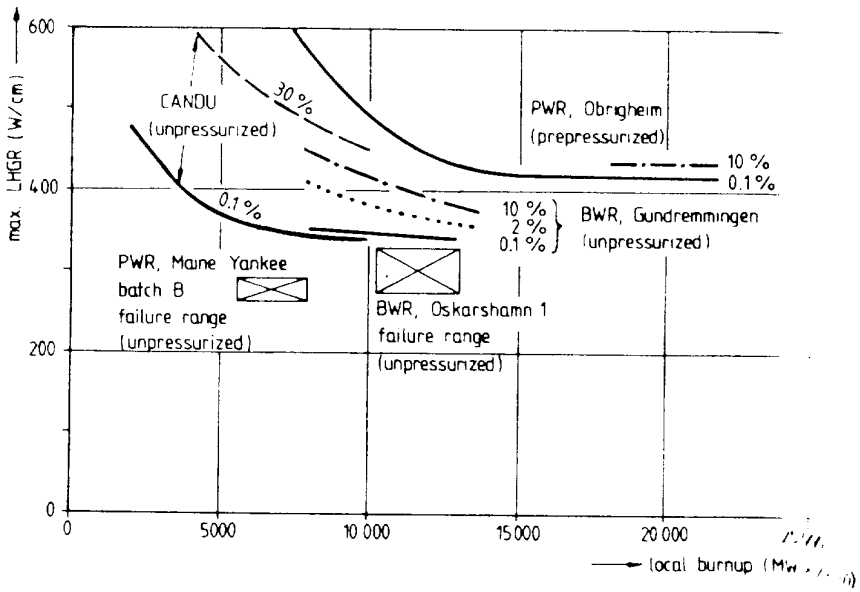


*FIG.33. Correlation between maximum power during a fast ramp and the defect rate by PCI of fuel rods of various designs* [16, 62, 63].

Since the failure probability of a fuel rod may be influenced by the pre-ramp power history, a standard ramp with constant preirradiation power level, as shown in Fig.31, is the most common basis for designing or evaluating ramp tests. Mainly five operational parameters are involved.

(a) Burnup accumulated prior to the ramp at low power (BU)
(b) Maximum rod power during the ramp (P)
(c) Ramp height, i.e. the power increment beyond the preirradiation power level ($\Delta P$)
(d) Average ramp rate ($\overline{\dot{\Delta P}}$)
(e) Dwell time at high power (T)

For defects to occur, all five parameters have to be in a critical range **simultaneously**. Experience shows that critical or threshold values exist for P and $\Delta P$ that depend on burnup. This can be seen from CANDU experience in Fig.32, as well as from the evaluations by KWU of BWR and PWR ramp occurrences or tests (Gundremmingen, Obrigheim, Biblis) in Fig.33. Figure 33 indicates that similar power threshold curves may apply for unpressurized CANDU and BWR fuel approaching about 350 W/cm at high burnup, whereas higher threshold curves (> 400 W/cm) are obtained for pressurized PWR fuel. The different behaviour of unpressurized and pressurized fuel is emphasized by the fact that no PCI problem has been observed in the high-rated Atucha fuel, which is the only prepressurized HWR fuel. Above the power threshold the failure probability

increases slowly for unpressurized rods, reaching the 10% line about 50 to 100 W/cm beyond the threshold (Fig.33).

Data analysis for the threshold ramp height so far has only been published for CANDU fuel (Fig.32(b, d)) with the result that the threshold ramp height is a hyperbolic function of burnup approaching about 100 W/cm at small dwell time but a near-zero value at large dwell time. However, the failure probability reaches the 10% line only about 120 W/cm beyond the threshold.

These results are consistent with individual ramp tests of unpressurized rods, where – with the exception of a few rods – failures occurred only above these 10% failure lines, i.e. $P > 400$ W/cm and $\Delta P > 150$ W/cm for high burnup. One must be careful, however, in generalizing these figures. For two other ramp occurrences (Maine Yankee, Oskarshamn-1, both unpressurized fuel) the reported threshold values [16,62] seem to be below the CANDU/BWR curves, as can be seen from Fig.33. The analysis shows that fuel temperature and fission gas release rather than rod power are the basic parameters.

No systematic data analysis has been published for the dependence of the failure probability on the ramp rate. A review of the data in the literature leads to the conclusion that no significant influence of the ramp rate can be found in the range of about 1 to 500 W/cm · min. As a consequence, there is generally also no influence of the ramp shape (stepwise or continuous). Below this range, however, the benefit of fuel creep to relax clad stress and to reduce failure probability seems to be substantial. As can be estimated from the operating recommendations (section 3), the critical or threshold value for the ramp rate is expected to be in the range of 2 to 20 W/cm · h (0.5 to 5%/h) and may depend on burnup, maximum power and design (e.g. prepressurization).

A more extensive analysis for establishing the influence of the dwell time is only available from CANDU fuel [56], giving a time dependency $[1 - \exp(-\lambda T)]$ with a time constant of $\lambda = 2.3\ h^{-1}$, which is in reasonable agreement with laboratory tests.

The question of to which extent fuel handling prior to the ramp has an influence on the PCI thresholds is not yet finally solved. The influence reported by the Canadian workers [61] could also be due to differences in fuel orientation (vertical/horizontal). The data from other test series (e.g. startup and in situ Petten ramp tests of KWU/CE [60]) are at present not sufficient to draw final conclusions. It seems, however, that the effect is not very pronounced. In addition, the length of the fuel rods has no significant influence on the PCI thresholds, as can be seen from the agreement between the results of CANDU fuel (short rods) and BWR fuel, or Petten tests (short rods) and PWR fuel, respectively.

With respect to the PCI mechanism, interesting test series have been reported by Canadian workers [65] and by GE [52]: No failures were observed by ramping fresh fuel in irradiated cladding tubes. This indicates that fission product availability is the dominating factor and not clad embrittlement by fast neutron irradiation.

### 4.3.3. *The influence of design; PCI modelling*

Within the conventional design variations of Zircaloy-clad $UO_2$ fuel there seems to be surprisingly little influence of geometric design variables on PCI behaviour. This is already indicated on the one hand by the close similarity of the behaviour of CANDU and BWR fuels, which are quite different in design, and on the other by the enormous difference in the PCI threshold powers between the Obrigheim and Maine Yankee (batch B) fuels, which are very similar in geometry (Fig.33). These observations and ramp test series show that, in particular at high burnup, the PCI threshold is fairly insensitive to variations in rod diameter, clad metallurgical condition, clad thickness, initial fuel to clad gap (in a limited range), rod length, pellet length and pellet dishing, at least in a first approximation. Of course, there may be second-order effects, and any design change to reduce the overall stress and local stress concentration during ramping must be considered as an improvement. An earlier hypothesis, that the threshold power increases with decreasing rod diameter [66], has not been confirmed, either by experiments or by more detailed theoretical investigations. The assumption that annealed cladding could be less susceptible to PCI failures than stress-relieved cladding, as often mentioned in discussions, has also been disproved by later experience (Oskarshamn). The analyses of ramp occurrences show that the only design parameters that have a first-order effect on PCI threshold powers are those affecting fuel temperature and fission product release characteristics, i.e. fuel structure and densification, prepressurization and, in extreme cases, the fuel-to-clad gap.

At the present time there is no generally accepted PCI model. Earlier approaches have been purely mechanical, e.g. the POSHO model of Scandpower [67]. However, wrong conclusions can arise if such models are applied in a general sense. Once calibrated against a fuel type, purely mechanical models may be capable of predicting approximately failure rates for the same fuel type but grossly underestimate or overestimate failure rates of other fuel types with different correlations between rod power and fission product release.

The same difficulty arises with a generalized application of the CANDU fuelograms to LWR fuel. In addition, the CANDU model is based on data at burnups below 10 GW · d/t(U), whereas the range above 10 GW · d/t(U) is the most important one for LWR fuel.

All the more detailed attempts, e.g. to incorporate thermal-mechanical feedback or SCC criteria into the PCI models, as reported at several recent conferences, are in a preliminary stage. In particular, we refer to the ANS Topical Meeting in St. Charles (May 1977), the SMIRT-4 Conference in San Francisco (August 1977) and the IAEA Specialists Meeting in Blackpool (March 1978). Since the widespread analytical aspects of PCI modelling are outside the scope of this review, we shall confine our discussion to a general description of the assumed mechanism in the following section.

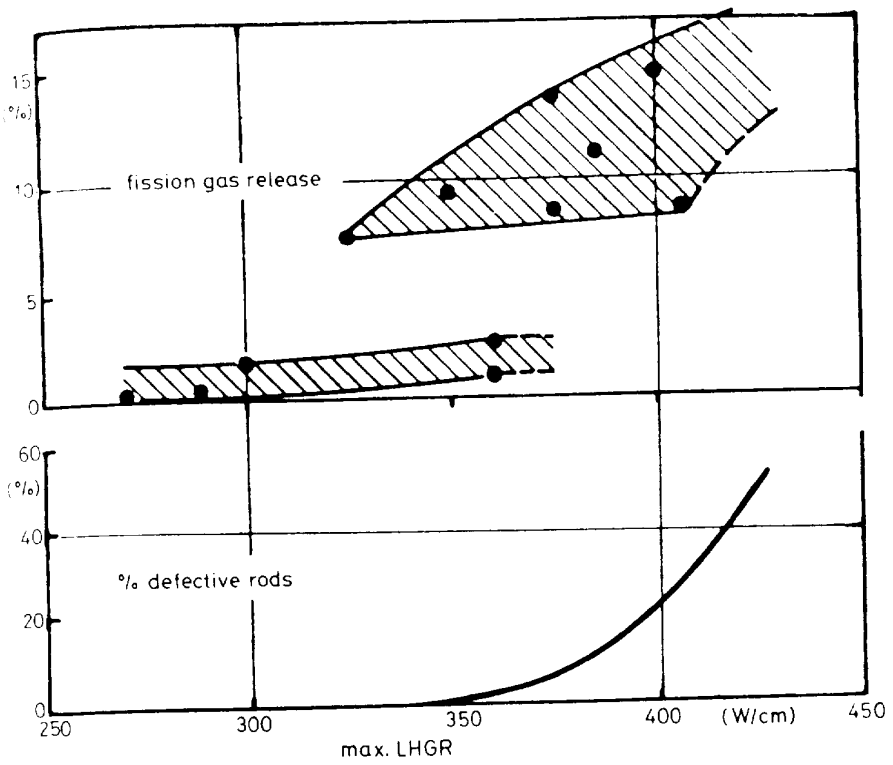


*FIG.34. PCI failure rate and fission gas release plotted against maximum rod power after a fast ramp* [63].

### *4.3.4. The mechanism of PCI failure*

It is a general observation that PCI failures start at power levels where the fission gas release increases sharply, showing large scattering from rod to rod. This is shown in Fig.34 and was also reported by Fuhrmann et al. [16] and Wood and Hardy [64]. As shown in Ref.[63], increased fission gas release is also associated with an increased release of other volatile fission products such as iodine and caesium. SEM examination of the deposits on cladding inner surfaces of rods with relatively large fission gas release [68,69] revealed different types of deposits containing the fission products caesium, iodine, tellurium and other volatile fission products combined with uranium, zirconium and oxygen.

The close correlation between the release of volatile fission products and PCI failures together with metallographic examinations (see section 4.3.1) point to fission product-induced stress corrosion cracking (SCC) as PCI failure mechanism. Several studies on possible chemical reactions between fission products and Zircaloy cladding revealed that stress corrosion cracking can only be caused by iodine or by iodides with low chemical stability, and by cadmium and silver.

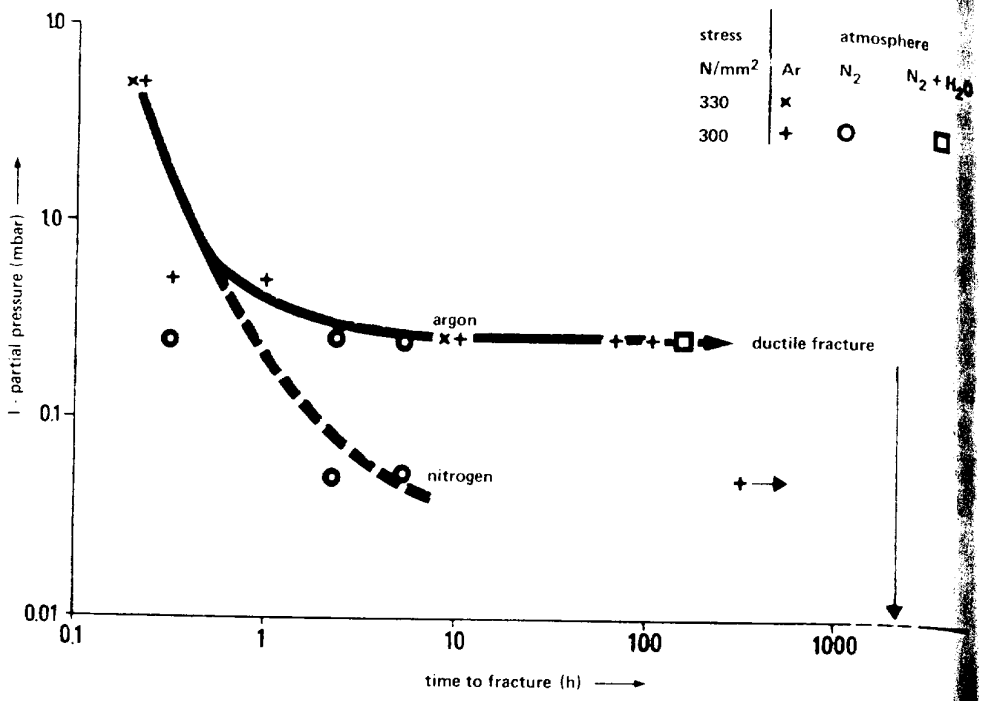


*FIG.35. Fracture behaviour of Zircaloy in tangential direction at 350°C under various iodine partial pressures* [63].

However, the latter species are only available in very small amounts, even in high-burnup fuel.

Since iodine is the most probable fission product to cause SCC, iodine-SCC of Zircaloy has been studied extensively during recent years (e.g. Refs [63, 64, 69–74]). It was found that a certain iodine concentration is necessary to initiate SCC. The time to fracture in relation to the iodine partial pressure at 350°C is given in Fig.35. The critical partial pressure in these tests was found to be between about 0.03 and 0.3 mbar, depending on other environmental conditions. An atmosphere leading to a non-passivating surface film (e.g. nitrogen) reduces the critical partial pressure compared with air-contaminated argon, whereas strongly passivating species (e.g. moisture) markedly increase this level. About the same critical iodine concentration was reported in Ref.[73], whereas most of the other published experiments indicated a much higher critical iodine concentration [70]. These discrepancies may partly be due to small differences in the environment (e.g. impurities of oxygen).

Furthermore, it was concluded from different studies that there exists either a strain rate-dependent minimum strain or a minimum stress for the occurrence of I-SCC. Time-stress relations for the time to failure for stress-relieved Zircaloy cladding tubes are plotted in Fig.36. These tubes were internally pressurized and

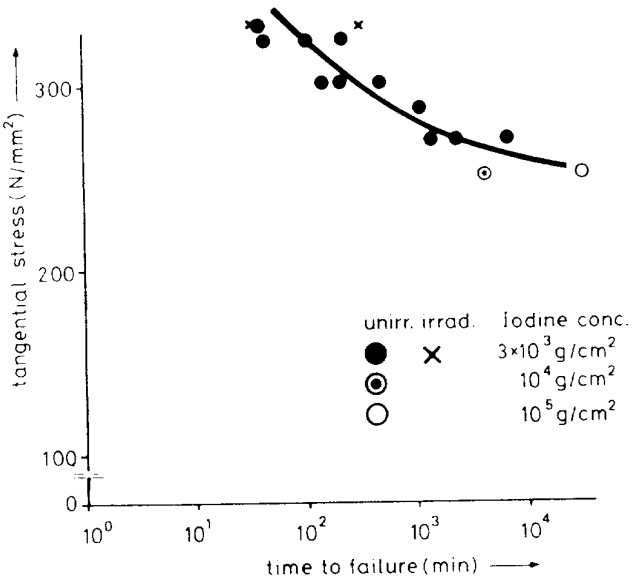


*Time of iodine SCC failure as a function of stress measured for stress-relieved* [63].

tested at 350°C with rather high iodine concentrations. From this figure a time to failure between 30 minutes and 500 hours is derived, depending on the stress in the range of 250–350 N/mm². These numbers are in general agreement with the findings of other experiments, e.g. Refs [70–75]. The threshold stress was found to depend on temperature and material condition.

The effect of irradiation was studied in Ref.[74] on samples irradiated in water and air environment. The tests showed that irradiation in water markedly increased the SCC susceptibility at fast neutron doses above $10^{20}$ n · cm$^{-1}$, whereas irradiation in air did not have any significant influence. Reference [75] reports that cladding from irradiated fuel rods has a lower minimum stress for I-SCC than unirradiated samples.

All investigations, however, have shown that I-SCC is possible only with elementary iodine or iodides with a low chemical stability (e.g. $ZrI_4$), but not with the more stable caesium iodide. Theoretical analyses (e.g. Ref.[69]) on the other hand lead to the conclusion that iodine should be totally bonded to caesium which is generated in excess. However, there is still some uncertainty in the theoretical data for the formation of complex oxides such as caesium uranate and caesium zirconate found at the pellet/cladding interface. The reaction of caesium iodide with zirconium and uranium oxides could result in the partial dissociation of the caesium iodide. From the available results it is not yet clear whether a sufficient amount of iodine is available under steady-state conditions in a chemical form that can produce I-SCC in a Zircaloy-clad fuel rod. It is

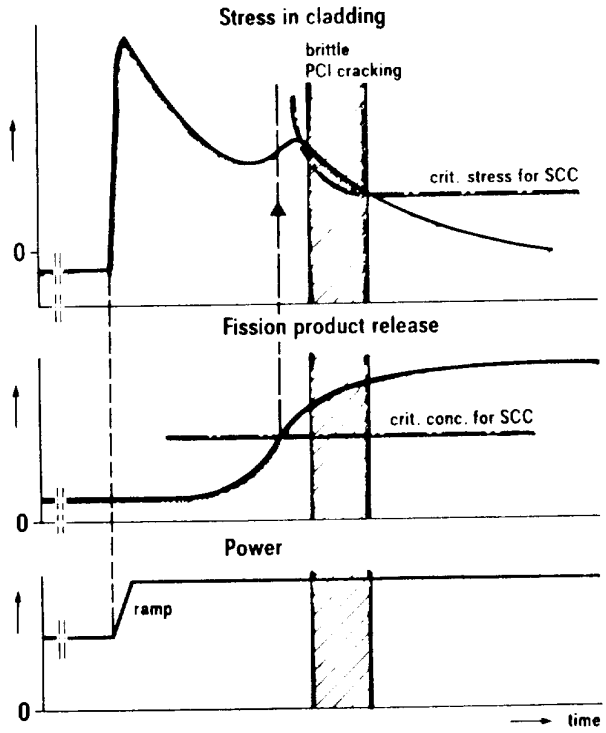


*FIG.37. Basic model of PCI cracking* [63].

possible that active iodides only exist under transient conditions or are formed by radiolysis, as suggested by Cubicciotti and Davies [76].

Post-irradiation examination of rods subjected to both power ramps and analytical evaluation suggests that a thermal feedback effect, induced by transient fission gas release, plays an important role. This may be one reason for the observation that pressurization reduces the tendency to PCI failures markedly [15]. According to Ref.[77], the sequence of events in the thermal feedback effect during ramping is as follows: (1) A fuel rod with a sufficiently high amount of stored fission gas in the fuel is ramped. (2) The fuel temperature becomes high enough to start increased fission gas release. (3) The fission gas released leads to further increase in fuel temperature by a decrease in the gap conductance, since the thermal conductivity of fission gas is about 20 times less than that of helium. (4) This in turn increases the fission gas release. The result is a substantial increase in fuel temperature and fuel thermal expansion, particularly in the case of fuel fragment misalignment or fuel chips in the gap, which impair an improvement of the gap conductance by contact pressure. (5) This transient release of fission gases is accompanied by the release of other volatile fission products which are responsible for stress corrosion cracking.

Based on the above hypothesis, the occurrence of PCI failures was explained as follows (Fig.37). After long exposure at low power a sufficiently high power

ramp generates tensile stresses in the cladding leading to local plastic deformations (i.e. ridging). The tensile stresses in the clad slowly relax by creep of fuel and cladding. During or some time after the ramp the fission product release rate shows a peak. This may lead to an additional temperature increase and thermal expansion in the fuel and a delay of the relaxation of stresses in the cladding. Brittle PCI cracking is possible if both the fission product concentration and the stress condition simultaneously exceed critical values. Future efforts in PCI modelling should be concentrated on a quantitative description of these effects.

### 4.3.5 *Corrective action*

As already discussed in section 3, the first corrective action to reduce PCI failure risks was changing the refuelling strategy and the implementation of operating guidelines, which was very successful. The broad introduction of fuel with smaller rod diameters and therefore reduced heat ratings for high-rated plants will also be beneficial with respect to PCI. The same is expected for the change to prepressurized BWR 8 X 8 fuel made by KWU. Additional design improvements (short chamfered pellets and annealed cladding [7]) will probably not significantly improve the PCI behaviour according to the discussion in the preceding section.

The present activities to further improve the PCI resistance of the fuel concentrate on testing of remedies like protective layers between fuel and clad (barriers, liners, chemical getters) or special pellet shapes differing from conventional designs. Furthermore, any measure to reduce transient fission product release by suppressing the onset of substantial grain growth in the pellet centre can be of great benefit. Additives to the $UO_2$ could improve the fuel plasticity, act as internal getters, and stabilize the grain size. It is also known that the texture of the Zircaloy influences the susceptibility to iodine stress corrosion [73]. However, it seems that significant changes in present fabrication routines would be necessary which could not be accepted without intensive testing.

The only remedy that has found commercial application up to now is graphite coating in CANDU fuel rods (CANLUB fuel). It has been demonstrated that the critical power for CANLUB fuel is higher than that for the original CANDU fuel by at least 100 W/cm [59]. Again, most of this experience is limited to the burnup range up to about 10 GW · d/t(U). Although several data points reported in Ref.[61] are in the range of 10–20 GW · d/t(U), it is still an open question whether coatings may also be beneficial under the different design conditions and in the high burnup range typical for LWR fuel.

Substantial worldwide efforts in developing and testing PCI remedies for LWR fuel rods are currently being made by the major fuel suppliers and also by plant operators within the scope of DOE and EPRI programmes. It will take several years before final conclusions can be drawn for commercial application.

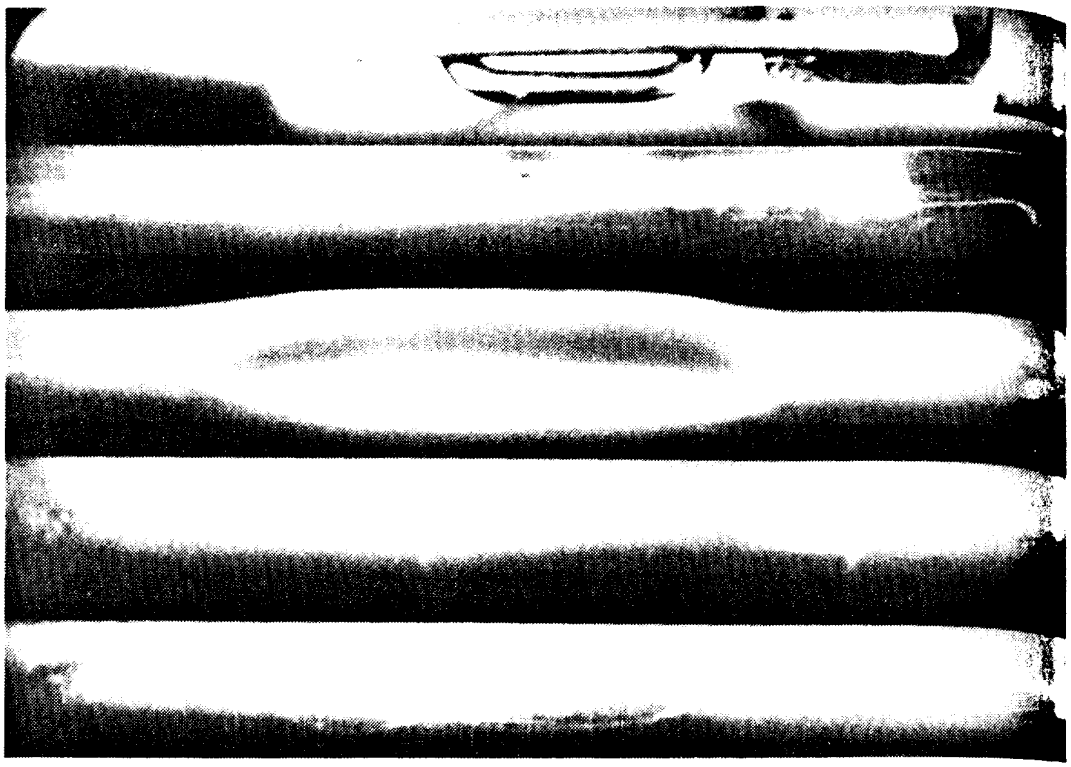

*FIG.38. Example of cladding collapse from Beznau I PWR [79].*

## 4.4. Fuel densification and clad collapse

### *4.4.1. General observations and consequences*

Flattened fuel rods were first detected in region II of Beznau Unit I during the 1971 refuelling after cycle 1 (Fig.38, Table V). Approximately 2% of the region II rods were found to contain a single flattened length of 15–75 mm in the upper 40% of the fuel column. No flattened rods were observed at that time in regions I or III, although a small fraction of the region I rods was found to be flattened after cycle 2. Flattened rods were also found in regions I, II and III of Ginna during the 1972 refuelling after cycle 1 and later in region I of the Point Beach Unit 1, H.B. Robinson Unit 2 and Mihama Unit 1 reactors. None or only weak flattening was observed in other regions of these reactors in rods with low pressurization level [78, 80, 81]. Flattening has never been observed in rods with the currently used high pressurization level.

Based on non-destructive examinations in the Beznau pool and destructive examinations in the hot cells, fuel densification and axial settlement was identified as the cause of gap formation in the fuel column. Subsequently, irradiation-enhanced creep of the cladding under the coolant pressure resulted in a flattening

TABLE V. PERIPHERAL FUEL ROD FLATTENING OBSERVATIONS [78]

| Plant | Cycle | Region[a] | Rod prepressurization | Fuel density (% T.D.) | Per cent flattened |
|---|---|---|---|---|---|
| Beznau 1 | 1 | 1 | No | 94 | 0 |
| | | 2 | No | 92 | 2.3 |
| | | 3 | No | 90 | 0 |
| | 2 | 1 | No | 94 | 0.8 |
| | | 2 | No | 92 | 4.5 |
| | | 4, 4B, 5 | Yes | 91 & 92 | 0 |
| Ginna | 1B | 1 | No | 94 | 2.0 |
| | | 2 | No | 92 | 7.3 |
| | | 3 | No | 90 | 3.5 |
| | | 4, 4A, 4B | Yes | 92 & 94 | 0 |
| | 2 | 1 | No | 94 | 3.8 |
| | | 2 | No | 92 | 6.5 |
| | | 4A | Yes | 92 | 0 |
| Mihama 1 | 1B | 1 | No | 94 | 1.0 |
| | | 2 | Yes | 92 | 0 |
| | | 3 | Yes | 91 | 0 |
| Point Beach 1 | 1 | 1 | No | 94 | 3.2 |
| | | 2 | Yes | 92 | 0 |
| | | 3 | Yes | 91 | 0 |
| | 2 | 2 | Yes | 92 | 0.7[b] |
| | | 3 | Yes | 91 | 0.05 |
| | | 4 | Yes | 94 | 0 |
| H.B. Robinson 2 | 1 | 1 | No | 94 | 1.1 |
| | | 2 | Yes | 92 | 0 |
| | | 3 | Yes | 91 | 0 |

[a] Typical core consists of three fuel regions which differ in design parameters and are intended to be sequentially discharged. Letters designate partial regions.

[b] An additional 0.3% exhibited high ovality.

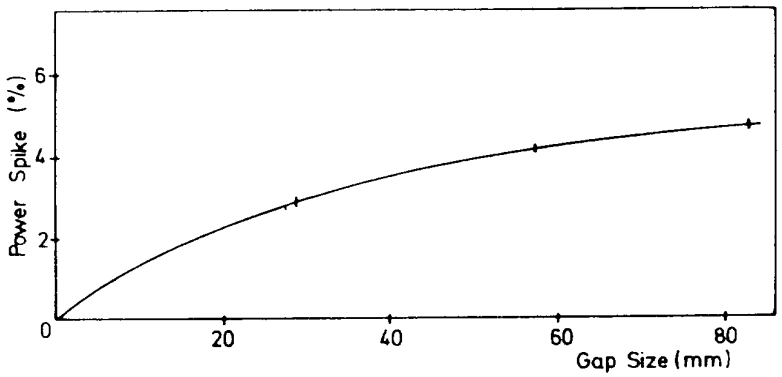


*FIG.39. Power spike in adjacent rod as a function of gap size for a regular fuel lattice.*

of the fuel rods in unsupported sections [78–81]. Examination of over 1000 rods from Obrigheim, which were also unprepressurized but contained a more stable fuel, did not show any collapsed sections. This confirms that unstable fuel was the primary reason for the collapsing observed.

In general, the flattening observed was always limited to the upper part of fuel rods since gaps of sufficient size are not formed at the bottom of the fuel column. The lengths of flattened sections ranged from about 13 mm, the minimum observed at those plants, to 75 mm as observed at Ginna. The largest flattened sections occurred near the top of the fuel column where densification and settlement of the fuel column may add up most effectively. Long flattened sections were generally completely flattened, but occasionally fuel pieces remaining in the gap prevented total flattening. Short and only partially flattened sections were often found as a result of end support by the pellets preventing flattening into the short gap [81].

Only a small fraction of the flattened fuel rods (3–22%) developed leaks due to the high local strain (~25%) during collapsing [78, 80, 81]. Another consequence of clad collapsing is local power spiking. This occurs both in the adjacent rods and in the collapsed rod itself. Even in the case of gap formation without collapsing such a spiking only due to the reduced absorption of thermal neutrons is predicted (Fig.39). Therefore, it is necessary not only to avoid collapsing but also to prevent larger gaps due to in-pile densification of the fuel.

The main effects that influence local collapsing are creep-down behaviour of the cladding under external pressure and the dimensional stability of the fuel.

### *4.4.2. Creep-down behaviour of the cladding*

Under the external pressure the cladding creeps down and ovalizes due to irradiation-induced creep until it contacts the pellets. Continued creep-down after the first contact leads to reduction of the ovalization and an increase of

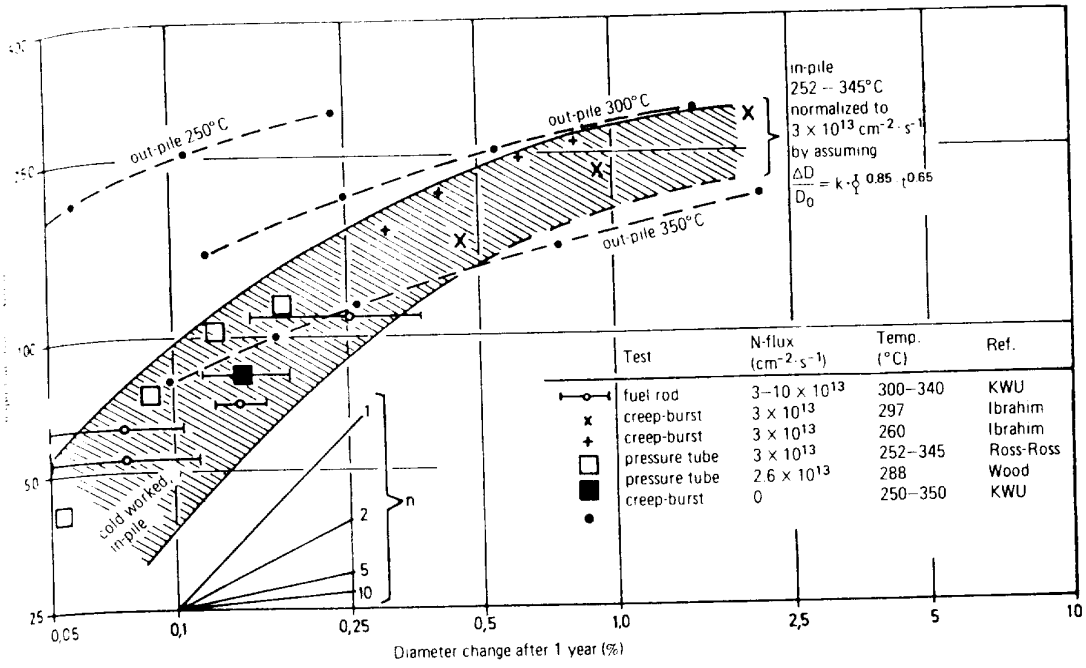


*FIG.40. Stress dependence of in-pile and out-of-pile creep of cold-worked and stress-relieved Zircaloy ([83–85], KWU data).*

the area of contact until the cladding is totally pressed against the fuel column [82]. Figure 40 shows the in-pile and out-of-pile creep deformation of Zircaloy tubes after one year of exposure as a function of stress for different temperatures in the range between 250 and 350°C. In this temperature range creep deformation is mainly due to irradiation creep in the interesting stress range of 50 to 120 N/mm$^2$. Various equations for irradiation creep have been published and most of them are based on the following basic relation:

$$\epsilon = k\, \phi^p\, \sigma^m\, t^n$$

where $\epsilon$ = creep deformation
$\phi$ = fast neutron flux
$\sigma$ = stress
t = exposure time
k, p, m, n = material constants.

The flux and time exponents were found to be in the range between 0.5 and 1 [45, 86]. The stress exponent is close to 1 at stresses below 100 N/mm$^2$ for cold-worked Zircaloy and increases to higher numbers above 100 N/mm$^2$, as can be seen from Fig.40. The change in the ovality in non-supported tubes can be

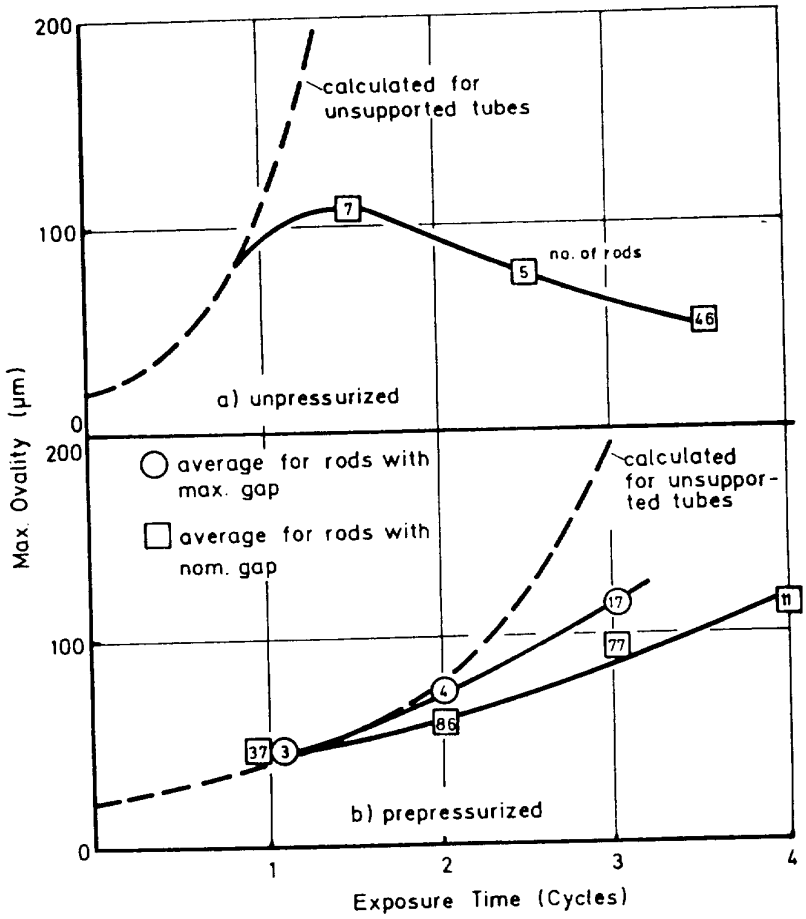


*FIG.41. Development of ovality in prepressurized and unpressurized PWR fuel rods* [45].

predicted from several codes. Reference [79] uses the following approximate expression for materials where the creep rate depends on the square of the applied stress:

$$O_\epsilon = O_0 \exp\left[8\,\epsilon\,\frac{r^2}{s^2}\right]$$

where

$O_\epsilon$ = final ovality
$O_0$ = initial ovality
$\epsilon$ = average creep deformation under the external pressure
r = clad radius
s = wall thickness.


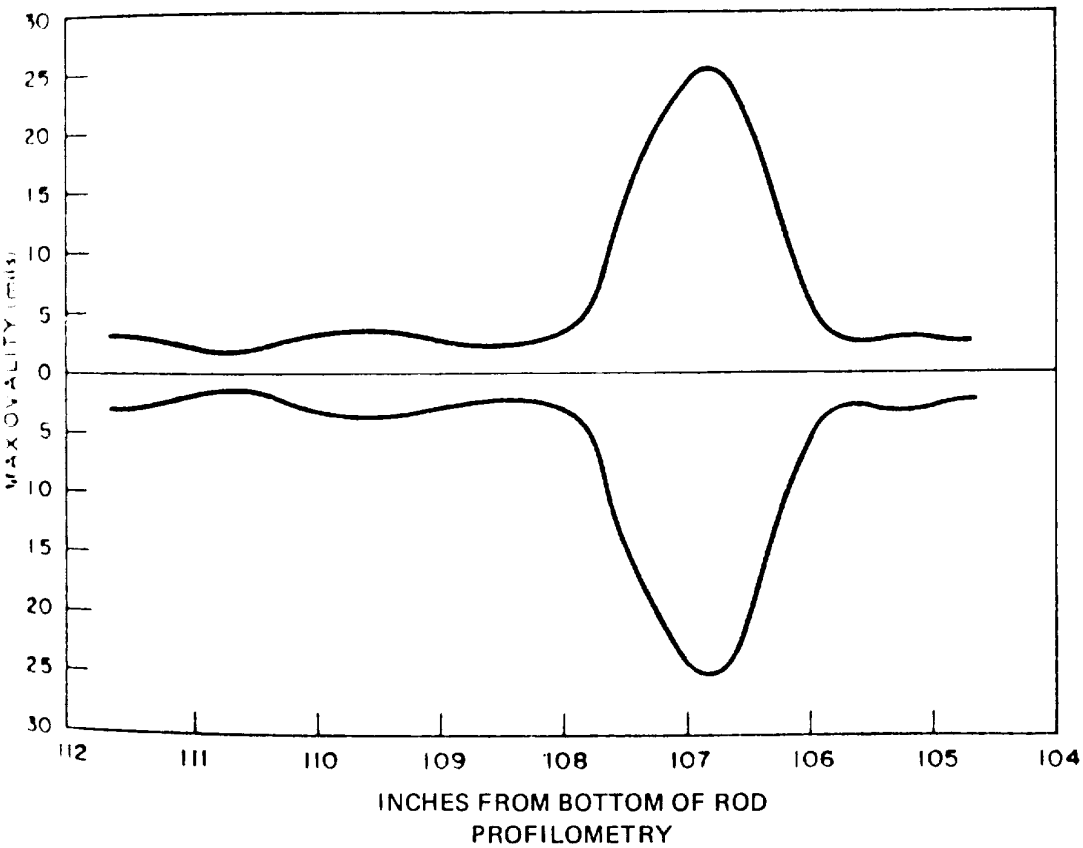


*FIG. 42. Section of Beznau I Region 2 fuel rod with a short gap in the fuel column.*

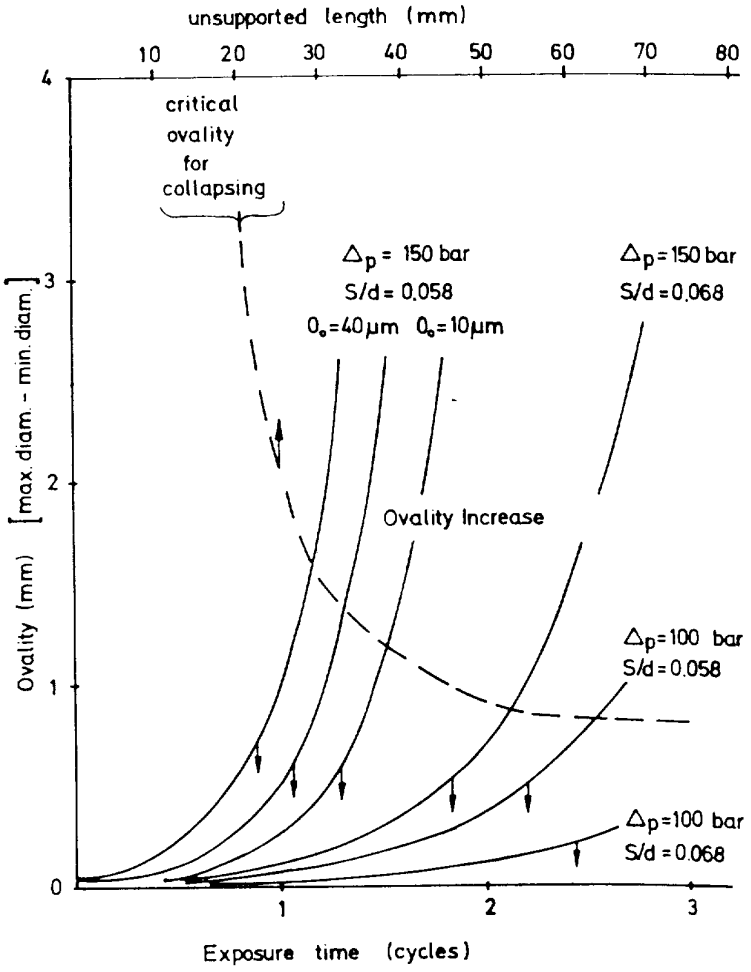


*FIG.43. Critical ovality for collapsing and ovality increase versus exposure for various overpressures (Δp) and wall thickness to diameter (s/d) ratios derived from Ref.*[79].

Figure 41 shows the ovality plotted against exposure time in pressurized and unprepressurized PWR rods calculated with the above relation for unsupported tubes, together with the maximum ovality found in various fuel rods. The theoretical curve gives a good approximation for the initial period of operation. Deviations from the predicted curve occur after 1 to 2 cycles due to the support of the fuel pellets. The onset of the support depends on the size of gaps between the pellets and on the creep-down and ovalization rate, which is much faster in unpressurized than in prepressurized fuel rods. In sections with gaps in the fuel column the ovalization is more severe leading to local ovality loops, as can be seen from Fig.42. The probability of collapsing depends mainly on the magnitude of the external overpressure (Δp), the wall thickness to diameter ratio

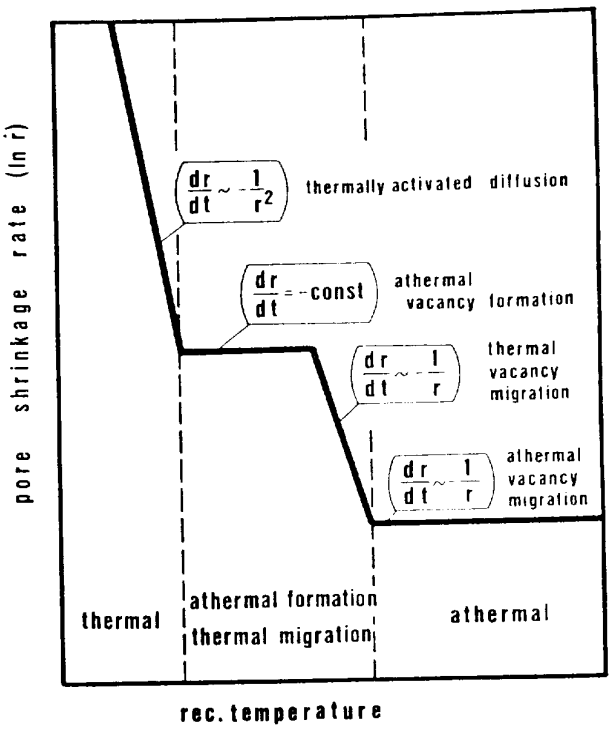


*FIG.44. Arrhenius plot for the pore shrinkage rate* [90].

(s/d), the initial local ovality, the eccentricity, and the size of the gap in the pellet columns. Figure 43 shows the ovalization in unsupported areas for typical PWR fuel rods with different s/d ratios for two different values of external overpressure, together with the critical ovality for collapsing as a function of the gap length. For the unpressurized design with an s/d ratio of 0.058 corresponding to Beznau and Ginna first core collapsing should mainly occur in positions where the gap size in the fuel column exceeds about 50 mm. After two cycles collapsing should have occurred at all gaps larger than 20 mm. An increased s/d ratio (e.g. 0.068 for the KWU design) as well as prepressurization reduces strongly the probability of collapsing even if large gaps exist (see Fig.43).

### 4.4.3. *Fuel densification*

When it became evident that an in-pile densification phenomenon was the reason for the local flattening observed in early Westinghouse fuel many studies were initiated to clarify the mechanism and the rate-controlling parameters of $UO_2$ in-reactor densification (e.g. Refs [87–93]).

Thermally activated densification (final stage sintering) was first analysed by Coble [94] using vacancy diffusion models. He described the densification of a body made up from identically shaped pore free particles with pores left only at the corner points. All pores have the same initial size and disappear

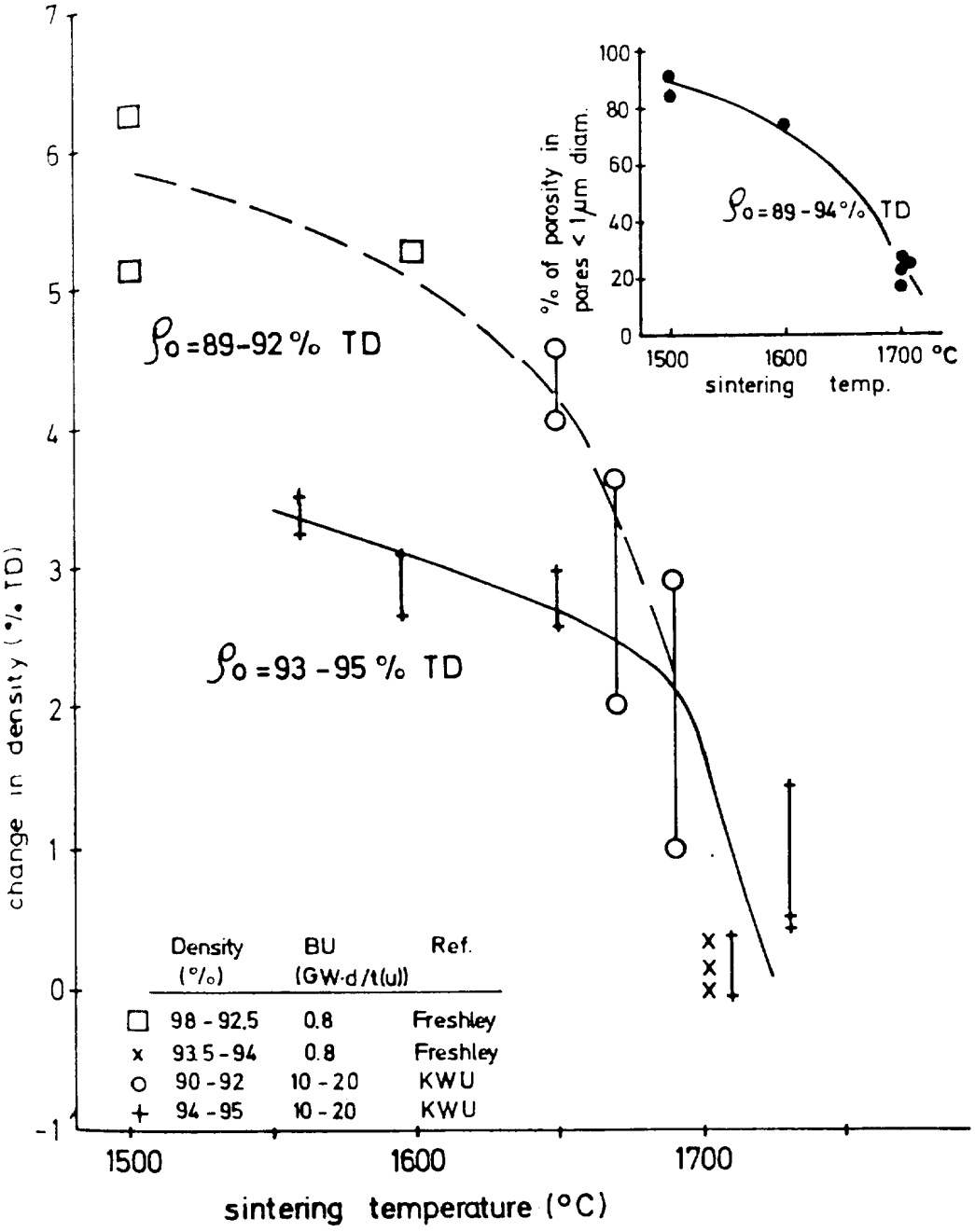


*FIG. 45. Correlation between densification propensity and sintering temperature (data from [93] and KWU).*

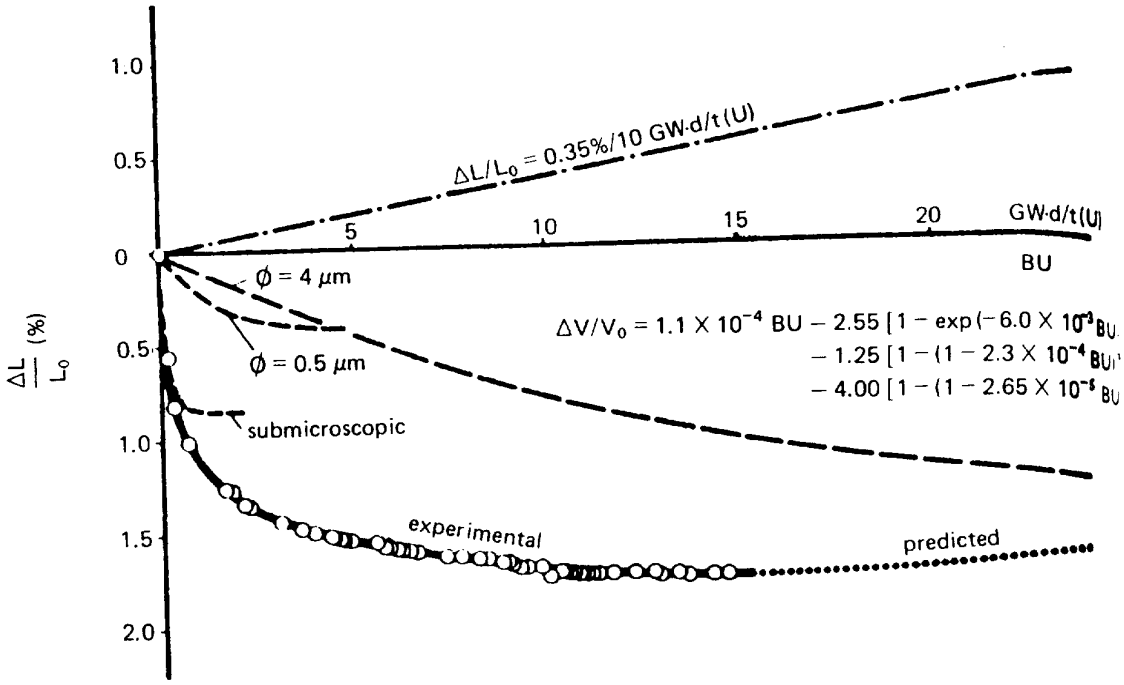


*FIG.46. Continuous stack shortening of an experimental unstable fuel (IFA 418 rod 3). Comparison with theory* [100].

high in-pile densification propensity, whereas fuel pellets sintered at high temperatures (with rather large pores) show a relatively high stability against in-pile densification. This can be seen from Fig.45. Large changes in the density due to in-pile densification occur only in pellets sintered at temperatures below 1700°C. After sintering at 1500–1600°C most of the pore volume is contained in pores with a diameter below 1 μm, whereas sintering at 1700°C leads to a small volume of pores with <1 μm diameter (see insert in Fig.45).

The influence of burnup on the densification can be seen from Fig.46, which shows the relative $UO_2$ column length change of an experimental unstable fuel with a large fraction of the porosity in submicroscopic or very small pores. The irradiation was performed in the HBWR (Halden Boiling Water Reactor, IFA-418, rod 3) [100]. The net change in volume of the $UO_2$ during burnup is determined by the superposition of the matrix swelling and the simultaneous shrinkage of the pores with different sizes. The data points could be described by the equation inserted in Fig.46. There are only four terms: the first one represents the matrix swelling, the second one describes the fast disappearance of the submicroscopic porosity (2.55% of pellet volume), and the last two terms represent the slower shrinkage rate of two classes of coarser pores, with pore diameters of 0.5 and

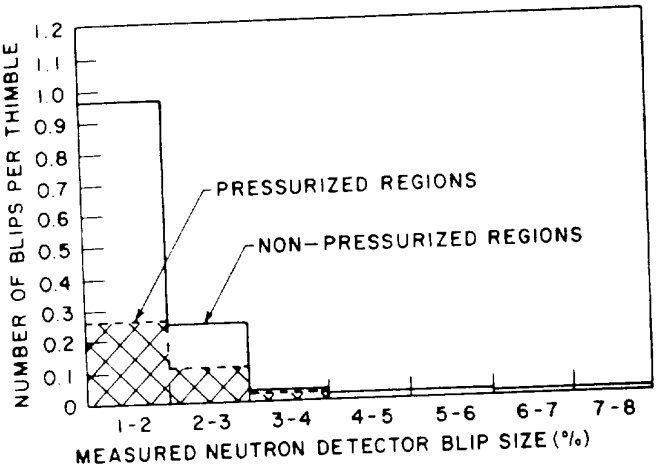


*Fig. 47. Measured size and frequencies of fuel column gaps indicated by flux blips for prepressurized and unpressurized fuel rods* [78].

4 μm, representing 1.25 and 4.00% of pellet volume, respectively. The contributions from swelling and from the shrinkage of the different classes of pores are shown separately. It is obvious that shrinkage of the small pores occurs early in life, whereas the shrinkage of larger pores is considerably slower.

The fuel used for Beznau, Ginna, Mihama 1, Point Beach 1, and H.B. Robinson was sintered at rather low temperatures and therefore experienced significant densification (about 4.5%) early in life. However, modern fuel is sintered near or even above 1700°C and shows a much higher in-pile densification resistance.

### 4.4.4. *Gap formation in the fuel column*

Gaps in the fuel column are a consequence of two effects: (1) differential axial length change of the cladding and the fuel column by growth of the cladding and densification of the pellets, and (2) the 'hang-up' of single pellets which prevents settling of the pellets. The maximum possible gap size increases with increasing height of the gap (axial position in the fuel rod), with increasing densification and with increasing growth of the cladding. The pellet hang-up probability should depend on local deviations in the creep-down and ovalization characteristics of the cladding and on the dimensional behaviour and cracking pattern of the pellets. The probability of gap formation should be higher in unpressurized than in prepressurized fuel rods. This is consistent with the results shown in Fig.47, which illustrates the frequency and size of flux blips (localized increases in neutron flux which are detected by the incore instrumentation). These flux blips have been shown to be the result of fuel column gaps or flattened sections [80]. It is obvious from this figure that about three times more gaps

TABLE VI. PROBABILITY OF AXIAL GAP SIZE DUE TO PELLET DENSIFICATION [80]

| Fraction of maximum gap size | Probability |
|---|---|
| 0 – 0.143 | 0.273 |
| 0.143 – 0.286 | 0.227 |
| 0.286 – 0.429 | 0.182 |
| 0.429 – 0.572 | 0.130 |
| 0.572 – 0.715 | 0.104 |
| 0.715 – 0.858 | 0.055 |
| 0.858 – 1 | 0.024 |

are formed in the unpressurized rods than in the prepressurized ones. In the pressurized rods (fuel with 92% TD) nearly every rod could have a gap accor to the analysis reported in Ref. [80], and one could conclude that each third may have a gap even in prepressurized rods with unstable fuel. However, this inconsistent with measurements on Stade first core. These rods had a lower densification propensity than the Beznau rods but still a larger in-pile densifi (about 2.5%) than modern fuel. The γ-scans performed in the pool showed o one of the 80 rods examined with a 15 mm gap (about 1/3 of the total differ between fuel column and clad length change). This indicates that other para- meters like wall to diameter ratio, densification propensity itself etc. influenc the probability for gap formation, too. Results from Westinghouse [80] have shown that the gap size follows a certain distribution function, as given in Table VI. The results indicate that hang-up of single pellets from the beginni of life only occurred in a small percentage of the rods showing gaps, most of them experiencing the hang-up only after long exposure or after some differe axial movement of fuel and clad.

The probability that a maximum gap is formed should also decrease wit increasing internal pressure (decreasing probability of an early hang-up) and decreasing densification tendency (smaller differential axial movement of cla and fuel).

Modern fuel rods may show a maximum differential length change betw fuel and clad of 10–30 mm (e.g. Ref. [82]). Therefore, the maximum gap in positions operating at high powers cannot exceed 25 mm, and the maximum power spiking is less than 2.5%, according to Fig.39. However, the probabilit of such gaps in modern fuel is extremely small.

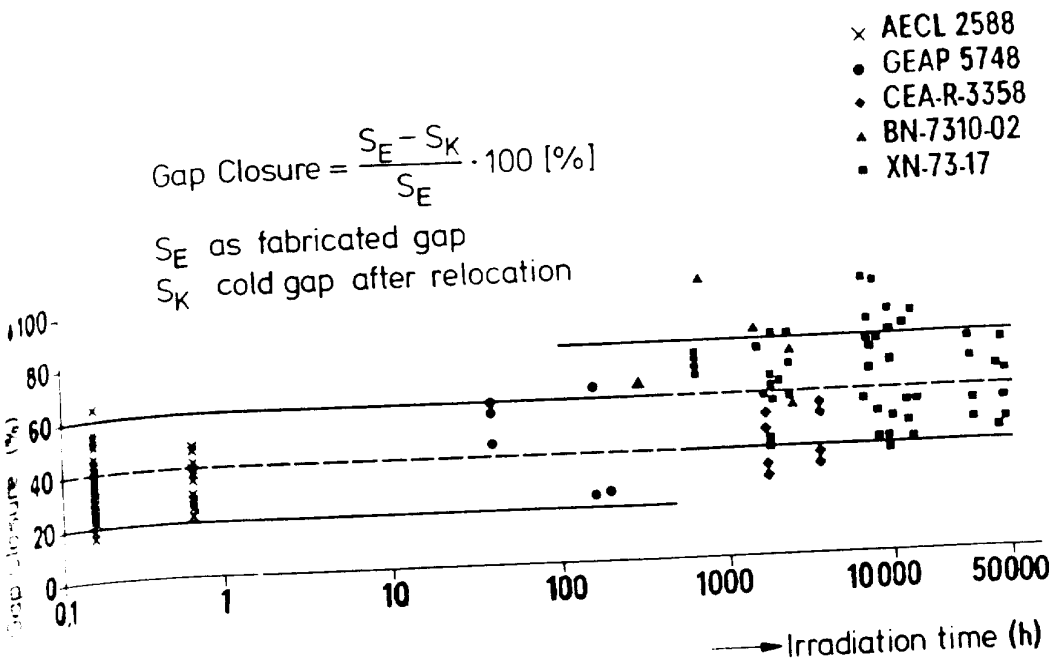


FIG. 47. *Closure of gap between pellet and cladding due to relocation plotted against exposure* [101]

ones. In the un-
e a gap according
at each third rod
lowever, this is
had a lower
n-pile densification
ool showed only
ie total difference
at other para-
f etc. influence
use [80] have
is given in
n the beginning
aps, most of
some differential

decrease with
ang-up) and
ement of clad

change between
ximum gap in
he maximum
the probability

### 4.4.5. *Relocation*

Another consequence of densification which has been widely discussed is an increase in the fuel temperature due to an increase in the radial gap between clad and pellet (decreasing gap conductance). A detailed analysis of the gap width as function of burnup showed that this effect is compensated by relocation of the fuel pellets (e.g. Ref.[101]), which crack in several fragments due to thermal stresses. These fragments relocate in an outward direction resulting in partial closure of the initial gap during startup (about 40%) and later in life about 20% additional closure, see Fig.48) [102]. This relocation is partly reversed under steady-state operating conditions by clad restraint. Only during fast power ramps should the pellet relocation be considered as being mostly irreversible.

## 4.5. Bowing and growth of fuel rods and assemblies

Changes in the length of fuel assemblies and rods are mainly caused by irradiation growth of Zircaloy. A knowledge of the irradiation growth characteristics is necessary at the design stage to take account of differences in the growth of the fuel rods and other components as well as the bowing of fuel rods and assemblies.

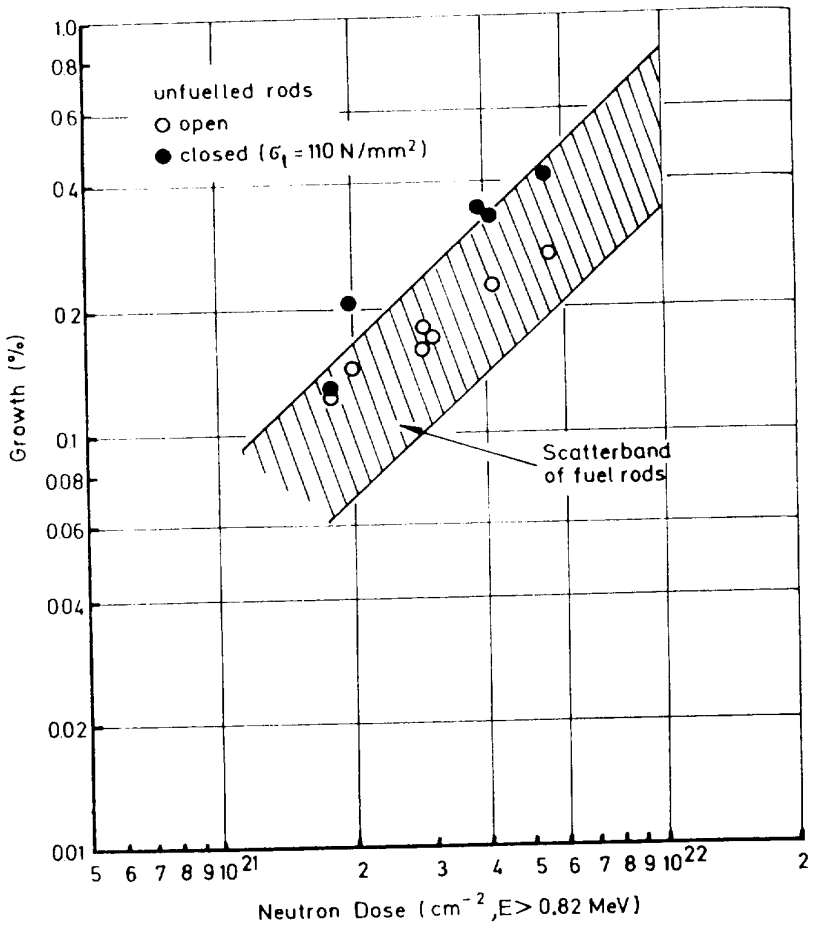


*FIG.49. Influence of differential pressure on the growth of unfuelled rods compared with the growth of fuel rods* [45].

### *4.5.1. Axial growth*

The amount of fuel rod growth and the scattering in the growth data experienced under operation was not anticipated in the earlier fuel designs. The risk of interaction between the assembly end-fittings and the fuel rods led to repair or premature discharge of the first PWR assemblies with Zircaloy cladding. In BWR assemblies the risk of disengagement from or interaction with the upper tie plate due to differential growth has been no general problem but has led to repairs in a few exceptional cases.

The length increase of Zircaloy-clad fuel rods arises, in general, from three different mechanisms [45]

Anisotropic creep-down

Irradiation growth

Mechanical interaction between fuel and cladding (ratchetting).

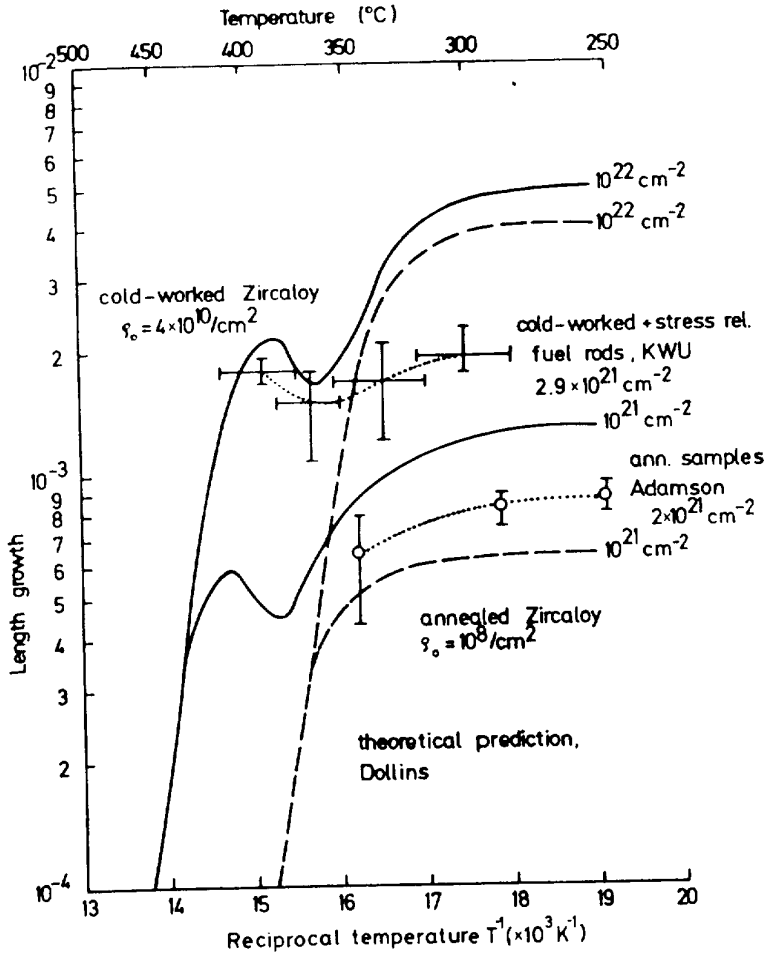


FIG. 50. *Influence of temperature on radiation growth of Zircaloy. Comparison of measurement* [45, 104] *and prediction* [105].

The creep-down of the cladding (axial to tangential stress ratio = 1 to 2) would not result in a length change if the material properties were isotropic. Zircaloy tubings, however, have a pronounced texture causing anisotropic behaviour (e.g. Ref.[103]) resulting in increases in length. Figure 49 shows the scatter band for the fuel rod growth of KWO fuel rods and some length growth data of unfuelled rods (open and closed tubes). It can be seen that the rods with high compressive tangential stress (closed tubes) show a larger length increase than the rods with zero tangential stress (open tubes). The relative length increase due to the anisotropic creep was about 10% of the relative diameter decrease.

Irradiation growth is strongly influenced by the metallurgical condition of the material [104]. Both heavy cold working and a strong texture enhance the growth. The dependence of the irradiation growth ($\epsilon$) on the fast fluence ($\phi t$) can be described by the empirical relation

$$\epsilon = \text{const.}\ (\phi t)^n$$

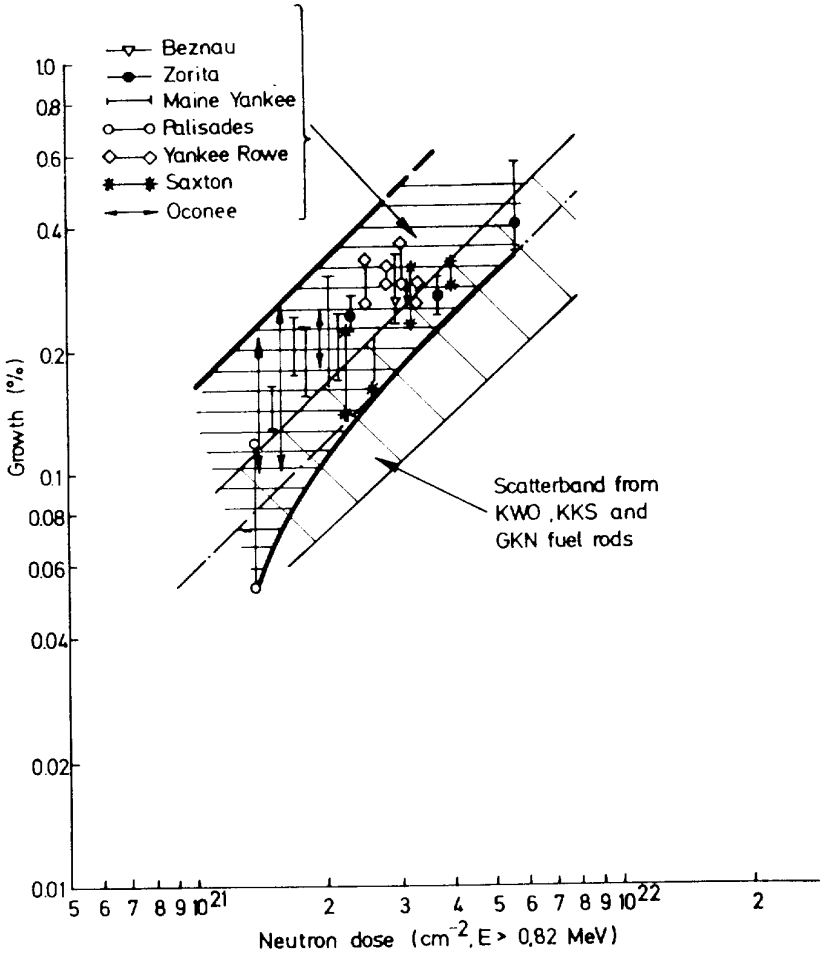


*FIG.51. Growth of PWR fuel rods* [45, 107–109].

The exponent n is generally in the range 0.45–1.0 and depends on temperature and material condition. For the cold-worked condition n is around 1, while for the fully annealed condition n is close to 0.5. The temperature dependence is weak below 330°C and becomes strong at higher temperatures, especially for annealed material (Fig.50).

The third contribution to fuel rod growth is the interaction of the fuel with the cladding. According to Ref.[106], growth due to fuel-clad interaction can be significant, especially in the lower part of the rods. The amount of growth induced by fuel-clad interaction is certainly different for various designs, and may be influenced by the operating mode. An analysis of the growth of SGHWR fuel rods showed that about half the measured length changes were due to irradiation creep of the cladding under the axial stresses caused by fuel-clad interaction [107]. On the other hand, an analysis of the length increases of fuel rods from the PWRs Obrigheim (KWO), Stade (KKS) and Neckarwestheim (GKN) revealed that the

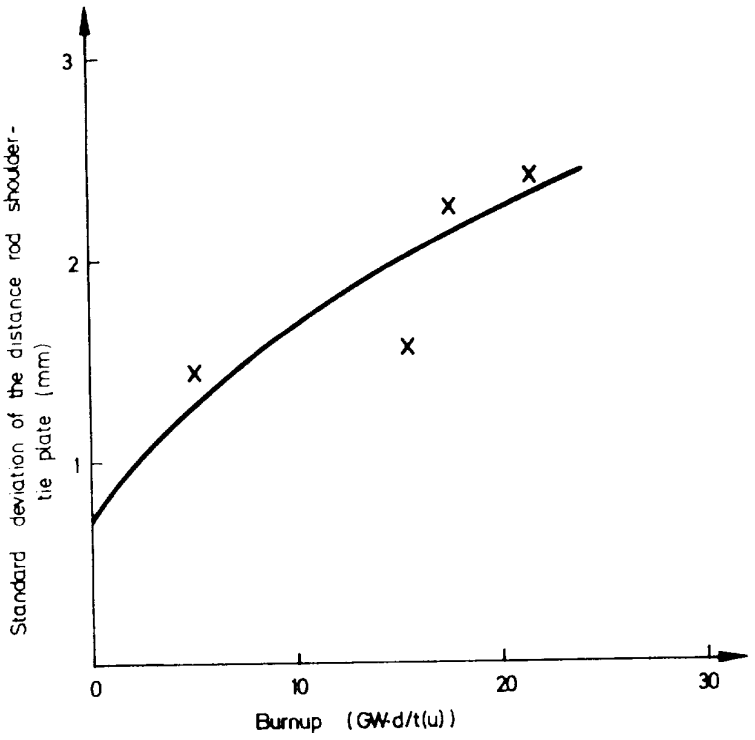


FIG. 52. *Influence of burnup on the standard deviation of the distance between the rod shoulder and the tie plate in BWR bundles.*

length increases were only due to irradiation growth and anistropic creep. Most fuel rods from other PWRs showed more growth than the fuel rods from KWO, KKS and GKN, as can be seen from Fig.51. The significant differences in the growth behaviour may partly be caused by the differences in the material condition (texture, cold work etc.) and partly by pellet-clad interaction early in life.

As can be seen from Fig.51, the length growth of various fuel rods exposed to the same neutron dose may vary from rod to rod quite markedly. This has to be taken into account, especially in BWR assembly designs where most of the rods are guided in holes of the upper tie plate. To determine a safe guide length it is necessary to take into account the manufacturing tolerances and particularly the scattering of differential growth with increasing burnup. Analysis of measurements of the distance between the top end shoulder of the fuel rods and the upper tie plate after various burnups revealed a Gaussian distribution. The standard deviation is shown in Fig.52 as a function of burnup for samples of rods from various tube suppliers with large differences in yield strength. It can be seen that the standard deviation for such tubings increases nearly linearly with increasing burnup in the given range.

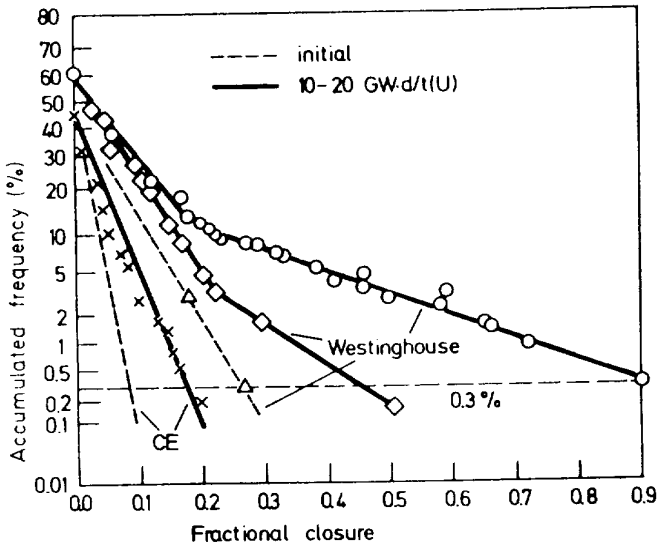


*FIG.53. Distribution of gap closure between adjacent rods due to bowing in various types of assemblies before and after irradiation* [8,110].

Length increases of the poison rods from Palisades Core I were noted to be greater than for fuel rods. These rods, which have Zircaloy cladding and are filled with $Al_2O_3$-$B_4C$ pellets, form an integral part of the fuel assembly. This larger growth of the poison rods cannot only be due to irradiation growth of Zircaloy. Interaction of cladding and pellets can be assumed to be responsible for the incremental length increase. The design was modified to provide more margin for the differential growth [17] and to reduce mechanical pellet-clad interaction.

### *4.5.2. Fuel rod bowing*

Fuel rod bowing may result from in-pile relaxation of the internal stresses or from an interaction between rods and the spacer grids of the assembly structure. Excessive fuel rod bowing can lead to local coolant flow restriction, which may result in a decreasing departure from nucleate boiling heat flux, and under certain circumstances even in enhanced corrosion at this point.

#### 4.5.2.1. Relaxation of internal stresses

The only fuel rod failures reported to be caused by rod bowing were found during the first two cycles of Dresden I. The Zircaloy tubes used for these fuel rods were 15–25% cold drawn without any subsequent annealing treatment.

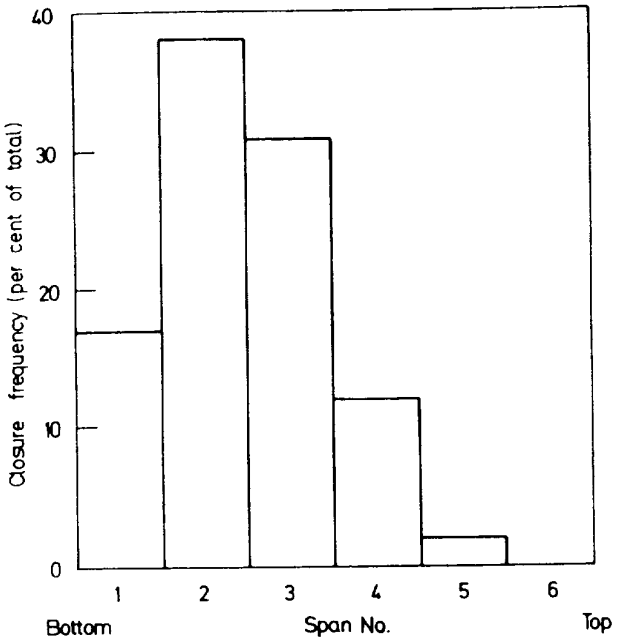


FIG. 54. *Axial distribution of significant gap closure between adjacent rods due to bowing* [111].

During operation the relaxation of the residual stresses caused bowing especially in areas of high power, and some of the bowed corner rods touched the inner side of the flow channels in the corner. This resulted in local restriction of the coolant flow and a noticeable local increase in the cladding temperature and, finally, in fuel rod failures due to excessive local corrosion. A stress-relieving annealing of the tubes for the subsequent reloads prevented the reoccurrence of this defect mechanism [17].

4.5.2.2. Grid restraint

Substantial bowing of the fuel rods and partial closure of the gaps between fuel rods has been observed in Westinghouse fuel assemblies with Zircaloy control rod guide tubes since late 1972 [110]. Since this type of bowing was not seen in earlier Westinghouse fuel with stainless steel guide tubes, it was concluded that the bowing mechanism is typical for assemblies with Zircaloy guide tubes. Therefore, extensive examination of fuel rod bowing was initiated also by other suppliers of fuel assemblies with Zircaloy guide tubes. The techniques used to measure the closure of the fuel rod spacing were (1) measurements with limited accuracy from television tapes, and (2) more accurate measurements by feeler gauges. Results of the distribution of gap closures between adjacent rods at all positions between two spacers of Westinghouse and non-Westinghouse assemblies

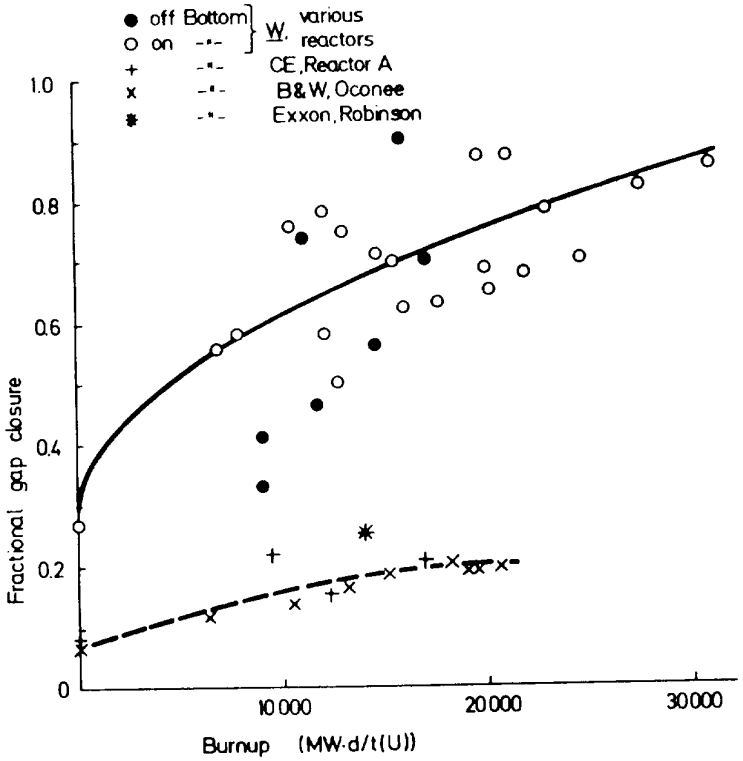


*FIG.55. Maximum gap closure between adjacent rods due to bowing (in 99.7% of all rod a function of burnup for PWR fuel assemblies from different suppliers* [8, 10, 110–112].

were reported in Refs [8,110] and are summarized in Fig.53. In all these case the deviation from the nominal gap can be well described by a Gaussian distribut As reported in Ref.[111], the maximum bowing of fuel rods is generally found between the second and the third spacer from the bottom almost independently of the design at the bottom (rods on or off bottom). Figure 54 points out this fact and shows that no significant gap closure has been seen in span 6 and that gap closure increases markedly from span 5 to span 2. The dependence of gap closure on burnup and fuel assembly design is shown in Fig.55, summarizing d from Refs [8, 10, 110–112]. The data points are verified by probability analy and give the maximum gap closure in 99.7% of all rods. It can be concluded from this figure that gap closure increases with increasing burnup, but depend on design and initial bowing. The orientation of the bowing was found to be random and reverses at each spacer grid [8, 111].

The mechanism of this bowing as proposed in Ref. [110] is the following An axial compressive end load is created by axial friction forces which result from grid spring and dimple to clad contact forces in the presence of differen fuel rod axial growth. The outermost spans in an off-bottom design (or the uppermost span in an on-bottom design) can elongate by stress-free growth. T

TABLE VII. RELATIVE STIFFNESS OF VARIOUS PWR ASSEMBLY DESIGNS

| Fuel assembly | Relative stiffness |
|---|---|
| CE, Reactor A | 2.5 |
| B&W Oconee 1 | 1.6 |
| W, 15 X 15 | 1.0 |

next span, however, must grow against the forces of one grid, the second next against the forces of two grids and so on. The maximum axial force is expected in the bottom span in an on-bottom design or in the middle span in an off-bottom design, and in an off-bottom design it should be half that in an on-bottom design. The axial compressive stresses cause bowing by creep mechanisms. The rate of bowing depends mainly on eccentricity and initial bow, and decreases with increasing time as a consequence of the relaxation of the spacer springs.

It was assumed from this analysis that an off-bottom design should show only about 40% of the maximum bowing experienced in an on-bottom design [110]. Later results, however, showed equal bowing for off and on-bottom fuel assemblies, and substantial bowing in the second span from the bottom in both cases [111]. The conclusion was that the mechanism is much more complex and should be described by a single empirical relation for the maximum gap closure in 99.7% of all rods

$$C = C_0 + 0.00342\,(BU)^{1/2}$$

where

$C$ = fractional closure
$C_0$ = fractional closure at the beginning
$BU$ = burnup in MW·d/t (U).

This empirical relation is valid for the type of assembly (design and fabrication) examined in Ref.[111]. Assemblies with different design or fabricated with other procedures do not follow the same empirical rod bowing relationship, as evident from Fig.55. In spite of the obvious contradiction of the results with on and off-bottom assemblies, the grid restraint axial growth mechanism is still considered the most probable mechanism [8]. The observed deviation from the earlier conclusion, that an off-bottom design should show significant gap closure only in the middle span, may be due to differences in the growth of the various axial spans. Assuming that some fraction of the total growth is attributed to pellet-clad interaction, the growth should be larger in the lower span than in the middle one [106].

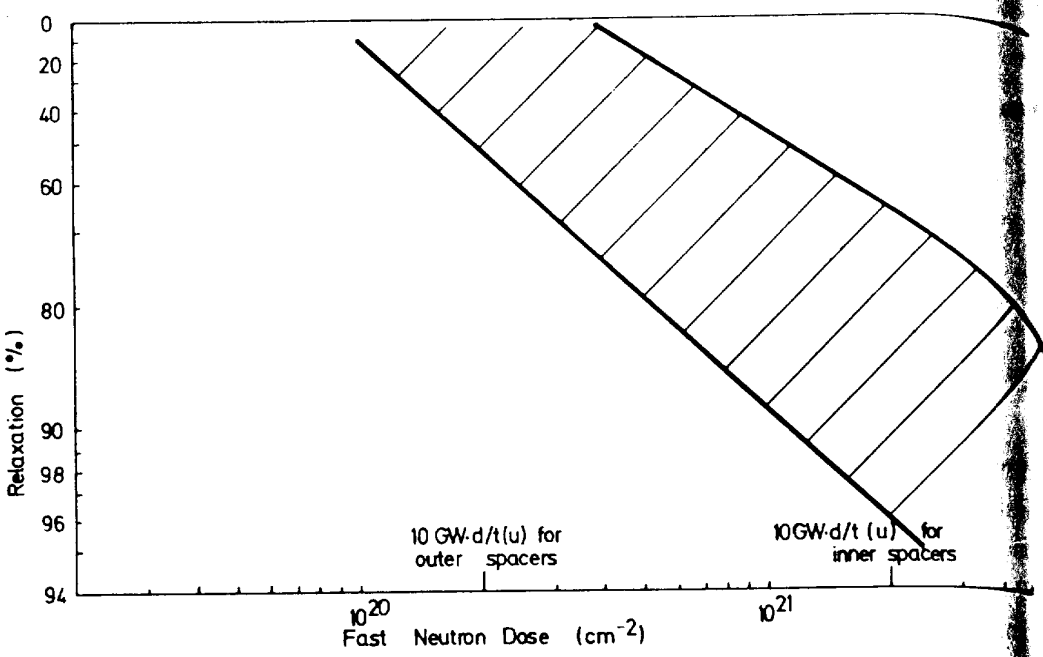


*FIG.56. Relaxation of spacer spring contact forces.*

Reference [8] points out that the magnitude of bowing depends on the distance between grid spacers, the moment of inertia of the cross-section of the cladding and the forces exerted by the grids. It is assumed that these effects can be examined by applying the equation for the elastic deformation ($\delta$) of a beam with uniform moments:

$$\delta = \frac{ML^2}{8EI}$$

$M = F\delta_0$ denotes the bending moment due to the grid forces (F) acting on a fuel rod with an initial bowing of $\delta_0$. L is the grid-to-grid distance, E is the modulus of elasticity of the cladding material, and I is the moment of inertia.

This formula can also be used to compare the stiffness of different fuel designs, as shown in Table VII. The difference in the stiffness may be one of the reasons for the reported differences in the bowing characteristics of different fuel designs.

The magnitude of the compressive axial force caused by the grids may depend on the technique used during assembling. A pushing procedure, for instance, results in compressive forces early in life, whereas a pulling procedure initially leads to tensile stresses, and the maximum compressive forces due to differential growth of the fuel rods are built up later in life. The maximum axial forces are given by the restraint of the grids, which are determined by the friction coefficient and the spring load of the spacer springs. Both vary from design to

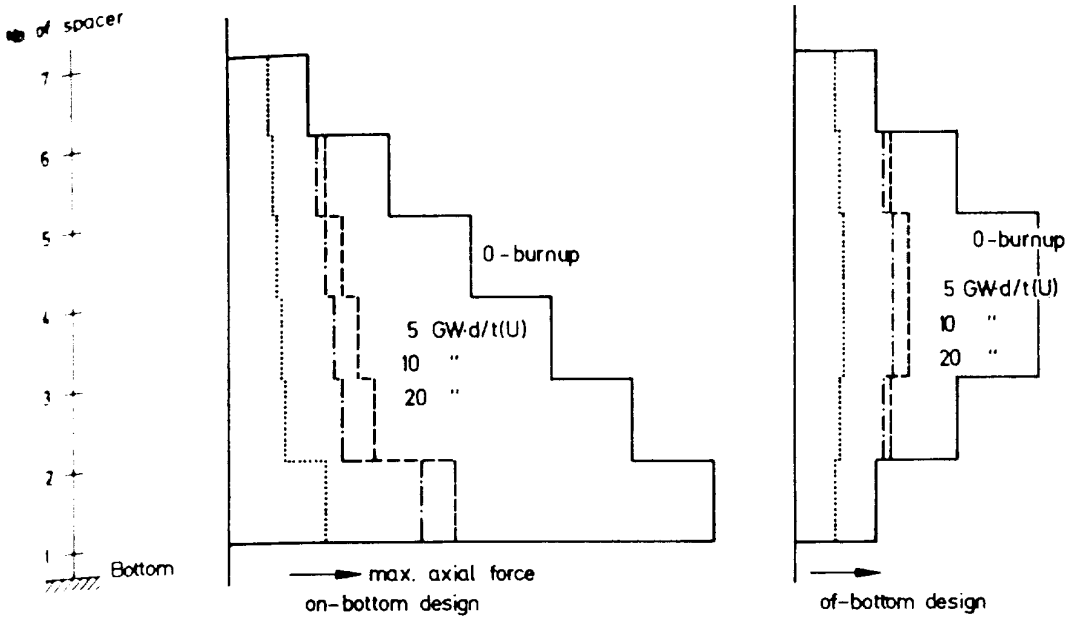


*FIG.57. Maximum axial force between different spacers (schematically).*

design but the spring load is drastically reduced during the exposure by radiation-induced relaxation, as can be verified from Fig.56. This figure shows the range of relaxation found in different spring materials plotted against fast neutron fluence. Because the neutron flux at the positions of the first and the last spacer grid is about one order of magnitude less than at the positions inbetween, the springs of the inner spacers relax faster than those of the first and the last ones. Figure 57 shows the maximum possible compressive forces over the length of the fuel rod for an on-bottom and an off-bottom design. The forces relax rapidly in the burnup range up to 5 GW·d/t (U). Since the forces at burnups in excess of 5 GW·d/t (U) are mainly estimated from the restraint forces of the two outermost spacer grids, the difference between the two designs diminishes.

The initial bowing has also an important influence on the fuel rod bowing, because the rate of bowing increases exponentially with increasing initial bowing. Accordingly, the highest bowing would be expected in those assemblies with the highest initial bowing and the highest initial compressive forces. The standard deviation in the gap width between two fuel rods as found by the various PWR fuel manufacturers is given in Table VIII. The lowest initial standard deviation in the gap width is found in fuel assemblies where fuel rods are pulled into the skeleton (KWU). The difference in the bowing tendency for different designs and fabrication routines (Fig.55) may thus be partly attributed to different initial bowing and different initial axial forces.

TABLE VIII. AS-FABRICATED STANDARD DEVIATION OF GAP WIDTH BETWEEN ADJACENT RODS IN PWR ASSEMBLIES

| Manufacturer | As-fabricated standard gap width deviation (% of nominal) | Reference |
|---|---|---|
| B & W | 2.6 | [10] |
| CE | 2.9 | [8] |
| KWU | 1.9 | KWU measurements |
| W | 9.9 [a] | [111] |

[a] This number is not derived from accurate measurements but is thought to be typical for a distribution found by TV. The actual initial standard deviation may be less.

The reason why assemblies with stainless steel structure have never shown any significant bowing is certainly the large difference in the thermal expansion coefficient of the Zircaloy fuel rods and the stainless steel control rod guide tubes leading always to tensile stresses early in life. About half a cycle of operation is needed to reverse the stress by rod growth.

In spite of the frequent observations of significant gap closure in some PWR fuel assemblies with Zircaloy guide tubes, there have been no defects or other anomalies caused by fuel rod bowing. This is in agreement with theoretical safety considerations [111] and tests to measure the effect of rod-to-rod contact. The reduction in the 'departure of nucleate boiling' (DNB) heat flux was found to be relatively small and could be balanced by generic margins in the DNB limits [9]. Furthermore, it was shown by analytical treatment [111] that the vibration-induced fretting of contacting rods is negligible.

### *4.5.3. Fuel assembly bowing*

Fuel assembly bowing may lead to problems in PWR systems during unloading and loading. The bowing of PWR fuel assemblies is determined by the behaviour of the control rod guide tubes under (1) the influence of cross-flow and hold-down forces, and (2) the growth of guide tubes. Fuel channel bowing in BWRs can cause mechanical interaction with the control rod blades. The bowing of assemblies is always determined by the channels, which are much stiffer than the fuel rod bundle. The bowing may result from (1) the relaxation

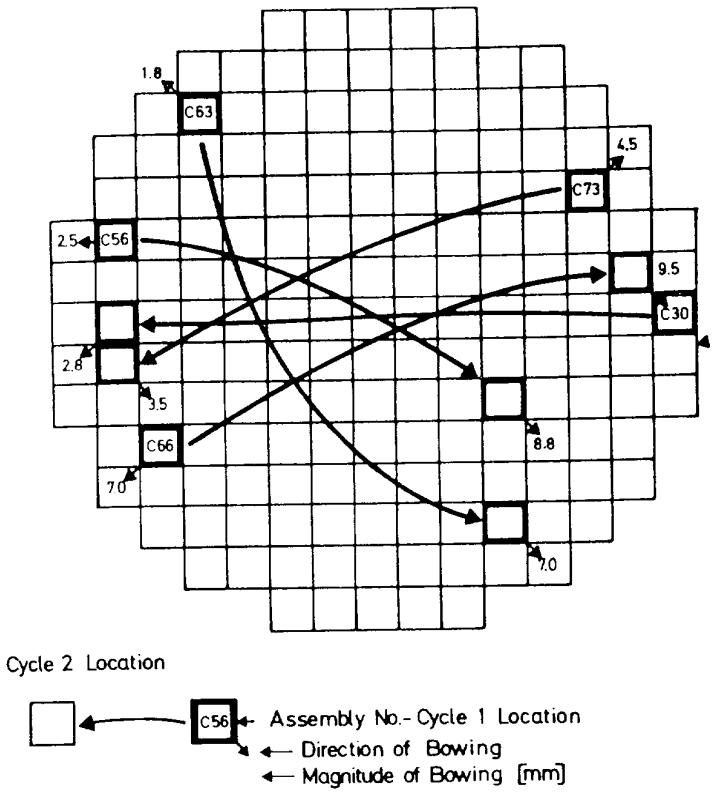


*FIG.58. Fuel assembly bowing in Oconee-1 at the end of cycles 1 and 2* [10].

of internal stresses, (2) differential growth due to material inhomogeneities, (3) differential growth due to flux gradients, (4) irradiation creep, and (5) differential thermal elongation.

Assembly bowing was already observed in PWR assemblies with stainless steel guide tubes. However, larger bowing may be experienced by assemblies with Zircaloy guide tubes. Measurements on the bowing of several assemblies with Zircaloy guide tubes were reported in Ref.[10] and are shown in Fig.58. At the end of cycle 1 this assembly bowing was outwards from the centre of the core. The magnitude (vector sum of the perpendicular components) varied from 1.8 to 7.0 mm. Observations on approximately 30 additional discharged assemblies at the end of cycle 1 showed similar direction and magnitude. After cycle 1 the five assemblies shown in Fig.58 were shuffled across the core without rotation, i.e. they began cycle 2 with the bowing directed towards the centre of the core. At the end of cycle 2 the bowing was reversed, again showing an outward tendency. The magnitude was slightly higher, on average, and some assemblies appeared to retain a portion of their EOC-1 bowing. This bowing is probably initiated by the cross-flow from the centre to the core periphery and is due to irradiation creep under the action of the hold-down forces. However, no detailed

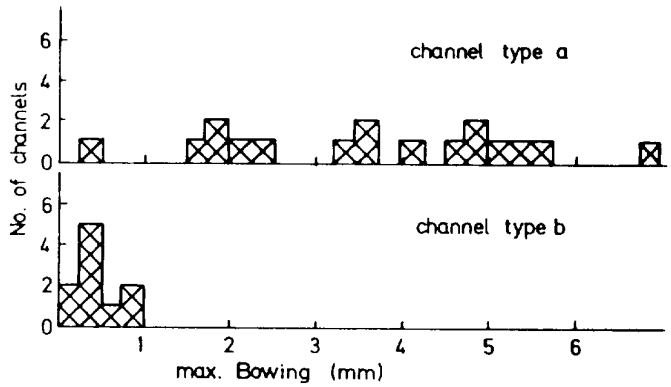


*FIG.59. Comparison of the maximum bowing of various channels after 4–54 GW·d/t (U) burnup.*

Substantial BWR channel bowing up to 8.5 mm independent of burnup was first reported in Ref.[113]. Later KWU measurements showed that the magnitude of bowing depends on the fabrication routine, as can be seen from Fig.59, and that some of this bowing may result from differences in the growth due to the gradient in neutron flux. The maximum gradient in the fast flux of about 20–30% exists at the core periphery (two outer rows of fuel assemblies). However, after one year of operation the channel bowing resulting from this effect should be less than 1 mm (0.8–0.9 mm) according to measurements on modern channels. It is suggested that the larger bowing observed on older channels resulted mainly from internal stresses or from different growth characteristics of the two half-shells from which the channels were fabricated.

Channel bowing can be minimized by appropriate fuel management schemes and the use of fabrication routines resulting in low internal stresses and little inhomogeneities in the material. The half-shells should be selected from the same batch of sheet raw material.

## 4.6. Wear and fretting corrosion

### *4.6.1. General mechanism*

Wear can result from the following three basic mechanisms: adhesion, abrasion, and surface fatigue. Adhesive wear is caused by the generation and destruction of microwelds between the surfaces of two contacting and sliding components. Abrasive wear is obtained when a hard asperity or particle slides over a soft surface. Motion between soft and hard surfaces causes the asperity or particle to plough or cut a groove into the softer material. The fatigue process results when a surface is subject to repeated strain cycling by continuous sliding,

sliding or impacting motions. This cycling can initiate cracks on or near the surface.

Fretting corrosion involves both chemical and mechanical effects. In materials whose corrosion resistance is due to the passivity of a preformed oxide layer continual removal of the oxide film results not only in mechanical wear but also in a high local corrosion rate. The fretting of Zircaloy components under operation may be caused by a combination of all these mechanisms.

The extent of fretting depends mainly on the contact pressure, on the number, frequency and amplitude of cycles, and on the temperature. In KWU experiments the weight loss of Zircaloy was found to increase linearly with the contact pressure, whereas other results [114] showed a tendency for saturation. The influence of the number of cycles on the weight loss is normally found to be linear (Fig.60) after an initial period characterized by either rapid loss or incubation. The effect of the amplitude of the relative motion (slip) on the weight loss was also found to be linear in KWU experiments, a result that is in general agreement with other measurements (e.g. Ref.[114]).

For analytical predictions of the fretting wear of Zircaloy components the Archard equation [115] for sliding

$$V = \frac{S\,F\,L}{3H}$$

is often applied, where

V = wear volume ($mm^3$)
S = wear coefficient
F = normal force on contacting surfaces (N)
L = total length of relative motion (mm)
H = hardness ($N/mm^2$).

The wear coefficient has to be determined by experiments simulating the real conditions as closely as possible. According to KWU calculations and other published results, the wear coefficient is between $10^{-1}$ and $10^{-5}$, depending on the material in contact (stainless steel, Inconel or Zircaloy), the temperature, frequency and other details. Fretting of stainless steel or Inconel components with Zircaloy components causes much more metal loss in the Zircaloy component than in the other component.

As described in section 4.2, part of the hydrogen formed by corrosion of Zircaloy is picked up by the metal. Because the corrosion rate is enhanced in surface areas influenced by fretting, the hydrogen pickup should also be enhanced. According to out-of-pile tests at 300°C the hydrogen pickup is between 1 to 50 $mg/cm^2 \cdot d$ depending on frequency and other test details (e.g. Refs [116, 117]). However, KWU examinations of the wear area of fuel rods from Gundremmingen first core, where fretting was caused by loose stainless steel wires,

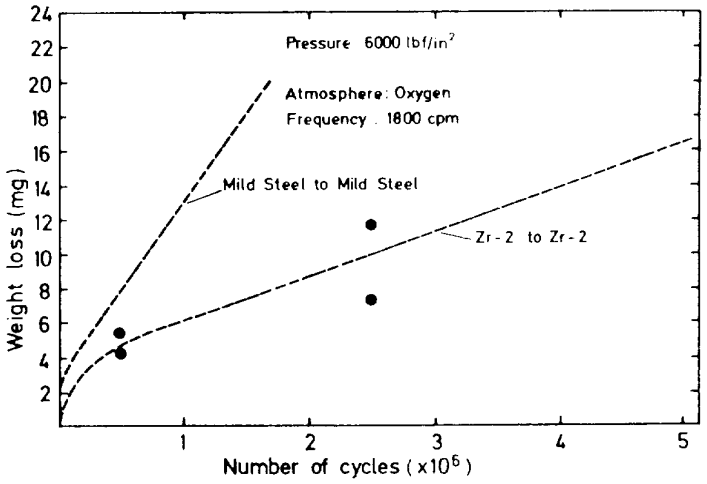


*FIG.60. Effect of time on fretting of Zircaloy.*

showed the same hydride concentration in the wear areas as in other non-fretting areas or cross-sections from non-fretting fuel rods.

Similar examinations of fuel rods defected by fretting against stainless steel spacers in the VBWR [118] and of pressure tubes fretted by excessive assembly vibration [119] also did not indicate any noticeable increase in the hydride concentration near the fretting marks. The discrepancy between these results and the expected behaviour may be partly due to the high diffusivity of hydrogen at operating temperatures, leading to fast migration of the excess hydrogen away from the fretting mark. Therefore, an increase in the hydride concentration due to fretting corrosion in water reactors should only be expected if very large areas are influenced by fretting.

### *4.6.2. Observations from fretting incidences*

During operation all fuel pins, fuel assemblies and core internals vibrate to a certain extent. The assembly components that have suffered from severe fretting in the past and the cause of the fretting already have been summarized in Table IV.

Spring-type spacer grids are used in all modern fuel assemblies. The spring forces are designed to prevent fuel pins lifting off the fixing supports (dimples) under vibrational forces. The vibrational driving forces on fuel rods are largest at the lower end of the assembly because of the coolant turbulence at the bottom nozzle. Therefore, nearly all the fretting problems have been observed at the lowest spacer grid or at the lower end support. The fretting effects at spacers observed in PWRs were caused by low spring forces of the spacers or spring

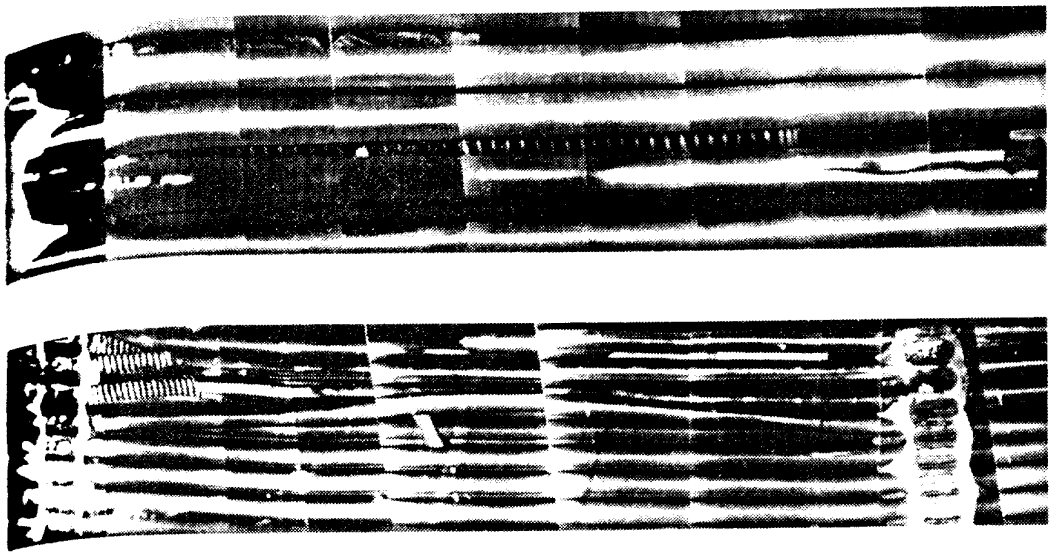

*FIG. 61. Defects due to baffle leaks in Zorita PWR (private communication).*

deformations that resulted in a loss of contact. Since significant fretting has never been observed on the upper spacers, it can be concluded that loss of contact at higher positions is less critical. This is in agreement with out-of-pile test where loss of contact at the springs of intermediate spacers did not lead to noticeable fretting [8].

In BWR assemblies the situation may be more complex since an additional peak of the vibrational driving forces is expected about at the mid-plane of the assemblies. Vibration measurements under two-phase flow conditions showed that the vibration amplitude increases with increasing void, reaches a maximum at 10–20% void, and decreases again to the same amplitude as in single-phase flow conditions at about 50% void [120]. However, no fretting problems have been seen with spacers in BWRs. The only fretting defects observed were located at the lower tie plate (Gundremmingen). The clearance between bore and pin is normally in the range of 0.1–0.2 mm. In the case of the fretted pins the clearance was probably in excess of 1 mm. Another rod found with a 1 mm clearance in the top nozzle did not show any signs of mechanical interaction, confirming that the vibrational driving forces are very small at the upper end.

Fretting incidences with loose particles have been rather seldom. This is due to the design of the inlet nozzle, which prevents larger particles from entering the assembly. Small stainless steel wires caught in the spacer grids caused fretting in the Gundremmingen first core. A later improvement of the spacer design significantly reduced the risk of fretting due to such small particles. The fretting observed in Stade after the first cycle is also a special case not possible in a more modern PWR. Here at some corner assemblies the core baffle does

not extend along the entire length of the fuel rods and allows the contact of loose particles at the lower end of the rods. Fretting damage was seen in Westinghouse PWRs on a few peripheral assemblies and was caused by high velocity coolant cross-flow leaking through gaps in the corner joints in the baffle. The cross-flow caused excessive rod vibration and fretting through cladding in the grid support areas (Fig.61). Corrective action was taken by repairing the baffle joints to eliminate the leakage. Baffle designs in later eliminated the gaps completely [17].

Fretting defects in some first core assemblies in Borssele were a result hold-down spring forces being below the design limit. Axial oscillations of assemblies during startup led to the distortion of some outer spacer grid bands by wear and later to fretting failures of the grids at these positions.

Fretting of flow channels were caused by excessive vibration of temporary control curtains, in-core flux monitors and secondary neutron sources in some BWRs. The amount of damage varied from minor to extensive. The most significant damage was observed in Mühleberg and Pilgrim where the wall was perforated in 8 and 6 channels respectively, resulting in a narrow vertical slot. In earlier BWR designs leakage between the lower tie plate and the channel box was the only source of bypass flow in the gap between the assemblies, but later plants had additional bypass flow holes in the core support plate. Because no significant wear was observed in over 6000 channels from reactors without bypass holes, the vibration of the curtains and in-core flux monitors was attributed to cross-flow close to the bypass flow holes in the core support plate. This was later confirmed by simulation tests [17]. The corrective action was plugging of the bypass flow holes.

## 5. OPERATIONAL BEHAVIOUR OF DEFECTIVE FUEL

An understanding of the behaviour of defective fuel under continuous irradiation is necessary because the primary failure may occur early in life, i.e. early in the operational cycle of a reactor. In most European (all Federal German) reactors sipping is performed at the end of each operational cycle during refuelling if fuel failures are expected from the coolant activity, in order to limit the exposure time of defective fuel to a maximum of one cycle. However, sometimes no sipping testing is done during refuelling and the behaviour of defective fuel under continued exposure up to several years is of interest.

### 5.1. Operational consequences of defective fuel rods

Defective fuel rods release fission products into the primary coolant. The resulting coolant activity is a balance between the release of active species through

TABLE IX. POSSIBLE INFLUENCE OF CONTINUED EXPOSURE AFTER FUEL ROD DEFECTION [123]

| Changes caused by defects | Consequences |
|---|---|
| Clad | |
| Oxidation of inner surface and enhanced general $H_2$ pickup | Low temperature embrittlement |
| Localized $H_2$ pickup | Secondary hydride defects |
| Fuel | |
| Oxidation | Volume increase and diameter increase |
| | Decrease in thermal conductivity, increase in fuel temperature |
| Leaching and loss of fuel | Circuit contamination |

the cladding perforation, the decay and the removal of active species by the purification system of the primary circuit.

The fission product release rate is a complex function of the plant operation characteristics. Systematically, the following cases can be distinguished [121]:

(a) Slow or sudden release of stored fission products immediately after clad perforation
(b) Steady-state release of fission products from existing fuel failures during constant power operation of a reactor
(c) Fission product spiking during shutdown
(d) Moderately increased release rate during non-steady operation of a plant [122].

Taking into account the plant layout, the fission product release rates of different isotopes can be calculated from the coolant activity under steady-state conditions. These steady-state release rates are frequently used for an estimation of the number of defective rods in a core using empirical data for calibration. However, the release rates depend on the rod power at the defect position, on the size of the defect, and on several other variables. Therefore, uncertainties up to a factor of at least 2 must be accepted. On the other hand, a defective rod may experience some degradation (changes in the number and size of the defects and in material properties) during continued operation so that a perfect 'steady state' will never be reached.

In the case of high coolant activity a cautious mode of operation avoiding severe load changes can be adopted with the intention to keep the time-averaged coolant activity as low as possible (avoiding spiking effects).

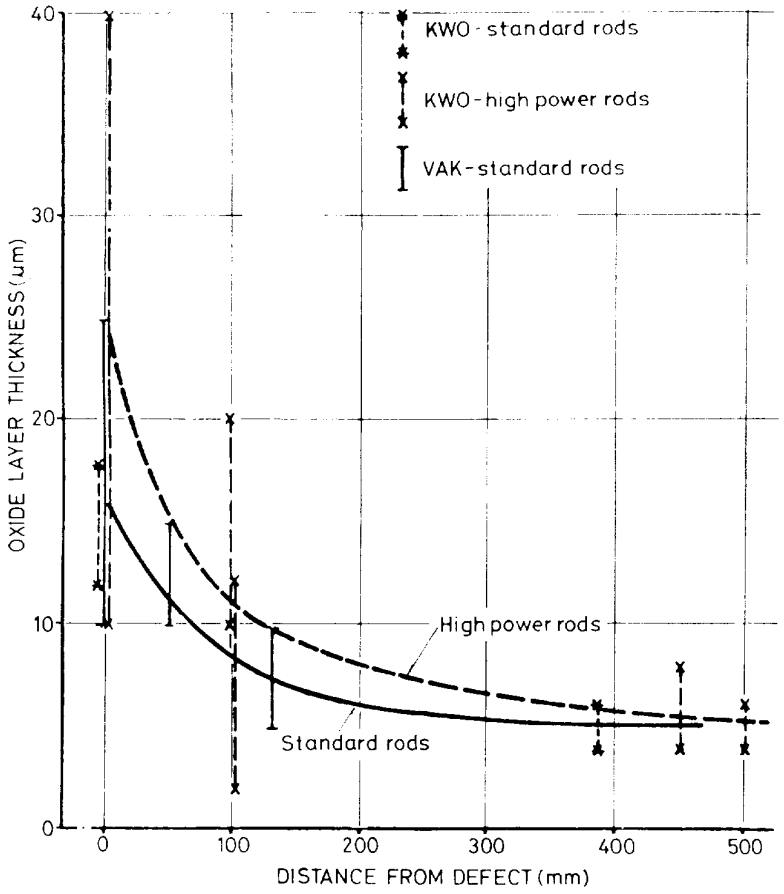


*FIG.62. Inner oxide layer thickness as a function of the distance from the cladding defect* [123]

## 5.2. Defective fuel rod behaviour

Once a fuel rod is perforated, water or steam can enter. The possible effects of continued exposure after perforation are summarized in Table IX together with their consequences. None of these consequences would in general forbid further operation. However, by operation through several cycles the primary coolant activity might increase to an inconvenient level by additional failures or secondary failures of already perforated rods.

### *5.2.1. Cladding behaviour*

The water or steam entering a perforated fuel rod provides a large source of hydrogen and oxygen. This leads to oxidation accompanied by a high hydrogen uptake at the inside of the cladding. The corrosion rate at the inside of the cladding is larger than at the outside of the cladding because of its higher

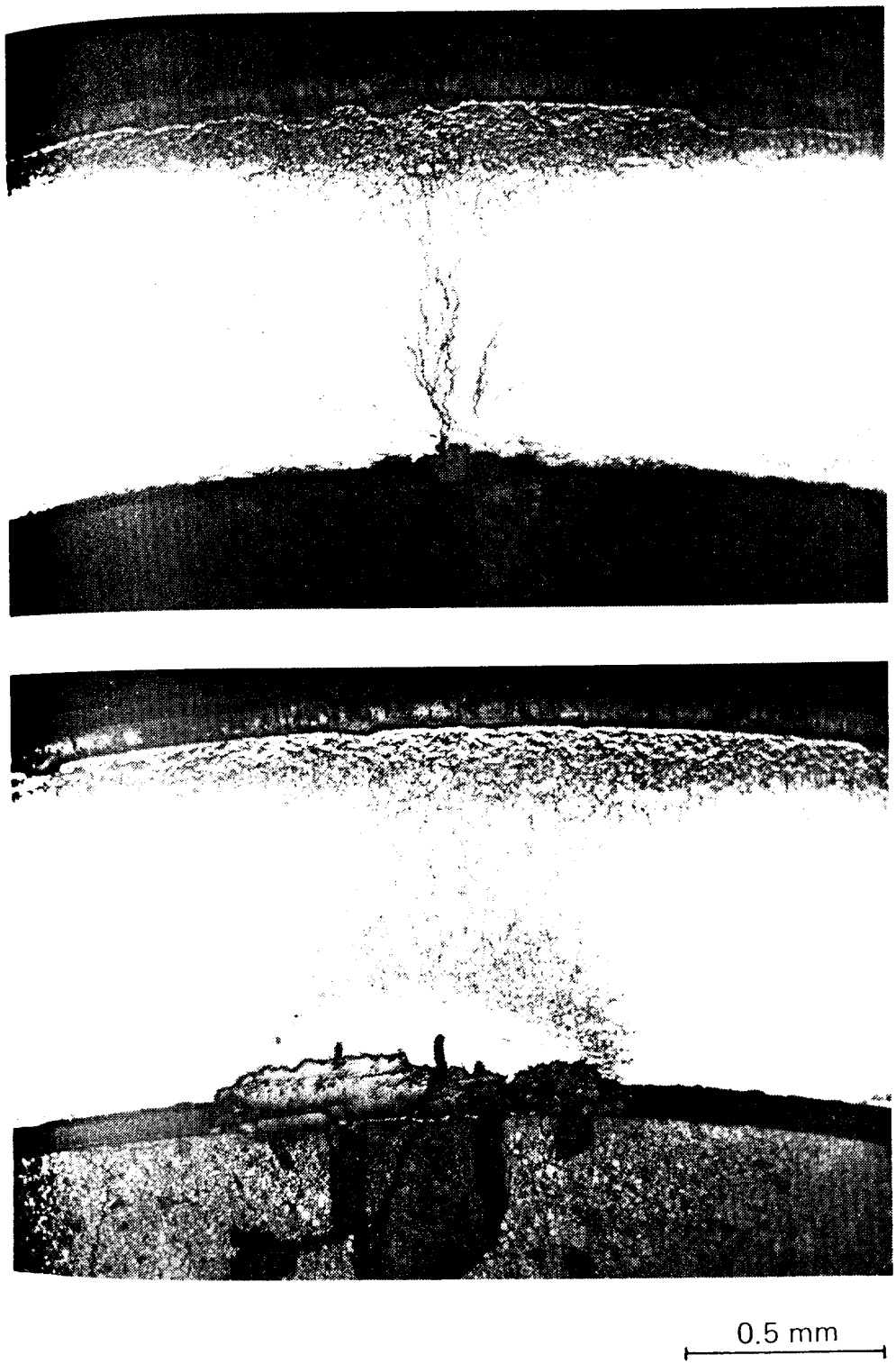


FIG. 63. *Oxide patches and enhanced hydriding of the inner clad surface of defective rods* [123].

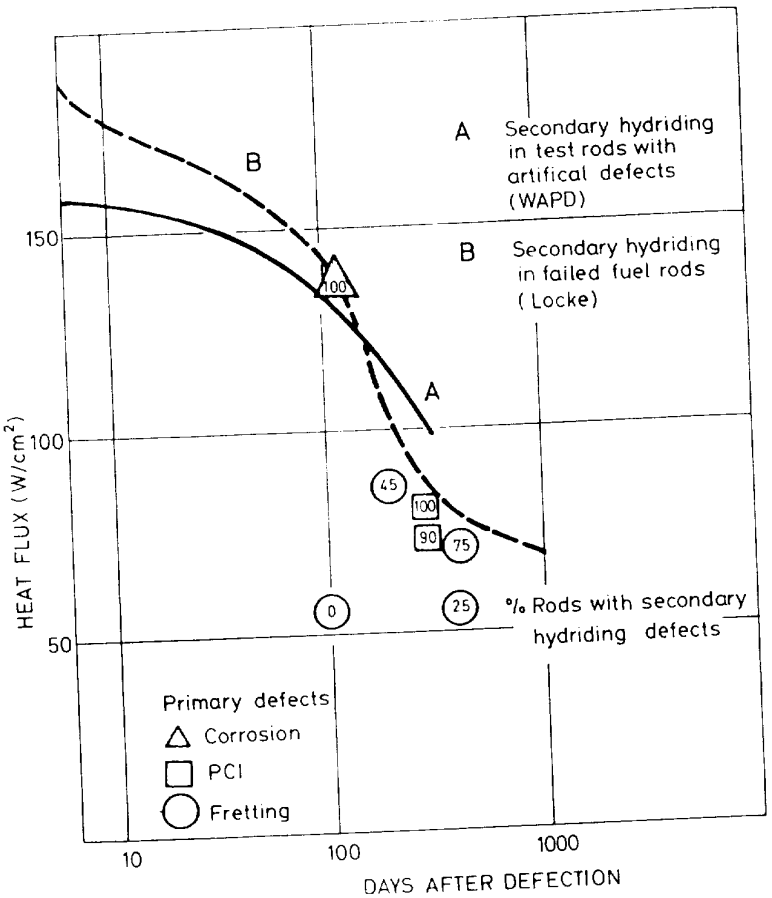


*FIG.64. Development of secondary hydriding defects after a primary defect* [123–125].

temperature (350–430°C). The corrosion rate on the inner side of the cladding may reach rates of 0.02–0.24 μm/d (if out-of-pile rate constants are assumed). According to post-irradiation examinations [123], mainly a uniform oxide layer is formed, the thickness of which decreases rapidly with increasing distance from the defect, as can be seen in Fig.62. From these results it can be concluded that the supply of oxygen is limited to the area near the perforation as a consequence of gap closure and oxygen starvation.

Besides the uniform oxide layer, occasionally local oxide patches with thicknesses up to 300 μm are observed opposite radial pellet cracks. It is suggested in Ref.[123] that these oxide patches are the result of local depassivation of the uniform oxide layer by fission products like iodine and caesium.

The oxidation of the cladding and the fuel as well as radiolysis leads to the formation of hydrogen. This hydrogen is mostly absorbed by the cladding and can be the reason for secondary defects at positions where the hydrogen pickup is locally enhanced (see section 4.1). Two different theories have been published

in recent years on the mechanism responsible for locally enhanced hydrogen pickup in defective fuel rods [123, 124]. One of these mechanisms is based on the oxygen starvation mentioned above, which is accompanied by an increasing hydrogen partial pressure (see section 4.1). The other mechanism is based on observations from post-irradiation examination: it is suggested that absorption is uniform in areas where the oxide layer is uniform, but markedly enhanced at the areas of oxide patches. It is assumed that local loss of passivity due to fission products is responsible for these oxide patches (Fig.63). Localized hydriding appears first in the form of blisters, bulges and finally as cracked areas and holes. Hydriding of the upper end plug welds has also often been observed.

Secondary defects due to localized hydriding are generally concentrated at axial rod positions of maximum cladding temperatures. For PWR fuel rods this is in the upper half of the rod, for BWR fuel it is at the position of maximum rod power and thus depends on the position of the control rods [123].

The first analyses of the conditions leading to secondary hydride failures were performed by Lustman [125]. From intentionally defected fuel rods of the Shippingport core 1 blanket (Fig.64, curve A) a correlation was derived between the time of formation of secondary hydride failures and the heat flux. Later, a more extended analysis by Locke [124, 126] revealed a similar correlation, which is also shown in Fig. 64 (curve B). As can be seen from the figure, later observations from BWRs and PWRs [123] fit well with these correlations.

Uniform hydrogen pickup, which is the normal mode of absorption, has no real detrimental effect on the cladding behaviour. Although relatively low concentrations reduce the room temperature ductility, a significant influence on the mechanical properties at operating temperatures occurs only at very high concentrations well above 1000 ppm.

### 5.2.2. *Fuel pellet behaviour*

In sound fuel rods the fuel remains almost stoichiometric, but in a defective fuel rod the fuel is oxidized. The degree of oxidation depends on

The time of exposure after the cladding defect occurred

The size of the defect

The fuel temperature

The water chemistry.

Measurements on the O:U ratio of defective fuel are very rare. According to Ref.[123], the increase in O:U ratio is most pronounced at the outer surface of the pellets. A dense surface layer (probably $U_3O_8$) is often found in ceramographic cross-sections of pellets from defective rods. The thickness of this layer varies, depending on the type of defect and the rod power. According to Ref.[123] the $U_3O_8$ layer is small (10–30 $\mu$m) opposite small cladding defects,

even after one year of operation. Thick $U_3O_8$ layers (up to 1000 $\mu$m) develop at large cladding defects. However, in low-rated fuel rods they rapidly decrease in thickness with increasing distance from the defect. Only in high-rated fuel rods does the $U_3O_8$ layer extend over longer distances apart from the position of the cladding perforation. The increase in stoichiometry results in a decrease in thermal conductivity of the $UO_2$ [127] and, consequently, in a rise of the pellet centre temperature. Since the self-diffusion and probably also the sublimation process is enhanced in $UO_{2+x}$ [123], equiaxed and columnar grain growth is often observed in defective fuel rods, even at positions of low linear heat generation rates.

Another consequence of the increase in the U:O ratio and of the formation of an $U_3O_8$ layer is a small diameter increase (maximum 100 $\mu$m) of a defect fuel rod [123].

$UO_2$ exhibits excellent corrosion resistance to the coolant water. Direct exposure of fuel to the coolant causes only some minor leaching of the fuel. The amount of fuel loss through a defect is typically in the range of $10^{-3}$ to 10 g/a, depending mainly on the size of the defect [123].

### *5.2.3. Rod behaviour*

A postulated secondary defect mechanism, which was discussed in the early days, is waterlogging of a defective fuel rod. This mechanism can be described as follows. Coolant water may be trapped in a defective fuel rod during reactor shutdown. If the steam formed during a fast return to power is not able to escape through the hole fast enough, the rod may burst as a result of the high internal overpressure.

Waterlogging has been observed in fuel rods containing low-density fuel of less than 80% theoretical density (TD) [128]. This effect is extremely rare in fuel rods with the currently used densities of 94–95% TD [123].

It has been argued that long-term operation of defective fuel rods can lead to fretting defects in neighbouring fuel rods through debris or through the broken ends of the defective rods. However, this effect has been observed in only a few cases and has never been severe [123].

## 5.3. Discharge criteria

All power reactors can be operated with a certain amount of leaking fuel rods without exceeding any licensed limits of site activity release especially if they have a gaseous waste delay bed. Since the defect level of modern fuel is generally in the range of zero to only 0.1%, there is usually a wide margin available. Therefore, the practice used especially in PWRs in USA of operating defective fuel over its full reactivity lifetime is acceptable.

However, there are trends in several countries to reduce the allowed failure rate by more restrictive specifications, particularly for the activity in the coolant water. These trends are based on the desire to decrease the possible activity release to the environment in the event of coolant leakage. The authors think that a practicable way to fulfil the above requirements is to remove the defective fuel assemblies at each refuelling outage after being identified by sipping if a certain coolant activity is exceeded.

In pressure tube reactors all fuel assemblies can be monitored in respect to fission product release and can be discharged during operation. Reference [129] points out that under such easy conditions defective fuel assemblies should be discharged before severe leakage of fission products occurs.

## REFERENCES


[1] BOBE, P.E., Rep. NUREG-0032 (1976).
[2] LOCKE, D.H., Nucl. Eng. Des. 33 (1975) 94.
[3] ZEBROSKI, E., LEVENSON, M., Annual Review of Energy (HOLLANDER, J., Ed.), 1 (1976) 101.
[4] ROBERTSON, J.A.L., Proc. Joint Top. Meeting Commercial Nuclear Fuel Today, Toronto (1975) 2–1.
[5] PICKMAN, D.O., INGLIS, G.H., Nuclear Power and its Fuel Cycle (Proc. Conf. Salzburg, 1977) 2, IAEA, Vienna (1977) 607.
[6] FANJOY, G.R., BAIN, A.S., Nuclear Power and its Fuel Cycle (Proc. Conf. Salzburg, 1977) 2, IAEA, Vienna (1977) 595.
[7] PROEBSTLE, R.A., BAILY, W.E., KLEPFER, H.H., Am. Nucl. Soc. Topical Meeting Water Reactor Fuel Performance, St. Charles (1977) 38.
[8] ANDREWS, M.G., Am. Nucl. Soc. Topical Meeting Water Reactor Fuel Performance, St. Charles (1977) 50.
[9] BOMAN, L.H., CAYE, T.E., CERNI, S., Am. Nucl. Soc. Topical Meeting Water Reactor Fuel Performance, St. Charles (1977) 60.
[10] MONTGOMERY, M.H., MAYER, J.T., FRECH, D., Am. Nucl. Soc. Topical Meeting Water Reactor Fuel Performance, St. Charles (1977) 71.
[11] STRASSER, A.A., LINDQUIST, K.O., Am. Nucl. Soc. Topical Meeting Water Reactor Fuel Performance, St. Charles (1977) 18.
[12] ALMGREM, B., Enlarged Halden Progress Group Meeting Water Reactor Fuel Performance, Sanderstølen (1977) 2/6.
[13] KNÖDLER, D., STEHLE, H., NUCLEX-75 Techn. Meeting No.6, 1975.
[14] OLSHAUSEN, K.D., Enlarged Halden Progress Group Meeting, Sanderstølen, 1976; Rep. HPR 195 (1976).
[15] HOLZER, R., KNÖDLER, D., STEHLE, H., Am. Nucl. Soc. Topical Meeting Water Reactor Fuel Performance, St. Charles (1977) 207.
[16] FÜHRMANN, N., PASUPATHI, V., CORSETTI, L.V., Am. Nucl. Soc. Topical Meeting Water Reactor Fuel Performance, St. Charles (1977) 262.
[17] Nuclear Power Engineering, Experience, Vol.PWR-2 and BWR-2, Experience, Section I - Fuel.
[18] KRAMER, F.W., Proc. Topical Meeting Commercial Nuclear Fuel Technology Today, Toronto (1975) 1–50.

[19] Discussion, Meeting Commercial Nuclear Fuel Technology Today, Toronto, 1975.
[20] CANDON, J.D., Am. Nucl. Soc. Topical Meeting Water Reactor Fuel Performance, St. Charles (1977) 13.
[21] PROEBSTLE, R.A., et al., Proc. Topical Meeting Commercial Nuclear Fuel Technolo Today, Toronto (1975) 2–15.
[22] PICKMAN, D.O., Nucl. Eng. Des. **33** (1975) 141.
[23] GARZAROLLI, F., et al., Reaktortagung Bonn (1971) 547.
[24] ASSMANN, H., et al., AED-CONF.-71-100-27 (1971).
[25] ARNESSEN, P., Enlarged Halden Programme Group Meeting, Rep. HPR-173 (1973)
[26] ASSMANN, H., MATHIEU, N., 79th Ann. Meeting American Ceramic Soc., Cincinn AED-Conf-76-194-007 (1976).
[27] GARZAROLLI, F., et al., Br. Nucl. Energy Soc. Conf. Nuclear Fuel Performance, L (1973) 71.1.
[28] FRESHLEY, M.D., FLAHERTY, W.J., Rep. HW-81600 (1974) 4.5.
[29] LUNDE, L., HPR 173 (1973) Paper 12.
[30] MARSHALL, R.P., J. Less-Common Met. **13** (1967) 45.
[31] SHANNON, D.W., Rep. HW-76562 Rev. (1963).
[32] GIBBY, R.L., Rep. BNWL-150 (1965) 3.11.
[33] BOYLE, R.F., KISIEL, T.J., Rep. WAPD-BT-10 (1958) 31.
[34] ZIMA, G.E., Rep. HW-66537 (1960).
[35] ADAMSON, M.G., AITKEN, E.A., EVANS, S.K., DAVIES, J.H., Thermodynamic Nuclear Materials 1974 (Proc. Symp. Vienna, 1974) **1**, IAEA, Vienna (1975) 59.
[36] JOON, J., Reaktortagung Hamburg (1972) 233.
[37] DUNCAN, R.N., et al., Nucl. Applic. **1** (1965) 413.
[38] ARMIJO, J.S., Corrosion **21** (1965) 235.
[39] GARZAROLLI, F., et al., Reaktortagung Bonn (1971) 566.
[40] KNAAB, H., STEHLE, H., Nukleonik 7(1965) 209.
[41] LUNDE, L., Nucl. Eng. Des. **33** (1975) 178.
[42] GARLICK, A., et al., J. Br. Nucl. Energy Soc. **16** (1977) 77.
[43] MATHERN, P.K., RIESS, R., Power Reactor Water Chemistry Session Annual A Soc. Conf. San Francisco (1975).
[44] STEHLE, H., et al., Nucl. Eng. Des. **33** (1975) 155.
[45] GARZAROLLI, F., et al., 4th Int. Symp. Zirconium in the Nuclear Industry, Stratford-on-Avon (1978).
[46] DELAFOSSE, J., POEYMENGE, N., Proc. Conf. Use of Zirconium Alloys in N Reactors, Marianske, Lazine, CSSR (1966) 271.
[47] BERRY, E., ASTM Spec. Tech. Pub. 368 (1963) 28.
[48] DOUGLASS, D.C., The Metallurgy of Zirconium, At. Energy Rev., Suppl. (19
[49] PARRY, G.W., EVANS, W., Nucleonics **22** (1964) 65.
[50] HARDIE, D., J. Nucl. Mat. **15** (1965) 208.
[51] GARZAROLLI, F., MANZEL, R., Reaktortagung, Mannheim (1977) 477.
[52] DAVIES, J.H., et al., Am. Nucl. Soc. Topical Meeting Water Reactor Fuel Per St. Charles (1977) 230.
[53] MOGARD, H., AAS, S., JUNKRANS, S., Peaceful Uses of Atomic Energy (Pr Geneva, 1971) **10**, UN, New York, and IAEA, Vienna (1971) 273.
[54] ROBERTSON, J.A.L., Eng. J. (Montreal), (Nov./Dec. 1972) 9.
[55] AAS, S., OLSHAUSEN, K.D., VIDEM, K., Br. Nucl. Energy Soc. Conf. Nuc Performance, London (1973) 55.1.
[56] PENN, W.J., LO, R.K., WOOD, J.C., Nucl. Technol. **34** (1977) 249.

[57] KNUDSON, P., Am. Nucl. Soc. Topical Meeting Water Reactor Fuel Performance, St. Charles (1977) 243.
[58] MOGARD, H., BERGENLID, U., BODH, R., LYSELL, G., Nuclear Power and its Fuel Cycle (Proc. Conf. Salzburg, 1977) 2, IAEA, Vienna (1977) 635.
[59] LYSELL, G., VELLI, G., Br. Nucl. Energy Soc. Conf. Nuclear Fuel Performance, London (1973) Paper 68.
[60] VOGEL, W., et al., Reaktortagung Hannover (1978) 533.
[61] HARDY, D.G., et al., Am. Nucl. Soc. Topical Meeting Water Reactor Fuel Performance, St. Charles (1977) 198.
[62] JUNKRANS, S., VÄRNILD, O., Am. Nucl. Soc. Topical Meeting Water Reactor Fuel Performance, St. Charles (1977) 219.
[63] GARZAROLLI, F., et al., Kerntechnik **20** (1978) 27.
[64] WOOD, J.C., HARDY, D.G., Am. Nucl. Soc. Topical Meeting on Water Reactor Fuel Performance, St. Charles (1977) 315.
[65] McDONALD, R.D., HARDY, D.G., HUNT, C.E.L., Trans. Am. Nucl. Soc. **17** 2 (1973) 216.
[66] ROLSTAD, E., Atomwirtsch., Atomtech. (1973) 121.
[67] PITEK, M.T., ROLSTAD, E., Am. Nucl. Soc. Topical Meeting Water Reactor Fuel Performance St. Charles (1977) 198.
[68] VIDEM, K., LUNDE, L., Proc. Eur. Nucl. Conf. Paris **3** 1, Pergamon Press, New York (1975).
[69] CUBICCIOTTI, D., et al., Am. Nucl. Soc. Topical Meeting Water Reactor Fuel Performance, St. Charles (1977) 282.
[70] COX, B., WOOD, J.C., Electrochem. Soc. Symp. Corrosion Problems, New York (1974) 275.
[71] GARLICK, A., J. Nucl. Mater. **49** (1973/74) 209.
[72] BUSBY, C.C., et al., J. Nucl. Mater. **55** (1975) 55.
[73] PEEHS, M., et al., 4th Int. Conf. Zirconium in the Nuclear Industry, Stratford-upon-Avon, 1978.
[74] WOOD, J.C., Nucl. Technol. **23** (1974) 63.
[75] ROBERTS, J.T.A., et al., EPRI-Rep. NP-737-SR (1978).
[76] CUBICCIOTTI, D., DAVIES, J.H., Nucl. Sci. Eng. **60** (1976) 314.
[77] WUNDERLICH, F., GARZAROLLI, F., Reaktortagung Hannover (1978) 525.
[78] JORDAN, K.R., Proc. Topical Meeting Commercial Nuclear Fuel Technology Today, Toronto (1975) 2–86.
[79] ROBERTS, G., et al., Am. Nucl. Soc. Topical Meeting Water Reactor Fuel Performance, St. Charles (1977) 114.
[80] UNITED STATES ATOMIC ENERGY COMMISSION, Technical Report on Densification of Light Water Reactor Fuel (1972).
[81] FERRARI, M.M., et al., Br. Nucl. Energy Soc. Conf. Nuclear Fuel Performance, London (1973) 54.1.
[82] MANZEL, R., STEHLE, H., Proc. 1st Eur. Nuclear Conf., Paris (1975) 253.
[83] IBRAHIM, E.F., J. Nucl. Mater. **46** (1973) 161.
[84] ROSS-ROSS, P.A., HUET, C.E.L., J. Nucl. Mater. **26** (1968) 2.
[85] WOOD, D.S., Proc. Eur. Conf. Irradiation Behaviour of Fuel Cladding and Core Components Materials, Karlsruhe (1974) 123.
[86] FIDLERIS, V., At. Energy Rev. **13** 1 (1975) 51.
[87] MARLOWE, M.O., Rep. NEDO 12440 (1973).
[88] MacEWEN, S.R., HASTINGS, I.J., Philos. Mag. **31** (1975) 135.
[89] ASSMANN, H., STEHLE, H., Reaktortagung Karlsruhe (1973) 409.
[90] STEHLE, H., ASSMANN, H., J. Nucl. Mater. 52 (1974) 303.
[91] ASSMANN, H., STEHLE, H., Atomwirtsch., Atomtech. **21** (1976) 239.

[92] ASSMANN, H., STEHLE, H., Trans. 4th Int. Conf. Structural Mechanics in Reactor Technology, San Francisco (1977) C3/1.
[93] FRESHLEY, M.D., et al., J. Nucl. Mater. **62** (1976) 138.
[94] COBLE, R.L., J. Appl. Phys. 32 (1961) 787.
[95] WHAPHAM, A.D., Nucl. Applic. 2 (1966) 123.
[96] ROSS, A.M., J. Nucl. Mater. **39** (1969) 134.
[97] BELLAMY, R.G., RICH, J.R., J. Nucl. Mater. **33** (1969) 64.
[98] TURNBULL, J.A., CORNELL, R.M., J. Nucl. Mater. **36** (1970) 161.
[99] TURNBULL, J.A., CORNELL, R.M., J. Nucl. Mater. **37** (1970) 355.
[100] CHALDER, G.H., et al., Enlarged Halden Program Group Meeting, Sanderstølen,
[101] BRZOSKA, B., et al., Enlarged Halden Group Meeting, Sanderstølen, 1977.
[102] BRZOSKA, B., et al., Reaktortagung Nürnberg, 1975.
[103] STEHLE, H., et al., 3rd Int. Symp. Zirconium in the Nuclear Industry, Quebec
[104] ADAMSON, R.B., 3rd Int. Symp. Zirconium in the Nuclear Industry, Quebec
[105] DOLLINS, C.C., J. Nucl. Mater. 59 (1971) 61.
[106] DANIEL, R.C., Nucl. Technol. **14** (1972) 171.
[107] WEDDINGTON, J.S., 78th Ann. Meeting Am. Ceramic Soc., Cincinnati, 1976.
[108] HARBOTTLE, J.E., CORNELL, R.M., Nucl. Eng. Des. **42** (1977) 423.
[109] DUNCAN, R.N., et al., Proc. Topical Meeting Commercial Nuclear Fuel Technology Today, Toronto (1975) 2–55.
[110] SHEPPARD, K.D., et al., Rep. WCAP–8346 (1974).
[111] REACIS, J.R., et al., Rep. WCAP–8692 (1975).
[112] GALLAUGHER, W.C., et al., Am. Nucl. Soc. Topical Meeting on Water Reactor Performance, St. Charles (1977) 48.
[113] EICKELPASCH, N., Reaktortagung Karlsruhe (1973) 397.
[114] McMULLEN, W.D., et al., Rep. WAPD-BT-15 (1959).
[115] ARCHARD, J.F., Rep. NASA-SP-181 (1967) 267.
[116] KIENZ, F.H., et al., AECL Rep. CRMet. 857 (1960).
[117] BHANCHET, J., et al., Corr. Traitement, Protection, Finition **20** (1972) 19.
[118] WILLIAMSON, H.E., et al., Rep. GEAP-4597 (1965).
[119] DEFFERDING, L.J., Rep. HW-73698 (1962).
[120] GORMAN, D.J., Nucl. Sci. Eng. **44** (1971) 50.
[121] NEEB, K.H., SCHUSTER, E., presented Am. Nucl. Soc. National Meeting, San Diego, June 1978.
[122] SCHUSTER, E., et al., Reaktortagung Mannheim (1977) 817.
[123] GARZAROLLI, F., et al., to be published in Kerntechnik.
[124] LOCKE, D.H., Nucl. Eng. Int. (1969) 648.
[125] LUSTMAN, B., et al., Rep. WAPD-BT-23 (1961).
[126] LOCKE, D.H., Nucl. Eng. Des. **21** (1972) 318.
[127] STEHLE, H., et al., Nucl. Eng. Des. **33** (1975) 230.
[128] EICHENBERG, J.D., et al., Rep. WAPD-183 (1057).
[129] LOCKE, D.H., Am. Nucl. Soc. Topical Meeting Water Reactor Fuel Performance, St. Charles (1977) 28.